Removal of Arsenic from Contaminated Water by Granular Activated Carbon Embedded with Nano scale Zero-valent Iron.

Md. Rashadul Islam Chowdhury

A Thesis
In the Department
of
Building, Civil and Environmental Engineering

Presented in Partial Fulfillment of the Requirements
For the Degree of
Doctor of Philosophy (Civil and Environmental Engineering) at
Concordia University
Montreal, Quebec, Canada

July 2015

CONCORDIA UNIVERSITY
SCHOOL OF GRADUATE STUDIES

This is to certify that the thesis prepared

By: **Md. Rashadul Isalm Chowdhury**

Entitled: **Removal of arsenic from contaminated water by granular activated carbon embedded with nano scale zero-valent iron.**

and submitted in partial fulfillment of the requirements for the degree of

Ph.D.

complies with the regulations of the University and meets the accepted standards with respect to originality and quality.
Signed by the final examining committee:

Gerard J. Gouw	Chair
David Blowes	External Examiner
Justin Powlowski	External to Program
Radu Zmeureanu	Examiner
Zhi Chen	Examiner
Catherine N. Mulligan	Thesis Supervisor

Approved by

Chair of Department or Graduate Program Director

Dean of Faculty

ABSTRACT

Removal of arsenic from contaminated water by granular activated carbon embedded with nano scale zero-valent iron.

Md. Rashadul Islam Chowdhury, Ph.D.
Concordia University, 2015

This study investigated the removal of arsenic from groundwater by granular activated carbon (GAC) supported nano scale zero-valent iron (nZVI). GAC supported nZVI (nZVI/GAC) composite was synthesized by hydrolyzing a Fe(III) salt on GAC, reduced by $NaBH_4$ and dried under vacuum. Synthesized nZVI/GAC was characterized using scanning electron microscopy (SEM) along with EDS, BET surface area analysis, X-ray diffraction (XRD), and Fourier transform infrared (FTIR) spectroscopy. The experimental results were produced through the batch and Rapid Small Scale Column Test (RSSCT). The adsorption depends on pH, initial concentration, and reaction time. Arsenite adsorption capacity varies from 800 to 1400 µg/g over the pH 2-11. Arsenate adsorption was higher (3000-3700 µg/g) over the acidic pH range 2-6.5. Among competitive ions, phosphate and silicate affected the most while sulfate, nitrate, chloride, fluoride, manganese, magnesium and calcium had insignificant impact. The experimental data were evaluated with Langmuir and Freundlich isotherms. The adsorption capacity for arsenate, calculated from Langmuir and Freundlich isotherms, were 5000 and 6000 µg/g, respectively at pH 4.5. The reaction kinetics followed the pseudo-second order model. The initial sorption rate (h), determined from pseudo-second order kinetic model, was 666 µg/g.min. The dynamic behaviour of the RSSCT was predicted by the HSDM model using the software FAST 2.0. From the RSSCT results, it was found that the number of bed volumes treated depends on the empty bed contact time (EBCT) as well as the initial arsenate concentration.

The regeneration of spent nZVI/GAC using 0.1M NaOH was effective as it desorbed 87% of adsorbed arsenic. The solid waste can be safely disposed of in a sanitary landfill without any treatment as the concentration of leached arsenate determined by TCLP was much lower than the regulatory limit. The arsenic removal mechanism was due to the combination of electrostatic and the complex formation, either monodentate or bidentate, between As(V) and nZVI corrosion products. The results indicated that nZVI/GAC is a promising adsorbent for arsenic removal.

ACKNOWLEDGEMENTS

First and foremost, I would like to express my sincere gratitude to my advisor, Dr. Catherine N. Mulligan, for her continuous support throughout this challenging journey that made this thesis possible. I am grateful for her invaluable advice, financial support, and compassion to scrutinize this manuscript.

The appreciation also goes to the examiners, Dr. David Blowes, Dr. Justin Powlowski, Dr. Radu G. Zmeureanu, and Dr. Zhi Chen for their time to examine the thesis. Special thanks to Dr. David Blowes and Dr. Justin Powlowski for their valuable comments and suggestions that gave a significant dimension to this thesis.

My heartfelt love to my wife Kazi Feroza Begum for her support and encouragement. Special love to our wonderful daughter Tasnim Chowdhury (Rodela), the source of our inspiration.

Last but not least, I like to thank all my friends and colleagues for their helping hands, sharing ideas and encouragement during this study.

DEDICATION

To my beloved wife, Kazi Feroza Begum

Table of Contents

Chapter 1 Introduction ____________________________ 1

Chapter 2 Sources, Chemistry and Toxicity of Arsenic_6

Chapter 4 Rapid Small Scale Column Test (RSSCT)__ 46

Chapter 5 Materials and Methods ________________ 59

Chapter 6 Results and Discussion ________________73

List of Figures

Chapter 2

Chapter 3

Chapter 5

Chapter 6

List of Tables

Chapter 2

Chapter 3

Chapter 4

Chapter 5

Chapter 6

Nomenclature

AA	Activated alumina
BAT	Best available technology
Bi	Biot number, $Bi = k_f r_p c_0 / (D_s \rho_p q_e)$ (dimensionless)
BV	Bed volume (cm^3)
c	liquid-phase concentration (µg/L)
C_e	liquid-phase equilibrium concentration (µg/L)
C(t)	liquid-phase concentration as a function of time (µg/L)
c_0	influent liquid-phase concentration (µg/L)
c*	liquid-phase concentration at exterior adsorbent surface (µg/L)
D_0	Dosage of adsorbent, µg/g
Dg	solute distribution parameter, $Dg = \rho_B q_e / \varepsilon_B c_0$ (dimensionless)
D_s	surface diffusion coefficient (cm^2/s)
EBCT	empty bed contact time, $EBCT = m/(\rho_B Q)$ (min)

Ed	diffusivity modulus, Ed = St/Bi (dimensionless)
GAC	Granular activated carbon
h	Initial sorption rate (μg/g.min)
K_F	Freundlich isotherm coefficient (μg/g)(L/μg)$^{1/n}$
k_f	liquid-phase mass transfer coefficient (cm/s)
L	length of fixed-bed (cm)
m	mass of adsorbent (g)
1/n	Freundlich isotherm exponent (dimensionless)
N	number of simulated data points (dimensionless)
Q	solid-phase concentration (μg/g)
q_e	solid-phase concentration in equilibrium (μg/g)
q_0	initial solid-phase concentration (μg/g)
q_t	solid-phase concentration at time t (μg/g)
q^*	solid-phase concentration at exterior adsorbent surface (μg/g)
Q	fluid flow rate, (cm^3/min)
R	radial coordinate (cm)
r_p	radius of adsorbent grain (mm)
R	dimensionless radial coordinate, $R = r/r_p$ (dimensionless)
Re	Reynold's number (dimensionless)
ΔR	discretization grid width for dimensionless radial coordinate (dimensionless)
Sc	Schmidt number (dimensionless)
St	modified Stanton number, $St = k_L m/r_p \rho_p Q$ (dimensionless)
T	dimensionless time coordinate, $T = t/(EBCT \varepsilon_B Dg)$ (dimensionless)

ΔT	discretization grid width for dimensionless time coordinate (dimensionless)
TCLP	Toxicity characteristics leaching procedure
v_F	superficial filter velocity, hydraulic loading rate (HLR) (cm/s)
x	Diffusivity factor (dimensionless)
X	liquid-phase concentration, $X = c/c_0$ (dimensionless)
X^*	liquid-phase concentration at exterior adsorbent surface (dimensionless)
Y	solid-phase concentration, $Y = q/q_e$ (dimensionless)
Y^*	solid-phase concentration at exterior adsorbent surface (dimensionless)
z	axial coordinate (cm)
Z	axial coordinate, $Z = z/L$ (dimensionless)
ΔZ	discretization grid width for dimensionless axial coordinate (dimensionless)
Vb	molar volume at normal boiling point, cm^3/mole
α	courant number of filter PDE (4.3), $\alpha = Dg\Delta T/\Delta Z$ (dimensionless)
β	numerical stability number of filter PDE (4.3), $\beta = 3\ StDg\Delta T$ (dimensionless)
γ	courant number of intraparticle PDE (4.6), $\gamma = Ed\Delta T/\Delta R^2$ (dimensionless)
μ	dynamic viscosity of the fluid, (g/cm.s)
ε_B	bed porosity (dimensionless)
ρ_B	bulk density of adsorbent in the fixed-bed, $\rho_B = \rho_p (1- \varepsilon_B)$ (g/cm^3)
ρ_p	density of adsorbent grain (g/cm^3)

Subscripts

i	index of grid cell for time coordinate (dimensionless)
j	index of grid cell for axial coordinate (dimensionless)
k	index of grid cell for radial coordinate (dimensionless)
SC	small column
LC	large column

Chapter 1

Introduction

1.1 Introduction

Arsenic is one of the toxic elements that has acute to chronic and carcinogenic effects on human health mainly through ingestion of drinking water (Borum & Abernathy, 1994). Long-term exposure to a high level of arsenic through drinking water may cause cancer to different human organs and skin lesions as well as muscular weakness and neurological disorders (Saha et al., 1999; Jain & Ali, 2000). Elevated levels of arsenic are found in groundwater due to natural processes (volcanic emissions, biological activities, burning of fossil fuels and weathering of arsenic bearing rocks and minerals) (Cullen & Reimer, 1989) and anthropogenic activities (applications of arsenical pesticides, insecticides, wood preservatives, paints, drugs, dyes, semiconductors, incineration of arsenic containing substances, industrial wastewater discharge, mine tailing/landfill leaching) (Korte & Fernando, 1991; Peryea & Creger, 1994; Azcue & Nriagu, 1994; Welch et al., 1988). Naturally occurring arsenic in drinking water supplies affects over 137 million people in more than 70 countries; of which the most affected countries are Bangladesh, west Bengal (India), China, Chile, Argentina, Mexico, Hungry, Taiwan, and Vietnam (Smedley & Kinniburgh, 2002; Berg et al., 2004; Ćavar et al., 2005). In order to minimize the health risk, the World Health Organization (WHO), United States Environmental Protection Agency (USEPA), and health Canada have reduced the maximum allowable contamination level (MCL) of total arsenic in drinking water from 50 to 10 μg/L (USEPA, 2001a; WHO, 1997; health Canada, 2006). This stringent regulation poses a major compliance challange to the existing water supply systems.

Therefore, it is an urgent need to develop cost effective and technologically feasible systems to meet the new drinking water standard for arsenic.

Adsorption is one of the most commonly used technologies to remove arsenic from water (Mohan & Pittman, 2007). It is simple to perform and is usually inexpensive. Good sorption properties of iron (hydr)oxide phases have been found promising for remediation of various contaminants. Iron oxides, especially amorphous iron oxides, have also been reported to be effective for the removal of arsenic (Reed et al., 2000). Several iron(III) oxides, such as amorphous hydrous ferric oxide (FeOOH), poorly crystalline hydrous ferric oxide (ferrihydrite) and goethite (α-FeOOH), are promising adsorptive materials to remove As(V) and As(III) from aqueous solutions (Pierce & Moore, 1982; Hsia et al., 1994; Wilkie & Hering, 1994; Raven & Jain, 1998; Sun & Doner, 1998). Recently, zero-valent iron (ZVI) has been used to remove arsenic from water. Compared with other methods, ZVI can simultaneously remove As(V) and As(III) without pre-oxidation (Lackovic & Nikolaidis, 2000; Farrell & Wang, 2001; Melitas & Wang, 2002; Daus et al., 2004). ZVI and most iron(III) oxides are available as fine powders. These particles are characterized by high surface area to volume ratio, high level of stepped surface, and high surface energy (Ichinose, 1992). However, ZVI and iron oxide nanoparticles are not suitable for fixed bed systems because of their low hydraulic conductivity and poor mechanical strength.

To overcome the foregoing problems, recent studies are focused on creating inexpensive and stable iron bearing adsorbents such as iron oxide coated sand (Gupta et al., 2005), iron oxide impregnated activated carbon (Vaughan & Reed, 2005), GAC based iron containing adsorbent (Gu et al., 2005), GAC composites incorporated with iron/palladium (Fe/Pd) bimetallic nanoparticles (Choi et al., 2008), and nZVI-supported GAC (Zhu et al., 2009). Examples are also extended to HFO particles, which were incorporated into diatomite, GAC, and anion exchange resin D-201, to enhance their mechanical strength (Jang et al., 2006, 2008; Zhang et al., 2008). GAC has a large surface area, high pore volume, and rigid structure to be an ideal backbone for hosting a considerable amount of iron. Moreover, due to its ease of liquid/solid separation (Schroeder, 1976), GAC is widely used in water and advanced wastewater treatment facilities and is designated as the best available technology (BAT) by the U.S. EPA for the removal of organic compounds, odor and taste, and trace metals (USEPA, 1987). But virgin activated carbon cannot be directly applied for arsenic treatment due to its lower arsenic adsorption capacity (Deng et al., 2005). Research revealed that iron incorporated granular activated carbon can effectively remove arsenic from water without losing the capability of removing organic contaminants (Huang & Vane, 1989; Reed et al., 2000; Chen et al., 2007; Hristovski et al., 2009). Moreover, the infrastructure for GAC supplies, markets, treatment infrastructure (vessels, pumps, handling, etc.), and disposal is very well established and would provide rapid deployment (market penetration) of iron-modified GAC composites into the water industry.

1.2 Objectives of the Study

To develop a new class of arsenic adsorption media by combining the benefits of GAC and iron compounds is the objective of this research. The overall objective of this research is to develop an effective means of removing arsenic from groundwater.

To accomplish the objectives, the work was broken down into four main categories: (1) to synthesize and incorporate nano scale zero-valent iron onto GAC (nZVI/GAC), (2) to characterize nZVI/GAC, (3) to determine the rate of adsorption of arsenic by this material, and (4) to explain the arsenic adsorption mechanism. For logical explanation of the studies, the following investigations were performed.

- Comparative study of virgin and nano scale zero-valent iron modified granular activated carbon (nZVI/GAC).
- Sorption behavior of arsenate (As V) and arsenite (As III).
- Studies on the factors controlling arsenic removal efficiency.
- Studies on the effect of co-existing ions on arsenic removal efficiency
- Batch adsorption isotherm and kinetic studies.
- Dynamic column studies
- Desorption to evaluate the reusability of the adsorbent.

1.3 Scope of the Study

The scope of the study involved in the following tasks:

- This study focused on the sorption behavior of nano scale zero-valent iron modified granular activated carbon (nZVI/GAC) in removing inorganic, soluble penta-valent arsenate [As (V)] and trivalent arsenite [As (III)].
- Experimental studies were limited to lab-prepared water.

1.4 Organization of the Thesis

This thesis consists of seven chapters. Chapter one includes the introduction where the statement of the problem and the need for further research are explained in addition to the objectives and scope of the study. In chapter two, the sources of arsenic in drinking water, relevant chemistry of arsenic to understand the mechanisms by which it is released to the environment, its toxicity and regulation are described. A comparative study of available arsenic removal technologies has been presented in chapter three. Theoretical background of Rapid Small Scale Column Test (RSSCT), Homogeneous Surface Diffusion Model (HSDM) and its numerical solution, and the scale up procedure have been described in chapter four. Chapter five, materials and methods, describes the chemicals used, synthesis and characterization of the adsorbent materials, as well as the experimental procedure. In chapter six, experimental results are presented with detailed explanation. Chapter seven includes the concluding remarks and the recommendations for future work.

Chapter 2

Sources, Chemistry and Toxicity of Arsenic

2.1 Sources of Arsenic in the Environment

Arsenic is ubiquitously present in air, soil, natural water, mineral deposits and rocks and biota (Matschullat, 2000; Miteva et al., 2005) in varying concentrations. It is the main constituent of some 245 mineral species (Valberg et al., 1997; Thronton & Fargo, 1997) of which approximately 60% are arsenates, 20% sulfides and sulfosalts; the remaining 20% includes arsenides, arsenites, oxides, silicates and elemental arsenic (As) (Onishi, 1969). As^0 and As^{3-} are rare in aquatic environments (Mandal & Suzuki, 2002; Goldberg & Johnston, 2001). Only a few of these hundreds of arsenic minerals are common in hydrogeochemical environments (Hering & Kneebone, 2002; Kanivetsky, 2000). For example, in reducing environments, arsenic is present in iron sulfide minerals such as arsenopyrite (FeAsS), realgar (AsS) and orpiment (As_2S_3). In oxidizing environments, arsenic is found in arsenolite (As_2O_3) and claudetite (As_2O_3). Under a wide range of geochemical conditions, arsenic has also been associated with minerals such as iron oxides (Fe_2O_3), iron hydroxides (FeOOH), other metal oxides and hydroxides like aluminum and manganese (Hem, 1985; Holm & Curtiss, 1988; Hounslow, 1980; Kinniburgh & Smedley, 2001b; Korte, 1991; Ryker, 2003; Sullivan & Aller, 1996; Yan et al., 2000). Arsenopyrite is the most common and is relatively insoluble in water. The sulfides in arsenopyrite, however, can be oxidized to more soluble forms allowing arsenic to leach into groundwater. The arsenic content of minerals is usually between 0.02-0.50%, but arsenopyrite can sometimes contain as much as 5%

(Hindmarsh, 2000). Arsenic can be released into the environment by both natural and anthropogenic processes.

2.1.1 Natural Sources

Natural weathering processes contribute approximately 40,000 tonnes of arsenic to the global environment annually, while twice this amount is released by human activities (Paige et al., 1996). Arsenic ranks twentieth in abundance of elements in the earth's crust with an average level of 1.8 mg/kg in the earth's crust (Greenwood & Earnshaw, 1984), and fourteenth in seawater (Mandal & Suzuki, 2002). Normal background concentrations are 0.2-15 mg/kg in the lithosphere, less than 15 mg/kg in soils, 0.02-2.8 ng/m^3 in the atmosphere, and less than 1 μg/L in the aquatic environment (Matschullat, 2000).

2.1.2 Anthropogenic Sources

Some of the anthropogenic sources of arsenic are mining activities, combustion of fossil fuel, use of arsenic-based pesticides, herbicides, and wood preservatives. Of the total arsenic added to the soil from anthropogenic activities, about 23% comes from coal fly ash and bottom ash, 14% from atmospheric fallout, 10% from mine tailings, 7% from smelters, 3% from agriculture and 2% from manufacturing, urban and forestry wastes (Bhumbla & Keefer, 1994).

2.2 Chemistry of Arsenic

Depending on the pH, different forms of arsenite [As(III)] are H_3AsO_3, $H_2AsO_3^-$, $HAsO_3^{2-}$ and AsO_3^{3-} whereas that of arsenate [As(V)] are H_3AsO_4, $H_2AsO_4^-$, $HAsO_4^{2-}$, and AsO_4^{3-}. Figures 2.1 and 2.2 show the protonation forms of arsenite and arsenate at various pHs. These diagrams are generated by the following equilibrium relationships.

For arsenite (As III),

$H_3AsO_3 \leftrightarrow H_2AsO_3^- + H^+$ $pK_{a1} = 9.22$

$H_2AsO_3^- \leftrightarrow HAsO_3^{2-} + H^+$ $pK_{a2} = 12.13$

$HAsO_3^{2-} \leftrightarrow AsO_3^{3-} + H^+$ $pK_{a3} = 13.40$

For arsenate (As V),

$H_3AsO_4 \leftrightarrow H_2AsO_4^- + H^+$ $pK_{a1} = 2.20$

$H_2AsO_4^- \leftrightarrow HAsO_4^{2-} + H^+$ $pK_{a2} = 6.97$

$HAsO_4^{2-} \leftrightarrow AsO_4^{3-} + H^+$ $pK_{a3} = 11.53$

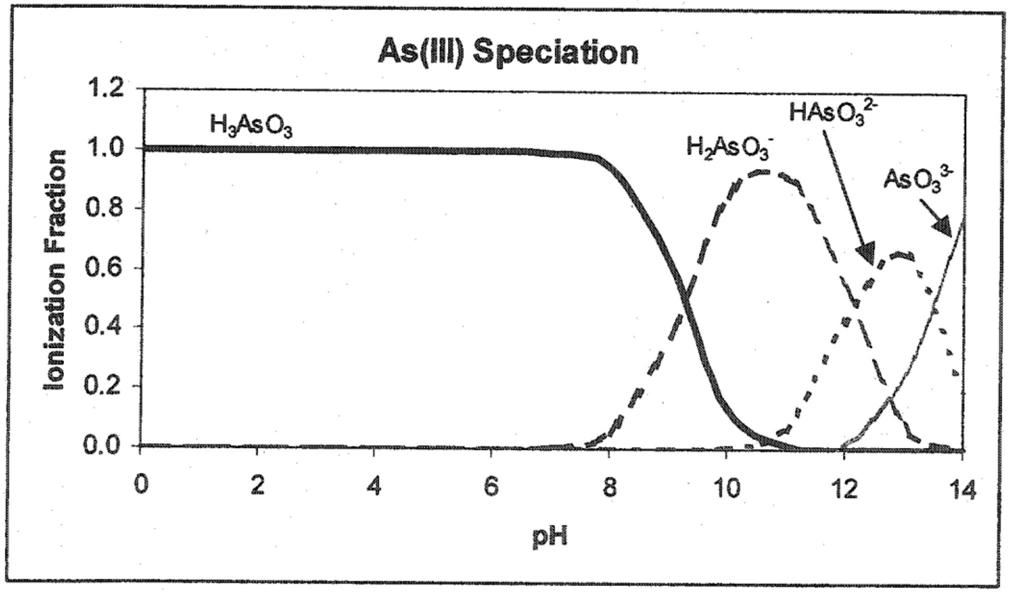

Figure 2.1 Speciation diagram for arsenite, As(III) (David & Allison, 1999)

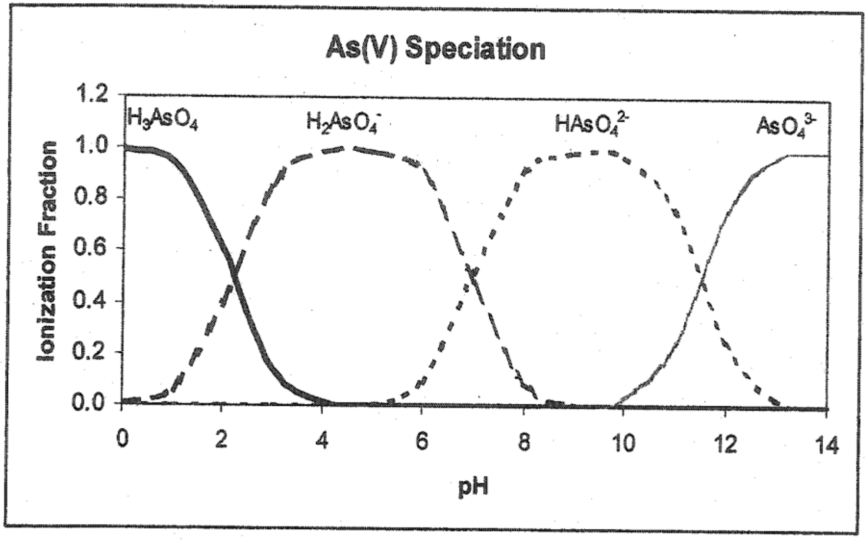

Figure 2.2 Speciation diagram for arsenate, As(V) (David & Allison, 1999)

The degree of protonation of both arsenite and arsenate is an important factor governing the mobility of these chemical species. For example, the pH of groundwater is often between 6 and 8. Within this range, arsenite is uncharged while arsenate is negatively charged. As a result, arsenite is more mobile than arsenate. The movement of arsenate is retarded by electrostatic attraction to positively charged particles, such as iron hydroxides (Domenico & Schwartz, 1998). This information is also useful in designing effective arsenic removal technologies and in determining the arsenic speciation by an ion exchange separation technique.

2.3 Speciation of Arsenic

Arsenic forms a number of inorganic and organic compounds. Naturally occurring inorganic arsenic is stable in oxidation states of -3 as in arsine gas (AsH_3), 0 as in crystalline/elemental arsenic, +3 as in arsenite [As(III)], and +5 as in arsenate [As(V)]. The elemental state is extremely rare whereas the -3 oxidation state is found only at extremely reducing conditions. Arsenate species

(H_3AsO_4, $H_2AsO_4^-$, $HAsO_4^{2-}$, and AsO_4^{3-}) are stable in oxygenated waters. Under mildly reducing conditions, arsenite species (H_3AsO_3, $H_2AsO_3^-$, $HAsO_3^{2-}$, and AsO_3^{3-}) predominate (Andreae, 1978; Ballantyne & Moore, 1988).

Organic arsenic species include monomethyl arsonic acid (MMAA), and dimethyl arsonic acid (DMAA). They may be produced by biological activity, mostly in surface waters, but are rarely quantitatively important. Organic forms may, however, occur where waters are significantly impacted by industrial pollution (Irgolic, 1982). The organic (methylated) arsenic usually occurs at natural concentrations of less than 1 μg/L and is not of major significance in drinking water treatment (Edwards, 1994). Generally, inorganic arsenic accounted for 85-99% of the total arsenic found in ground and surface water (Irgolic, 1982). The order of expected occurrence of arsenic in drinking water is arsenate (AsV), arsenite (AsIII), monomethyl arsonic acid (MMA) and dimethyl arsonic acid (DMA).

The occurrence, distribution, mobility and speciation of arsenic rely on many factors including the pH, reduction-oxidation reactions, distribution of other ionic species, aquatic chemistry and microbial activity (Oliver, 1997, as cited in Yong & Mulligan, 2004). Oxidation-reduction potential (Eh) and pH are the most important parameters controlling arsenic speciation. The relationships between Eh, pH and arsenic speciation are illustrated in Figure 2.3.

The Eh-pH diagram shows the arsenic speciation and oxidation states at a particular pH and redox potential (Villa-Lojo et al., 1997). The diagram also shows the expected change in arsenic state when environmental conditions differ. For example, anoxic groundwater usually has a low redox potential. When the water is pumped to the ground surface and exposed to the atmosphere, the presence of dissolved oxygen increases the redox potential. As a result, arsenite will naturally oxidize to arsenate.

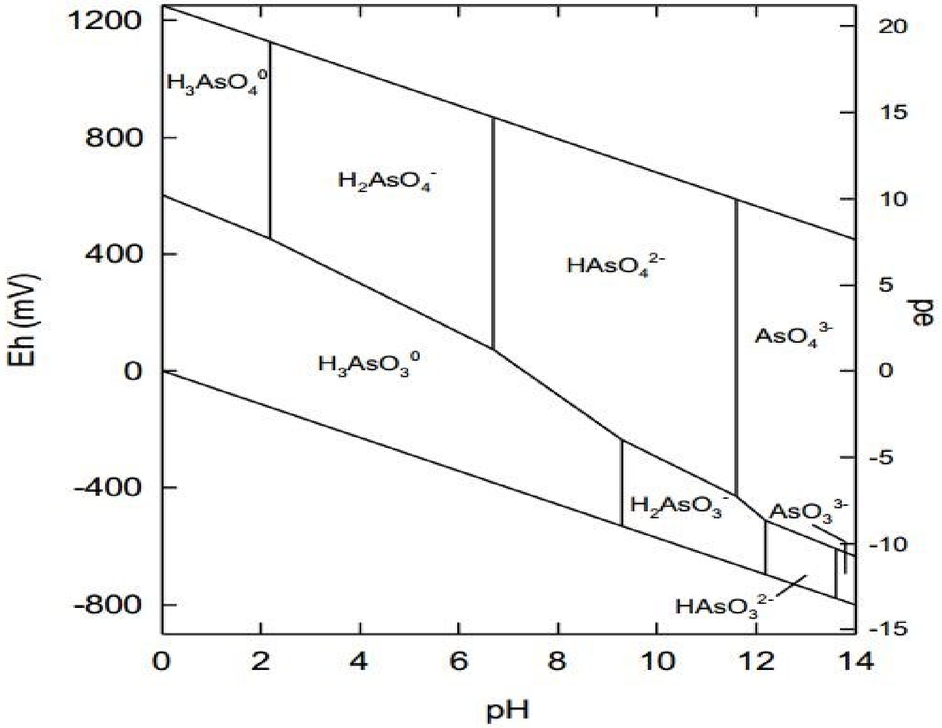

Figure 2.3. Eh-pH diagram of aqueous arsenic species in the system As-O_2-H_2O at 25ºC and 1 atm total pressure (Smedley & Kinniburgh, 2002)

High concentrations of arsenic are found in both oxidizing and reducing aquifers and areas affected by geothermal, mining and industrial activity. Bangladesh, India, Taiwan, Vietnam, Hungary and Romania are affected by groundwater arsenic problems because of the reducing environment. High levels of arsenic are present due to oxidizing environments in groundwater in the arid region of Mexico, Chile, and Argentina. Because of mixed oxidizing and reducing environments, the groundwater arsenic problem exists in southwestern USA (Smedley & Kinniburgh, 2002).

At the high redox potential values characteristic of oxygenated surface and ground waters, inorganic arsenate (As V) is the expected form of arsenic (Ferguson & Gavis, 1972). Irgolic (1982) developed analytical methods for inorganic arsenic speciation for highly contaminated waters and his method revealed a highly variable arsenite to arsenate ratio of 0.007 to 3.4.

2.4 Arsenic in Canadian Waters

Higher levels of arsenic occures in surface and groundwater due to mining, industrial, and geothermal activities in some regions of Canada. For example, Moira Lake (40-50 μg/L) and Moira River (2-140 μg/L) in Ontario have high concentrations of arsenic due to gold mining and mineral processing (Azcue & Nriagu, 1995; Zheng et al., 2003). Gegogan Lake, Nova Scotia has particulate (1500-5000 mg/kg) as well as dissolved arsenic (30-230 μg/L) from an abandoned gold mine (Wong et al., 1999). Coumans (2003) found the surface water arsenic in the Kam Lake, Northwest Territories (NWT) up to 1,570,000 μg/L as a consequence of gold mining. He also estimated that about 220 million tonnes of highly toxic arsenic trioxide were buried at the Giant gold mining site in Yellowknife, NWT which could pose a threat to the sourrounding area as well as far beyond the mining site ground and surface water.

The concentration of arsenic in groundwater was found up to 580 μg/L due to sulfide mineralization in Bowen Island, British Columbia (Boyle et al., 1998). Henning and Konasewich (1984) also reported higher levels of groundwater arsenic up to 11000 μg/L in the vicinity of an abandoned arsenical wood preservative facility near Vancouver, British Columbia. In the town of Virden, Manitoba, groundwater arsenic levels ranged from 65 to 70 μg/L (OSMONICS, 2002).

Due to geothermal activites, higher levels of arsenic were found in Meager Creek hot springs, British Columbia with an average concentration of 280 μg/L (Koch et al., 1999). In comparison, the arsenic concentration in the cold Meager Creek water was much lower (5.4 μg/ L). The higher concentration of arsenic in the hot spring water was due to the enhanced dissolution of arsenic-containing minerals by hot water.

2.5 Toxicity of Arsenic

Long term drinking of arsenic contaminated water may cause chronic arsenic toxicity (arsenicosis) that has detrimental effects on many parts of the bodily systems, including the gastrointestinal system, respiratory system (Morton, 1994), cardiovascular system (Franzblau, 1989; Morton, 1994), peripheral nervous system (Morton, 1994; Hindmarsh, 2000), skin (Hindmarsh, 2000; Morton, 1994; Mass, 1992), and mucous membranes (Franzblau, 1989). Arsenic has also teratogenic, reproductive, mutagenic (Morton, 1994; Vahter, 2000; Domingo, 1994; Fowler, 1977), and carcinogenic effects (Morton, 1994; Hindmarsh, 2000; Mass, 1992).

The process of arsenic uptake and distribution in organisms adapts the pathway of the element phosphorus, which is an important element for living organisms. Phosphorus forms nerve tissue, bones and teeth. Phosphorus and arsenic have similar oxidation states; these characteristics contribute to arsenic toxicity. Arsenate (H_3AsO_4) is an analogue of phosphate and is taken up via the phosphate transport system by most organisms. Arsenate has been postulated to replace phosphate in energy transfer phosphorylation reactions (Dixon, 1996). Replacing the stable phosphate with the less stable As(V) anion leads to rapid hydrolysis of high-energy bonds in compounds such as ATP. This leads to a loss of high-energy phosphate bonds and effectively "uncouples" oxidative phosphorylation. Arsenite binds with sulfhydryl groups in protein and disrupts sulfhydryl-containing enzymes and tissue proteins such as keratin in skin, nails, and hair. Since arsenite has a higher affinity for protein and has a longer half-life than arsenate, arsenite is more toxic. Arsenate can be reduced to arsenite by the activity of glutathione and results in the same toxicity. However, since not all of the arsenate can be converted to arsenite, the toxicity of arsenate is less than arsenite (Belton et al., 1985). Due to the bioaccumulation of arsenic in the body, the effects are irreversible.

2.6 Regulations for Arsenic

Arsenic is classified as a Group A carcinogen by the United States Environmental Protection Agency (USEPA) (Lien & Wilkin, 2005), World Health Organization (WHO, 1993) and International Agency for Research on Cancer (Welch et al., 1988). Due to the increasing awareness of the toxicity of arsenic, the regulatory authorities have reduced the maximum allowable contaminant level (MCL) of total arsenic in drinking water. Table 2.1 shows the MCL of some regulatory authorities.

Table 2.1 Maximum allowable contaminant level (MCL) for total arsenic of different regulatory authorities

Authority/Country	**Maximum allowable contaminant level (MCL), µg/L**	**References**
WHO	10	WHO, 1996
Australia	7	NHMRC, 1996
US EPA	10	US EPA, 2001a
European Community (EC)	10	European Commission Directive, 1998
Canada	10	Health Canada, 2006
Bangladesh, China, Mexico Taiwan, Vietnam, etc.	50	Nordstrom, 2002

Chapter 3

Arsenic Removal Technologies

3.1 Arsenic Treatment Options: an Overview

Various common arsenic treatment technologies are available; the selection of a particular technology depends on the source water characteristics in addition to the economic feasibility. Arsenic is present in groundwater as trivalent arsenites (As III) and pentavalent arsenates (As V), in different proportions. Arsenite is generally more difficult to remove than arsenate by conventional treatment methods (Kartinen & Martin, 1995; Lackovic et al., 2000). Hence, most methods require an oxidation step as pre-treatment that converts arsenites to arsenates for effective arsenic removal. Oxygen is the preferred oxidant because it avoids the formation of residuals and oxidation by-products, but the process is extremely slow (Jekel, 1994). For the selection of oxidants, in the case of drinking water treatment, some important factors like residuals of oxidants, oxidation by-products, and the oxidation of other inorganic and organic water constituents are considered. Some effective oxidants are free chlorine, hypochlorite, ozone, permanganate, and hydrogen peroxide (Jekel, 1994). Solar oxidation (Lara et al., 2006), ultraviolet irradiation (Lee & Choi, 2002), and MnO_2-based solid oxidizing media (SOM), Filox-R^{TM} (Clifford, 2001), were also successfully used. Oxidation alone does not remove arsenic from solution and it must be combined with an arsenic removal process. If oxidation is considered as a separate subject, all of the arsenic removal technologies can be put in two categories, membrane separations and adsorption processes. Membrane separations include reverse osmosis, nanofiltration and electrodialysis (Viraraghavan, 1999; Su & Puls, 2001; Prasad, 1994). Adsorption process include fixed bed adsorbent media, metal hydroxides precipitated from solution and ion exchange resins. Fixed bed adsorbent media can be both engineered adsorbents and biomaterials. Some engineered adsorbents are activated alumina, metal oxy-hydroxides, iron-based media, activated carbon, activated bauxite; manganese greensand and iron oxide coated sand (Chen et al., 1999; Frey, 1998; Chwirka et al., 2000; Clifford, 1999; Edwards, 1994; Jekel, 1994; Kartinen & Martin, 1995). Examples of biosorbents include modified fungal biomass, coconut coir pith, sea nodule, *Lessonia nigrescens* and orange waste, anaerobic biomass (Viraraghavan et al., 2006; Loukidou et al., 2003; Anirudhan et al., 2006; Maity et al., 2005; Hansen et al., 2006; Ghimire et al., 2003; Chowdhury & Mulligan, 2011). Arsenic is also removed from solution by adsorption-coprecipitation using coagulants e.g. alum or iron salts, lime softening; oxidation followed by filtration or precipitation (Banerjee et al., 1999; Kartinen & Martin, 1995; Chen, 1999).

3.1.1 Best Available Technologies (BATs)

Among the conventional techniques, the US EPA (US EPA, 2001b) has identified those presented in Table 3.1 as best available technologies (BATs) for effective arsenic removal from drinking water. Technologies are judged by the US EPA to be a BAT when they possess high removal efficiency, a history of full-scale operation, general geographic applicability, reasonable cost based on large and metropolitan water systems, reasonable service life, compatibility with other water treatment processes, and the ability to bring all of the water in a system into compliance. In the following sections, the best available technologies (BATs) are briefly described.

Table 3.1 Best available technologies (BAT) for arsenate removal (US EPA, 2001b)

Treatment Technology	Max. As(V) Removal (%)	Limitation
Ion Exchange	95	Sulfate ≤ 50 mg /L
Adsorption (Activated Alumina)	95	pH sensitive, low regeneration rate
Oxidation/Filtration	80	20:1 = iron: arsenic
Modified Lime Softening	90	pH > 10.5
Modified Coagulation/Filtration	95	pH < 7, high dosage required
Reverse Osmosis	>95	Low water recovery rate, high cost
Electrodialysis	85	Low water recovery rate, high cost

3.1.1.1 Ion Exchange (IX)

Ion exchange is a reversible physical/chemical reaction in which an ion on the surface of a solid phase is exchanged for an ion dissolved in the liquid phase. The solid phase is typically a synthetic resin selected to preferentially adsorb the particular contaminant ion (Korngold et al., 2001). For arsenic removal, chloride-form strong-base resins are generally used (USEPA, 2000). Feed-water is continuously passed through a bed of the ion exchange resin until all of the exchange sites have been filled (USEPA, 2000). The exchange resin is then rinsed with a regenerant solution (typically concentrated NaCl solution for chloride-form resins) to replenish the exchanged ions (Korngold et al., 2001). Anion exchange resin needs frequent regeneration as it is exhausted by sulfate. Frequent column bed regeneration leads to increasing costs and volumes of waste produced by the process.

3.1.1.2 Adsorption by Activated Alumina

Activated alumina (AA) is a porous, granular material with a typical diameter of 0.6 to 0.3 mm having high surface area of 50-300 m^2/g. The media, aluminum trioxide (Al_2O_3), is prepared through the dehydration of precipitated aluminum hydroxide, $Al(OH)_3$, at a temperature range of 300-600^{0}C.

Major factors affecting adsorption by activated alumina are pH, competing ions, EBCT (empty bed contact time) and arsenic oxidation state. Several different studies have established the optimum pH range as 5.0-6.0, and demonstrated greater than 98% arsenic removal under these conditions (USEPA, 2003). The AA column operated under acidic pH conditions is 5 to 20 times longer than under natural pH conditions (6.0-9.0).

3.1.1.3 Lime Softening

Lime softening is a chemical-physical treatment process used to remove calcium and magnesium cations from solution. To remove arsenate, additional lime is added to increase the pH above 10.5. In this range magnesium hydroxide precipitates and arsenate is removed by co-precipitation. Arsenate removal by co-precipitation with calcium carbonate (i.e., below a pH of 10.5) is poor (less than 10%) (USEPA, 2003). These precipitates are then amenable to removal by clarification and filtration.

3.1.1.4 Oxidation/Filtration

Oxidation/filtration refers to processes that are designed to remove naturally occurring iron and manganese from water. The processes involve the oxidation of the soluble forms of iron and manganese to their insoluble forms and then removal by filtration. If arsenic is present in the water, it can be removed via two primary mechanisms: adsorption and co-precipitation. First, soluble iron and arsenite are oxidized. The arsenates then adsorb onto the iron hydroxide precipitates that are ultimately filtered out of solution.

Although some arsenic may be removed by adsorption/co-precipitation with manganese, iron is much more efficient for arsenic removal. The arsenic removal efficiency is strongly dependent on the initial iron concentration and the ratio of iron to arsenic. In general, the Fe: As mass ratio should be at least 20:1, which may yield an arsenic removal efficiency of 80-95% (Selecky et al., 2003).

The effectiveness of arsenic co-precipitation with iron is relatively independent of source water pH in the range 5.5 to 8.5. However, high levels of natural organic matter (NOM), orthophosphates, and silicates weaken arsenic removal efficiency by competing for sorption sites on iron hydroxide precipitates (Fields et al., 2000).

3.1.1.5 Coagulation/Filtration

Coagulation is the process of destabilizing the surface charges of colloidal and suspended matter to allow for the agglomeration of particles. This process results in the formation of large, dense floc, which is amenable to removal by clarification or filtration through a granular media. The most widely used coagulants for water treatment are aluminum and ferric salts, which hydrolyze to form aluminum and iron hydroxide particulates, respectively.

The mechanism involves the adsorption of arsenate to an aluminum or ferric hydroxide precipitate. The arsenate becomes entrapped as the particle continues to agglomerate. Arsenite is not effectively removed because of its overall neutral charge under natural pH conditions. Therefore, pre-oxidation is recommended.

The efficiency and economics of the system depend on several factors, including the type and dosage of coagulant, mixing intensity, and pH. In general, optimized coagulation-filtration systems are capable of achieving over 90% removal of arsenate.

3.1.1.6 Coagulation-Assisted Micro-filtration (CMF)

Coagulation-assisted micro-filtration uses the same coagulation process described above except that the water is forced through a semi-permeable membrane by a pressure differential instead of passing through the granular media. The membrane retains the As(V) laden flocs formed in the coagulation step. The membrane must be periodically backwashed to dislodge solids and restore hydraulic capacity. Backwash water is typically a high-volume, low solids (less than 1.0%) waste stream. The specific amount of solids will depend on several factors, including coagulant type, dosage, filter run length, and ambient solids concentration (AWWARF, 2000).

3.1.1.7 Membrane Techniques

Membrane techniques like reverse osmosis, nano-filtration and electrodialysis are capable of removing almost all kinds of dissolved solids including arsenic from water. In this technique, arsenic is separated from water by passing it through a semi permeable barrier or membrane. Pressure difference is the driving force for the separation. The removal efficiency depends on the pore size in the membrane and the particle size of arsenic species. For better removal efficiency, water should be free from suspended solids and the arsenic should be in pentavalent form.

3.1.1.7.1 Reverse Osmosis (RO)

RO is a pressure-driven membrane separation process capable of removing dissolved solutes from water by means of particle size, dielectric characteristics, and hydrophilicity/hydrophobicity. In addition to arsenic, RO can effectively remove several other constituents from water including organic carbon, salts, and dissolved minerals. The treatment process is relatively insensitive to pH. In order to drive water across the membrane surface against natural osmotic pressure, feed water must be sufficiently pressurized with a booster pump. Reverse osmosis is capable of achieving over 97% removal of arsenate and 92% removal of arsenite in a single pass (NSF, 2001a; NSF, 2001b).

3.1.1.7.2 Electrodialysis

It is similar to reverse osmosis except that the driving force, an electric current, is applied to draw the ions (dissolved solids) through the semi permeable membrane. Since, dissolved solids exist as cations (such as calcium and magnesium) and anions (such as sulfate and arsenic), the cations are attracted to a negatively charged electrode and the anions are attracted to a positively charged electrode. Electrodialysis is more effective in removing arsenate than arsenite (Kartinen & Martin, 1995).

3.1.2 Arsenic Removal by Modified Granular Activated Carbon

Although the above methods are effective for the most part in removing arsenic from drinking water, some can be expensive due to separation techniques, or produce large amounts of waste, while some require expertise training to run and maintain the system. Hence, a continual effort is necessary either to develop new methods or to improve the existing ones for making arsenic removal feasible. Modified granular activated carbon (GAC) with iron compounds are promising for arsenic removal as will be illustrated in the following sections.

3.1.2.1 Activated carbon

Activated carbon is a heterogeneous adsorbent with regard to its pore size and surface chemistry. According to the International Union of Pure and Applied Chemistry (IUPAC) definition, activated carbon contains three types of pores: micro-pore (<2 nm), meso-pore (2-50 nm), and macro-pore (>50 nm). Activated carbon is comprised of graphene planes that are packed together and then bonded together. Each graphene plane consists of a hexagonal carbon lattice with some aromatic character. The edges of the graphene planes can host a number of oxidized sites, including the oxygenated substituents: carboxyls, phenolics, carbonyls, and lactones. In contrast, the interiors of the graphene planes can pose a localized low-redox potential since N can be substituted for C in the lattice structure, creating an electron-rich region (Leon & Radovic, 1994). Activated carbon is created by thermally treating carbon-based solids, such as bituminous coal, lignite coal, or wood. The pyrolysis step in thermal treatment creates narrow fissures between graphene planes; and the oxidation step facilitates the gasification of some graphene layers so as to create slightly wider spaces between the layers. Following activation, the edge sites can be left with incomplete electron configurations; and are therefore reactive. Oxygen can chemisorb to such reactive sites, and form oxygenated groups (Nowack & Stone, 2002). The spaces between graphene planes are generally planar, or slit-shaped. In conventional bituminous granular activated carbons (GAC's), the large majority of pores have widths of 4-30 Å; and organic molecules can just barely fit into these pores. Perhaps the most useful pore widths for adsorbing molecules are 1 to 13 times their dimension, i.e. 5-250 Å (Krupa & Cannon, 1996; Leyva-Ramos et al., 2005). Based on a mass/volume basis; a single continuous flat graphene plane would exhibit a surface area (top and bottom) of 2000 m^2/g; and commercial activated carbons generally have N_2 BET surface areas of 900-1200 m^2/g. This indicates that about half of all graphene planes have two surfaces exposed. These surface areas are 2-3 times higher than for granular iron media. The large surface area, high pore volume, and rigid structure of GAC render it an ideal backbone for hosting iron species or iron complexes.

3.1.2.2 Arsenic Removal by Granular Activated Carbon

A key attribute for activated carbon is its high specific surface area ranging from several hundred to around two thousand m^2/g, resulting from its porous structure. Activated carbon, either granular or powdered (GAC or PAC), is widely used as an adsorbent for water and advanced wastewater treatment. It is capable of adsorbing a wide variety of organic contaminants and heavy metals (James, 1985) and is designated as the best available technology (BAT) by the U.S. EPA for the removal of synthetic organic contaminants. The surfaces responsible for contaminant sorption are primarily internal pores with various dimensions. Use of activated carbon for water treatment is a mature technology for removal of synthetic and natural organic compounds, odor and taste, and trace metals, with numerous treatment systems in operation and a good track record. GAC adsorption is recognized as the most effective treatment technology for removing 51 of the 64 pollutants in the US EPA list of regulated organic contaminants (Pontius, 1999). Fixed-bed adsorption using GAC is most common, because of its suitable mechanical properties for water/solid separation (Schroeder, 1977). Arsenic adsorption onto virgin activated carbon is minimal, so it cannot be directly applied for arsenic treatment (Deng et al., 2005). Literature has, however, shown that the adsorption on activated carbon can be significantly increased by treatment with various iron compounds (Huang & Vane, 1989; Reed et al., 2000). It is likely that some iron compounds produced by the treatment are cross-linked to activated carbon, resulting in an enhanced arsenic sorption (Huang & Vane, 1989). Enhanced arsenic adsorption was similarly observed with copper-treated activated carbon (Manju et al., 1998) and zirconium loaded GAC (Daus et al., 2004).

3.1.2.3 Mechanisms of Arsenic Adsorption on Activated Carbon

Studies found that the arsenic adsorption on activated carbon is physical adsorption (Eguez & Cho, 1987; Reed et al., 2000). Eguez and Cho (1987) reported that the low isosteric heat of arsenic adsorption on activated charcoal, 0.75-4 kcal/mol for As(III) and 24 kcal/mol for As(V), indicated the adsorption is physical adsorption induced by Van der Waals force. Similarly, Reed et al. (2000) found the oxygen containing functional groups on activated carbon surface do not readily adsorb arsenic anions and the removal of arsenic by activated carbons is mostly attributed to physical adsorption.

However, some other studies found that arsenic adsorption on activated carbon is chemisorption (Huang & Fu, 1984; Lorenzen et al., 1995; Budinova et al., 2006). It was found that there was no correlation between adsorption capacity and specific surface area, and the oxygen functional groups played a prominent role in the process of arsenic adsorption (Huang & Fu, 1984; Lorenzen et al., 1995; Budinova et al., 2006). Lorenzen et a1. (1995) found that GAC with acidic surfaces tends to have high arsenic adsorption capacity, while Budinova et al. (2006) found that As(III) adsorption on GAC with an alkaline character is superior to GAC with acidic surfaces.

With the growing concern of arsenic in drinking water, GAC was used to remove arsenic from drinking water (Buche & Owens, 1996; Manju et al., 1998). Many studies reported that activated carbon exhibited limited arsenic adsorption capacity. Buche and Owens (1996) reported a maximum arsenic adsorption capacity of 24 µg/g and affinity of 0.00702 L/µg in a study of using GAC Hydrodarco to remove arsenic from contaminated groundwater (89 µg/L) in the city of Fresno, CA. Gu et a1. (2005) reported that GAC Darco 12x20 had a maximum arsenate adsorption capacity of 3.78 µg/g and Yang et al. (2007) found that the maximum arsenate adsorption capacity on GAC is 780 µg/g.

A few studies attempted to develop efficient and low-cost activated carbon from a variety of sources, such as agricultural by-products and other biomass materials (Budinova et al., 2006; Gupta, 2005). For instance, Budinova et al. (2006) studied the As(III) adsorption on activated carbon prepared from solvent extracted olive pulp and olive stones. They reported that the maximum As(III) adsorption capacity was 1.39 mg/ g. Although activated carbon was unable to remove arsenic effectively, once activated carbon was impregnated with iron, its arsenic adsorption capacity increased significantly (Reed et al., 2000; Gu et al., 2005; Chen et al., 2007). The methods of iron impregnation onto the surface of the activated carbon are described below.

3.1.2.4 Iron-Impregnation Methods

A number of studies found that iron impregnated activated carbon (Fe-GAC) significantly enhanced arsenic adsorption capacity (Pakula et al, 1998; Reed et a1., 2000; Gu et a1., 2005; Payne & Abdel-Fattah, 2005; Chen et al., 2007; Mondal et al., 2007; Jang et al., 2008; Hristovski et al., 2009). Though some other metals, such as silver and copper (Rajakovic, 1992), were tested for the improvement of arsenic adsorption of GAC, with consideration of cost and availability, iron is the most widely used to impregnate activated carbon for arsenic removal. The iron impregnation method falls in to four categories as follows.

3.1.2.4.1 Conventional Adsorption

Iron impregnation can be achieved through conventional adsorption process (Huang & Vane, 1989; Payne & Abdel-Fattah, 2005). Synthesis conditions, including the concentration of iron solution, iron species, nature of GAC, and reaction time, determined the amount of iron that can be impregnated on GAC.

Ferrous salts were preferred in the conventional adsorption method because of the electrostatic interaction between iron and surface of activated carbon (Huang & Vane, 1989). When pH is less than pHZpc (the pH that adsorbent has a net zero surface charge) of activated carbon, the surface of activated carbon is positively charged so that the adsorption of cationic iron ions is limited. When pH is above pHzpc, the surface of activated carbon is negatively charged so that the adsorption of cationic iron ions is favored. In this sense, high pH is favored for iron impregnation. However, ferric iron forms hydroxide precipitation at high pH; but ferrous iron is soluble at a wide pH range, that`s why it is preferred for iron impregnation in GAC using the conventional method (Huang & Vane, 1989; Payne & Abdel-Fattah, 2005). However, only a limited amount of iron can be impregnated in GAC through the conventional impregnation methods (Gu et al., 2005).

3.1.2.4.2 Iron Impregnation Followed by Chemical Modification of GAC Surface

The surface chemistry of GAC can be modified to facilitate the iron impregnation. The oxygen containing functional groups, such as carboxylic group, are considered to be responsible for iron adsorption (Pakula et al, 1998; Chen et al., 2007). It was found that oxidation of activated carbon in the liquid phase by nitric acid can increase the concentration of carboxylic acids on surface (Figueiredo et a1., 1999). Therefore, oxidation of activated carbon can increase the amount of iron impregnation in GAC. The selection of a proper oxidant is essential to increase the amount of impregnated iron. Chen et a1. (2007) investigated the performance of three combinations of oxidants, HNO_3, HNO_3/H_2SO_4, and $HNO_3/(CH_3COOH)/KMnO_4$, on oxidation of PAC (200x400) for iron impregnation and found that more iron was impregnated in PAC when stronger oxidants were used. The highest iron content of 15.4% was reported using wood-based activated carbon NORITC-Gran after HNO_3/H_2SO_4 treatment. Strong oxidation may help to increase the amount of impregnated iron in GAC. Strong oxidizing agents significantly weaken the mechanical strength of activated carbon. Chen et al. (2007) observed a high mass loss of wood-based activated carbon after acid oxidation process. Although this Fe-PAC can be prepared with iron content as high as 15.4%, it performed poorly in column tests compared with other Fe-PAC with lower iron contents.

3.1.2.4.3 In-situ Chemical Oxidation

The in-situ chemical oxidation method is the conventional adsorption method plus an in-situ oxidizing step. This method uses ferrous iron as a precursor because of its solubility at a wide range of pH. However, ferrous iron may not be stable after impregnation. The in-situ oxidizing step is to stabilize iron inside GAC through oxidation of ferrous to ferric ions. The first step is to diffuse ferrous iron into activated carbon, which is the same as the conventional adsorption process. In the second step, an oxidant is added into the mixture of ferrous iron and GAC to oxidize ferrous ion inside GAC.

Gu et al. (2005) investigated the performance of three different oxidants, oxygen, H_2O_2, and NaClO on iron impregnation through this in-situ chemical oxidation method and found that sodium hypochlorite performed the best with regard to the amount of impregnated iron.

Instead of preloading ferrous iron into GAC, Hristovski et al. (2009) preloaded oxidizing agent-potassium permanganate into GAC. Then, preloaded GAC was reacted with ferrous solution for iron impregnation. Challenges and questions were encountered with this in-situ chemical oxidation method. Whether the oxidation of ferrous iron occurred in-situ as designed is unsure because the oxidation of ferrous iron may happen in the bulk solution instead of inside GAC. According to the procedure described in the reference (Gu et al., 2005), once oxidant was added into ferrous solution, it was surrounded by ferrous bulk solution and reacted with ferrous iron immediately rather than diffusing into internal pores of GAC. Freshly formed ferric ion tends to precipitate at pH below 5. Ferric precipitates are difficult to penetrate into micro-pores of GAC because of their size. Even worse, they may block the outlets or channels on the exterior surface of GAC (Chang et al., 2010).

3.1.2.4.4 Precipitation and Evaporation

The precipitation method, also called precipitation-deposition, comprises inducing precipitation of a dissolved metal species which then deposits upon a finely powdered solid support. Conventionally, the most widely studied chemical method to prepare iron oxides has been the precipitation of iron ions from aqueous solutions of their nitrate, chloride, perchlorate, or sulfate salts (Lee et al., 1996). The precipitation of ferric ions is usually driven by thermolysis or by the addition of a base to the aqueous solution. The characteristics of the final product, i.e. oxide phase, particle size and surface area, depend highly on the precipitation conditions, especially the concentration of the iron ions, the nature of the counter-ions present, and the pH of the solutions. In the method of precipitation and evaporation, iron is impregnated on activated carbon through the precipitation of ferric iron by either pH adjustment or evaporation (Oliveira et a1., 2002; Zhang et al., 2007; Chen et al., 2007; Mondal et al., 2007; Kim et al., 2010). The common procedure is to mix activated carbon with ferric solution, adjust pH to form precipitates, and heat and dry to load iron on GAC. Ferric chloride and ferric nitrate were the two most commonly used ferric salts for iron impregnation using this method. One study attempted to use a mixture of $FeCl_3/FeSO_4$ (2:1, molar ratio) to impregnate more iron on GAC (Zhang et al., 2007). The iron hydr/oxides thus loaded into the pores of GAC can be reduced to nZVI by using a suitable reductant. The details of nZVI preparation are decribed in section 3.1.3.1.2.

3.1.3 Arsenic Removal by Iron Compounds

It has been found that iron-based materials are capable of removing arsenic from water effectively (Joshi & Chaudhuri, 1996; Wilkie & Hering, 1996; Fendorf et al., 1997; Raven et al., 1998; Driehaus et al., 1998; Appelo et al., 2002). Iron is inexpensive and widely available which makes it an attractive means to remove arsenic. Granular ferric hydroxide, hydrous ferric oxide (HFO), sulfur-modified iron, and zero-valent iron Fe(0) are common iron-based materials.

3.1.3.1 Arsenic Removal by Nano Scale Zero-valent Iron (nZVI)

Nanotechnology has revolutionized the science of controlling materials at the atomic and molecular level. Collectively, the term nano materials refer to all engineered or natural materials with a characteristic dimension below 100 nm (National Nanotechnology Initiative, 2009). Nano materials exhibit increased chemical reactivity due to the greater proportion of surface atoms, especially the more active edge and corner atoms, and distinct localized environments created by intermixing of atomic species (Mulvaney, 2001; Campbell & Parker, 2002). In environmental studies, nano materials with sizes in the range of a few to several hundred nanometers have been studied, the most well-known examples being iron oxides and alumina silicates, which have been extensively studied for their adsorptive properties for aqueous ionic species (Stumm, 1992; Morel & Hering, 1993). Zero-valent iron Fe(0) is a moderately strong reducing agent and electron donor. It reacts favorably with a large group of chemicals that have more positive electrochemical potential than iron (Gillham & O'hannesin, 1994). In the realm of environmental remediation, ZVI has been applied to the decontamination of halogenated hydrocarbons, azo dyes, munitions, nitrate, hexavalent chromium, arsenic, and heavy metals by transforming the contaminants into substances less harmful and more degradable (Matheson & Tratnyek, 1994; Johnson et al., 1996; Hundal et al., 1997; Gavaskar et al., 1998; Gu et al., 1998; Cao et al., 1999; Alowitz & Scherer, 2002; Wilkin et al., 2005). Since the early 1990s, granular ZVI has been employed in a type of engineering fixture known as permeable reactive barrier (PRB) for in situ remediation of ground water contaminated with chlorinated solvents or hexavalent chromium (Gavaskar et al., 1998; Gu et al., 1998; Wilkin et al., 2005). The effluent from a PRB typically has contaminants reduced to concentrations below the applicable USEPA regulatory levels. Several excellent review papers are available in the literature on the design, operation, and long-term assessment of PRB structures (Sacre, 1997; Gavaskar et al., 1998; Scherer et al., 2000). Nanoscale zero-valent iron (nZVI) can be regarded as an extension of zero-valent iron (ZVI) technology. Many studies found a wide range of contaminants are amenable to nZVI remediation. Pilot or large-scale field applications of nZVI have been conducted since early 2000, where nZVI was directly injected into the remediation site by gravity flow or under pressure into underground contaminant plumes (Elliott & Zhang, 2001). In this present study, an attempt has been made to combine the advantages of the nZVI and GAC by making a composite material (nZVI/GAC) that can be suitably used for dynamic column operation to treat arsenic contaminated water.

3.1.3.1.1 Preparation of nZVI

The preparation of nZVI can be categorized into two classes: top-down and bottom-up approaches. The latter entails piecing together iron atoms to form Fe(0) clusters at the nanometer scale. Typically, this is done by chemical reduction of ferrous (Fe(II)) or ferric (Fe(III)) salts (Glavee et al., 1995), or by vapor condensation in a vacuum or inert gas (Hahn, 1997). Various chemical reduction schemes have been used, among which the most widely adopted one is the borohydride reduction approach, where ferric or ferrous ions react with sodium borohydride in water under intensive mixing (Wang & Zhang, 1997). The reaction is shown in Eq. 2.1:

$$4Fe^{3+} + 3BH_4^- + 9H_2O \rightarrow 4Fe^0(s) + 3H_2BO_3^- + 12H^+ + 6H_2\,(g) \qquad (2.1)$$

This method, conducted under ambient temperature and pressure, can be routinely performed in common wet chemistry laboratories. However, the unit cost of wet chemistry synthesis is rather expensive due to the high cost of sodium borohydride and the labor required. This method is also difficult to scale up to an industrial scale due to the several separation steps involved and the large amount of wastewater produced (Li et al., 2009).

Other bottom-up approaches, such as decomposition of iron pentacarbonyl ($Fe(CO)_5$) in organic solvents, or reduction of goethite (α-FeOOH) or hematite (α-Fe_2O_3) by H_2 at high temperature, have also been reported (Capek, 2004; Nurmi et al., 2005; Majewski & Thierry, 2007). However, chemical reactions often consume expensive and toxic reagents, and produce not only nZVI but also byproducts such as $B(OH)_3$. For example, thermal decomposition of iron pentacarbonyl ($Fe(CO)_5$) generates small (10-20 nm) and uniform-sized nZVI (Suslick et al., 1991), but iron pentacarbonyl is a highly toxic reagent and thus raises critical safety concerns.

Top-down approaches start with bulk-sized iron materials, such as granular iron, and achieve size reduction through mechanical means. A precision ball-milling technique has recently been proposed, which uses stainless steel balls as the grinding media to fragment the starting iron materials into pieces less than 100 nm in diameter in approximately 3 hours. Laboratory batch experiments using such milled nZVI particles and several well-studied chlorinated contaminants confirm the milled nZVI (8-hour milling time) has slightly higher chemical reactivity over the chemically made nZVI (Li et al., 2009). Thus, precision ball-milling offers an attractive route to green manufacturing of iron nanoparticles at quantities sufficient for full-scale remediation.

3.1.3.2 Pathway of Arsenic Removal using Zero-valent Iron

Zero-valent iron can effectively remove arsenic from the aqueous phase (Farrell et al, 2001; Su & Puls, 2001; Manning et al., 2002; Kanel et al., 2005). Indeed, it is Fe(0) corrosion products rather than Fe(0) itself that remove arsenic (Leupin et al., 2005; Manning et al., 2002). As shown in Equation 3.1, Fe(0) corrodes first to form Fe(ll) as an intermediate. Then, oxidation of Fe(II) with dissolved oxygen (DO) leads to formation of iron oxides or HFO. Eventually, arsenic is adsorbed on the surface of iron oxides or HFO (Equation 3.2). As(V) removal rates depend on the continuous generation of iron oxide adsorption sites (corrosive rate). It was identified by X-ray absorption spectroscopy analysis that the iron corrosion product is a mixture of magnetite, ferric oxide, and possibly, iron hydroxides (Melitas et al., 2002).

3.1.3.3 Redox Reactions of Arsenic in the Removal Process using Zero-valent Iron

Redox reactions play an active role for the immobilization of arsenic on the surface of Fe(0). The reaction takes place between arsenic and the corrosion products of Fe(0). Studies found that As(IIl) can be oxidized to As(V) or reduced to insoluble As(0), while As(V) can be reduced to As(IIl) or As(0). Under anoxic conditions, Fe(0) can react with water to form Fe(II) and hydrogen gas. As As(V) and As(III) are stronger electron acceptors than water, thermodynamically, As(V) and As(III) can be reduced to As(0) by Fe(0) (Bang et al., 2005). Bang et al. (2005) found a fraction of As(III) was reduced to As(0) on an acid-pretreated Fe(0) under anoxic conditions.

Under anaerobic condition, As(III) oxidation to As(V) was observed. About 28% of arsenic was in the form of As(V) when As(III) was reacted with Fe(0). It was speculated that the oxidation of As(III) was due to the reaction between As(III) and carbonate green rust formed on the surface of Fe(0) (Lien & Wilkin, 2005).

Under aerobic condition, some researchers reported that As(III) was oxidized to As(V) in the process of arsenic removal using Fe(0) (Manning et al., 2002; Leupin et al., 2005). Manning et al. (2002) used X-ray Absorption Near Edge Structure (XANES and EXAFS) for ZVI powders reacted with As(III), where they proposed the oxidation of As(III) might be mediated by iron corrosion products such as magnetite/maghemite or lepidocrocite.

Leupin et al. (2005) found parallel oxidation of As(III) and corrosion-released Fe(II) by DO and subsequent adsorption on the HFO formed. They proposed a pathway of arsenic removal by Fe(0) under aerobic conditions, as shown in Equations 3.3-3.5. A reactive intermediate (RI) is formed during the oxidation of Fe(II) by DO and then this RI oxidizes As(III) to As(V). The RI can be $.O_2^-$, H_2O_2, and .OH formed in the oxidation of Fe(II) with DO; however, it is difficult to measure the intermediates directly.

$$Fe(0) \xrightarrow{Corrosion} Fe(II) \xrightarrow{Oxidation\ by\ DO} HFO \qquad (3.1)$$

$$HFO + As \xrightarrow{Adsorption} HFO - As \qquad (3.2)$$

$$Fe(0) + \ 0.5O_2 + 2H_2O \rightarrow Fe(II) + \ H_2O + 2OH^- \qquad (3.3)$$

$$Fe(II) + \ 0.25O_2 + H_2O \rightarrow Fe(III) + \ 0.5H_2O + OH^- + (RI) \qquad (3.4)$$

$$As(III) + \ RI \rightarrow As(V) \qquad (3.5)$$

Partial reduction of As(V) to As(III) was observed in the arsenic removal process using Fe(0). Su and Puls (2001) reported that the reduction of As(V) to As(III) in closed batch reactors occurred over 30-60 days and resulted a steady distribution of 73-76% As(V) and 22-25% As(III) in the solid-phase of corrosion products using X-ray photoelectron spectroscopy (XPS). Kanel et al. (2006) observed reduction of As(V) to As(III) after 90 days in a study of As(V) removal using nano Fe(0). It seems that the reduction of adsorbed As(V) in the solid phase to As(III) is a very slow process. Su and Puls (2001) did not observe the reduction of As(V) to As(III) at 5 days and Kanel et a1. (2006) did not observe the reduction of As(V) within 60 days. Reduction of As(V) to As(III) and As(0) was reported when As(V) was reacted with nZVI in 24 hours (Mauricio, 2010). Mauricio (2010) found a solid phase distribution of arsenic, as As(V)-76%, As(III)-11%, and As(0)-13%, established a fast kinetics as opposed to the previous studies. No significant change in arsenic distribution was observed even after 15 days under the same reaction conditions. Concomitant oxidation and reduction were also observed when As(III) was reacted with nZVI. Arsenic distribution on the nZVI surface was as follows: As(V)-14%, As(III)-51%, As(0)-35%. These reactions were done in anoxic conditions. Some studies reported that no reduction of As(V) occurred in the arsenic removal process using Fe(0). Manning et a1. (2002), under aerobic condition, found no reduction of As(V) to As(III) on Fe(0) and its corrosion products. Instead, they found that water was reduced (Equation 3.6) in the Fe(0) corrosion process and the pH of solution increased. Farrell et al. (2001), experimenting with opened batch reactors, found no measurable reduction of As(V) to As(III) on Fe(0), and all arsenic associated with the Fe(0) surface was As(V).

$$Fe(0) + 2H_2O \rightarrow Fe(II) + H_2 + 2OH^- \qquad (3.6)$$

3.1.3.4 Adsorption Mechanisms of Arsenic on Iron

The mechanism of arsenic adsorption through surface complexation with iron (hydr)oxides is documented (Goldberg & Johnston, 2001; Manning et al., 2002; Kanel et al., 2005). A number of surface complexation models (SCMs) were developed to interpret the interaction between ionic adsorbate and charged surface of adsorbent, including diffuse double-layer model, constant capacitance model, and triple-layer model (Drever, 1997). As to the double-layer model, the double-layer refers to two parallel layers of charge surrounding solid surface when it is placed into a liquid. The first layer, the surface charge (either positive or negative), comprises ions adsorbed directly onto the solid due to a host of chemical interactions. The second layer is composed of ions attracted to the surface charge via the columbic force, electrically screening the first layer. This second layer is loosely associated with the solid, because it is made of free ions, which move in the liquid under the influence of electric attraction and thermal motion rather than being firmly anchored. It is thus called the diffuse layer. To better understand the surface complexation between iron and arsenic species, a brief introduction of triple-layer model is presented below.

The triple layer model is essentially an extended Stern model with the compact double layer split into two parts-inner Helmholtz and outer Helmholtz plane. According to the triple-layer model (Yates et al., 1974; Yates, 1975; Davis et al., 1978), protons and hydroxide ions adsorb directly at the surface or O-plane (Fig. 3.l), resulting in surface charge, σ_o (Coulombs.m^{-2}). It is assumed that the ions, M^+ and L^- , of the ML-th electrolyte adsorb at the β-plane, resulting in charge, σ_β (Coulombs.m^{-2}). To neutralize the overall charge, (σ_o+σ_β), there is a diffuse layer of counter ions in the aqueous solution that has a closest distance of approach defined as the d-plane. Associated with each plane of charge are corresponding electric potentials (Volts) ψ_o, ψ_β, and ψ_d. These three layers of charge and potential are modeled as a parallel-plate capacitor of capacitances (Farads.m^{-2}) C_1, and C_2 (Fig. 3.1).

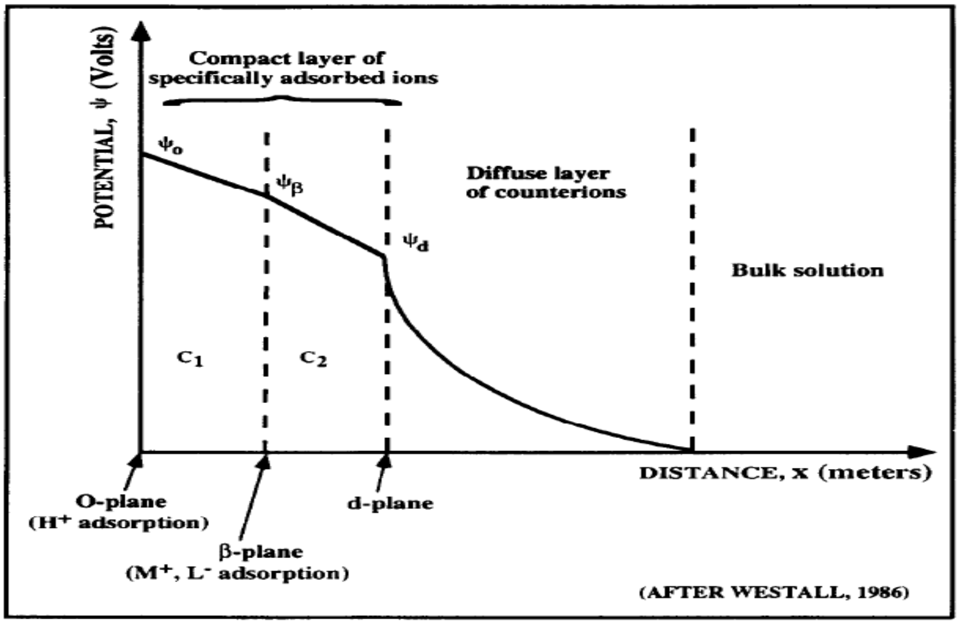

Figure 3.1 Schematic representation of potential, ψ, as a function of distance, x, from the surface according to the triple-layer mode1 (Davis et al., 1978). Protons and hydroxide ions adsorb at the surface or O-plane; electrolyte metal ion (M^+) and ligand (L^-) are assumed to adsorb at the β-plane. Closest distance of approach of counter ions is defined by the d-plane. The three layers of potential separated by intervening regions of dielectric constant ε_1 and ε_2 are modeled as a parallel plate capacitor of capacitances, C_1, C_2 (after Westall, 1986).

Adsorption is assumed to occur at specific sites on the mineral surface. All sites are considered energetically equivalent; that is, the adsorbing species does not prefer any one site to any other. It is further assumed that adsorption at the surface can be described by chemical equilibria analogous to aqueous complexation reactions.

When adsorbates are presumed to bind directly to a surface oxide ion (0 plane), they must lose the water of hydration. These types of surface complexes are relatively strong and are referred to as inner-sphere complexes. Some ions are also presumed to bind to the surface via chemical bonds (β plane), but to retain all their waters of hydration. They are therefore separated from the surface by a water molecule and form weaker complexes, referred to as outer-sphere complexes (Drever, 1997).

3.1.3.5 Surface complexation between iron and arsenic

Outer- and inner-sphere surface complexes can, and often do, occur simultaneously (Sparks, 2003) with one complex formed being predominant. Many studies found that arsenic forms inner-sphere surface complexation with iron oxides or iron hydroxides (Goldberg & Johnston, 2001; Farrel et al., 2001; Manning et al., 2002; Kanel et al., 2005). As shown in Figure 3.2, inner-sphere surface complexations include three possible complexes, monodentate mononuclear, bidentate mononuclear, and bidentate binuclear (Fendorf et al., 1997). X-Ray absorption spectroscopy was used to investigate the surface complexation between arsenic and iron. The interatomic distance between arsenic and iron in the inner-sphere surface complexation was measured as 0.360 nm, 0.325 nm, and 0.283-0.285 nm for monodentate mononuclear, bidentate binuclear, and bidentate mononuclear, respectively (Fendorf et al., 1997; Manning et al, 1998; Sherman & Randall, 2003). Although any of these three complexes may form in arsenic adsorption on iron-based materials, bidentate binuclear inner-sphere surface complexation was found to be the dominant type (Fendorf et al., 1997; Grossl et al., 1997; Manning et al., 1998; Farrell et al., 2001; Sherman & Randall, 2003). Fendorf et al. (1997) reported that arsenic developed all three types of surface complexes on goethite (α-FeOOH) while bidentate binuclear surface complexation dominated at high arsenate loading. Sherman and Randall (2003) explained the surface complexation of As(V) on Fe hydroxides through an energy viewpoint. They explained that a bidentate binuclear surface complex is more favored than bidentate mononuclear and the monodentate mononuclear surface complexation is unstable. Studies on arsenic adsorption onto goethite (pH 5.5, 6, 8, and 9), and ferric oxide (pH 5 and 8) observed that the surface complex formed was inner sphere, either bidentate binuclear or monodentate (Sparks, 2003). Arsenate adsorption mechanism studies have also been conducted with hydrated iron oxides (Roddick-Lanzilotta et al. 2002) and granular ferric hydroxide (Guan et al. 2008). These investigators found inner sphere surface complex formation. Arsenate adsorption on crystal γ-Fe_2O_3 nanoparticles showed formation of inner-sphere surface complex. FTIR-spectra analysis revealed that bidentate binuclear complex, $(FeO)_2AsO_2$, was formed.

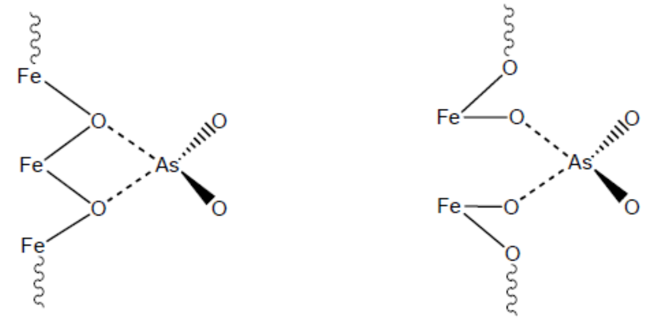

Bidentate Mononuclear

Bidentate Binuclear

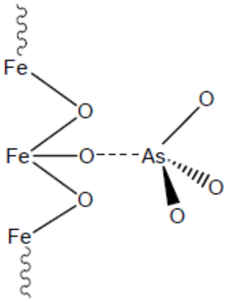

Monodentate

Figure 3.2 Possible configurations of the arsenate iron oxide complexes (adapted from Fendorf et al., 1997).

3.1.4 Adsorption

Adsorption is one of the earliest technologies developed for separation and purification. It involves the separation of undesirable compounds from the liquid phase, the binding of components to a surface, and their accumulation at the surface of the adsorptive media. Binding by chemical and physical forces are termed as chemisorption (characteristic of covalent bonding) and physisorption (characteristic of weak van der Waals forces) respectively (Faust & Aly, 1987). Adsorption is one of the suitable technologies that needs less expertise to operate and maintain. Two main characteristics of any adsorption process are adsorption equilibria (i.e. adsorption isotherm) and the rate of adsorption (i.e. adsorption kinetics). These aspects are discussed below.

3.1.4.1 Adsorption Isotherm (Adsorption Equilibria)

The distribution of solute (adsorbate) between the liquid and the solid phase (adsorbent) at equilibrium condition and at a specified temperature is called an adsorption isotherm. It is a mass transfer process from the liquid to the solid phase. The adsorption isotherm is graphically represented by plotting the experimental data in terms of adsorption density versus the equilibrium concentration. The experimental data are also fitted with the isotherm model to find out the realistic information regarding the binding constant, adsorption density, and the maximum adsorption capacity. For single-solute adsorption, the Freundlich and the Langmuir are the most common isotherm models (LeVan, 1996; Snoeyink & Summers, 1999).

The Freundlich adsorption isotherm is an empirical equation developed based on the assumption that the adsorbent has a heterogeneous surface composed of different classes of adsorption sites. The equation is expressed as (Freundlich, 1906):

$$q_e = K_F C_e^{\frac{1}{n}} \qquad (3.7)$$

The linear form of equation 3.7 can be written as:

$$\ln q_e = 1/n \ln C_e + \ln K_F \qquad (3.8)$$

Where, q denotes the sorption of sorbate per unit mass of the sorbent (µg/g), C_e is the equilibrium sorbate concentration in the liquid (µg/L), K_F and 1/n are constants for a given system; 1/n is unitless, and the unit of K_F is determined by the units of q_e and C_e. K_F is the equilibrium constant indicative of adsorption capacity; the greater the value of K_F, the greater the adsorption capacity; 'n' is the adsorption equilibrium constant whose reciprocal (1/n) is indicative of adsorption intensity. The reciprocal of 'n' is called the heterogeneity factor, and its value ranges from 0 to 1; the more heterogeneous the surface, the closer the 1/n value is to 0 (Al-Duri & McKay, 1995).

The Langmuir isotherm equation is based on the assumption of a structurally homogeneous sorbent where all sorption sites are identical and energetically equivalent. Theoretically, the sorbent has a finite capacity for the sorbate. Therefore, when a saturation value is reached no further sorption can take place. The Langmuir isotherm is expressed as the following form (Langmuir, 1918).

$$q = \frac{q_{\max} bC_e}{1 + bC_e} \quad \text{or} \quad \frac{C_e}{q} = \frac{C_e}{q_{\max}} + \frac{1}{bq_{\max}} \qquad (3.9)$$

Where,

q = Amount of sorbate adsorbed per unit mass of sorbent, (µg/g)

q_{max} = Maximum sorption capacity of the sorbent, (µg/g)

C_e = Equilibrium sorbate concentration in the liquid phase (µg/L)

b = Adsorption equilibrium constant ($k_{adsorption}/k_{desorption}$), indicates the affinity of adsorbent for adsorbate.

Hall et al. (1966) showed that the Langmuir constant, b can be expressed in terms of an equilibrium parameter known as a separation factor (R) defined as follows:

$$R = \frac{1}{1 + bC_i} \tag{3.10}$$

When,

$R > 1$: Unfavorable adsorption

$R = 1$: Linear adsorption

$0 < R < 1$: Favorable adsorption

$R = 0$: Irreversible adsorption.

3.1.4.2 Adsorption Kinetics

The rate of adsorption is one of the most important factors in determining the efficiency of an adsorption system of which the size and efficiency of the water treatment unit depends. To evaluate the rate of adsorption of the adsorptive material four reaction kinetic models are widely used which are described here.

The first order rate equation based on the solute concentration in the aqueous phase can be expressed as (Benefield et al., 1982):

$$-\frac{dC_t}{dt} = k_1 C_t \tag{3.11}$$

Rearranging equation 3.11 and integrating within the boundary conditions $t = 0$ to t and $C_t = C_0$ to C_t, gives the linearized form as:

$$\ln C_t = \ln C_0 - k_1 t \tag{3.12}$$

Where,

C_0 = Initial sorbate (As) concentration in the liquid phase (µg/L)

C_t = Sorbate (As) concentration in the liquid phase at any time t (µg/L)

k_1 = First-order rate constant (/min)

The pseudo-first order kinetic model based on the sorption capacity of the solid phase can be represented as (Lagergren, 1898):

$$\frac{dq_t}{dt} = k_{s1}(q_e - q_t) \qquad (3.13)$$

Integrating within the boundary conditions t = 0 to t and q_t = 0 to q_t equation 3.13 gives the linearized form as:

$$\ln (q_e - q_t) = \ln q_e - k_{s1}t \qquad (3.14)$$

Where,

q_e = Equilibrium sorption capacity of the sorbent (µg/g)

q_t = Sorption capacity of the sorbent at any time t (µg/g)

k_{s1} = Pseudo-first-order rate constant (/min)

According to Ho and Mckay (2000) the second order kinetic model can be expressed as:

$$-\frac{dC_t}{dt} = k_2 C_t^2 \qquad (3.15)$$

Rearranging and integrating equation 3.15 within the boundary conditions t = 0 to t and $C_t = C_0$ to C_t, gives the linearized form as:

$$\frac{1}{C_t} - \frac{1}{C_0} = k_2 t \qquad (3.16)$$

Where,

k_2 = Second-order rate constant (L/µg.min)

The pseudo-second order reaction kinetic model based on the equilibrium sorption capacity can be expressed as (Ho & Mckay, 2000):

$$\frac{dq_t}{dt} = k(q_e - q_t)^2 \qquad (3.17)$$

Rearranging and integrating equation 3.17 within the boundary conditions t = 0 to t and $q_t = q_0$ to q_t, gives the linearized form as:

$$\frac{t}{q_t} = \frac{1}{kq_e^2} + \frac{t}{q_e} \qquad (3.18)$$

Putting $h = kq_e^2$ in equation 3.18 we get,

$$\frac{t}{q_t} = \frac{1}{h} + \frac{1}{q_e}t \qquad (3.19)$$

Where,

h = Initial sorption rate (µg/g.min)

k = Pseudo-second-order rate constant (g/µg.min)

3.2 Arsenic Removal Technologies: a Comparative Study

It is crucial to choose a particular method based on many factors that contribute to the technical feasibility and economic viability. A comparison of commonly used processes is summarized here. Ion exchange, especially using anion exchange resins, is suggested at lower sulfate concentrations for removing arsenate (US EPA, 2000). The US EPA suggested 50 mg/L as an appropriate upper limit for sulfate concentration in anion exchange for removing arsenic. Ion exchange processes is selective of co-existing ions. The co-existing ions were ranked in order of selectivity for strong base anion (SBA) exchange resins: $SO_4^{2-} > NO_3^- > HAsO_4^{2-} > NO_2^- > Cl^- > H_2AsO_4^- > HCO_3^- >> Si(OH)_4, H_3AsO_4$ (Ghurye et al., 1999). It was found that sulfates and nitrates were more readily removed via anion exchange than arsenate. Adsorption by activated alumina (AA) is very pH sensitive and it has a low regeneration rate of 50-70% (USEPA, 2001b). Activated alumina is also highly selective, favoring arsenate over arsenite (Jang et al., 2006). AA has been found to be less effective for arsenic removal in the presence of chloride, fluoride, phosphate and sulfate (Pal, 2001). Oxidation/filtration is particularly effective for waters containing lower concentrations of arsenic and higher concentrations of iron (Subramanian et al., 1997). Co-precipitation techniques such as alum or iron coagulation and lime softening are commonly used for arsenic removal in large-scale treatment plants and produce a wet bulky material. Precipitation followed by coagulation is usually most effective when there is a high concentration of arsenic compounds in the water. Low concentrations of arsenic contamination in large volumes of water will greatly increase the cost of this technique due to high amounts of coagulants and sludge produced. To remove arsenic from water efficiently, the complete oxidation of arsenite to arsenate is needed before co-precipitation (Leist et al., 2000). Reverse osmosis (RO) technique might be reliable and meet the regulation limit of arsenic, but it may not be suitable in water-scarce regions because of low water recovery rates (75-85%) and high cost (Chen et al., 1999). In addition, since the alkalinity and hardness could be removed by reverse osmosis, the water would require a post-treatment to prevent corrosion problems and restore minerals back into the water. Electrodialysis is a type of membrane process. The method is expensive and it has low water recovery rate. It is more effective in removing arsenate than arsenite (Kartinen & Martin, 1995). Adsorption by modified GAC is simple and usually inexpensive. It can simultaneously remove arsenic and organic contaminants (Chen et al., 2007; Hristovski et al., 2009). Moreover, the liquid/solid separation is easy for solid disposal.

Factors that affect the efficiency of an adsorption process include media characteristics, solution characteristics, and design parameters. Media characteristics of concern are the particle size, surface area, surface chemistry, and pore size distribution. Solution characteristics include adsorbate concentration, pH, redox conditions, temperature, dissolved organic and inorganic constituents, and microbial activity. Design parameters that affect adsorption efficiency include contact time, surface loading, and design flow (Aragon, 2004). The optimization of these parameters along with the use of an effective adsorptive media can meet the maximum contaminant level (MCL) of total arsenic in drinking water.

Chapter 4

Rapid Small Scale Column Test (RSSCT)

4.1 Rapid Small Scale Column Test

The selection of appropriate adsorptive media requires long-term bench-scale and pilot-scale studies to generate performance data. To determine ideal water quality conditions for optimal treatment performance, it requires a substantial amount of time, months up to years. Since time is a critical constraint, new methodologies have been developed to reduce the amount of time required to predict the performance of full-scale treatment systems using data collected from bench-scale and pilot-scale studies. Preliminary studies have shown that the rapid small-scale column test (RSSCT) method, initially designed for determining the performance of granular activated carbon (GAC), has the potential to effectively and accurately predict the performance of a full-scale adsorption treatment system (Westerhoff et al., 2005). Rapid small-scale column tests (RSSCTs) are continuous flow column tests conducted at a laboratory scale. In the RSSCT, a small column loaded with an adsorbent ground to small particle sizes is used to simulate the performance of a pilot or a full-scale system. Due to its small size, the RSSCT requires a fraction of the time and water volume compared to pilot columns. By selecting the proper particle size, hydraulic loading, and empty bed contact time (EBCT) of the small-scale system, the breakthrough curve of RSSCTs can reasonably predict those of a full-scale column (Summers et al., 1995).

Crittenden et al. (1991) summarized the results of 22 studies in which the RSSCT method was used to correlate the performance of laboratory columns to larger activated carbon adsorption columns. These studies involved removal of organics, ranging from weakly adsorbing chlorinated aliphatic hydrocarbons to strongly adsorbing pesticides. RSSCT was also used to model arsenic removal in iron-based adsorbent columns (Badruzzaman & Westerhoff, 2005; Sperlich et al., 2005; Vaughan et al., 2007).

4.2 Mass Transfer Models

The theory behind the RSSCT procedure is based on the mass transfer processes and kinetic phenomenon associated with adsorption. Mathematical mass transfer models are used to estimate adsorbent usage rates, plan the scope of RSSCT and pilot plant studies, interpret RSSCT and pilot plant results, and to maintain perfect similarity between the performance of adsorbers in order to predict the optimum full-scale process design (Hand et al., 1997; Crittenden et al., 1986). The RSSCT procedure for modeling the performance of GAC columns is based on mathematical models of the adsorption process developed primarily by Crittenden and co-workers (1987).

Three conditions associated with the governing equations in the mass transfer models must be met in order for a small-scale process to give similar operating data to that of a full-scale process. These conditions are: (1) the boundary conditions for both large and small scale processes must occur at the same dimensionless coordinate values in the dimensionless differential equations, (2) the dimensionless parameters in the dimensionless equations must be equal for both large and small scale, and (3) there must be no change in adsorption mechanism with a change in process size (Crittenden et al., 1986).

A number of mathematical models for fixed-bed column adsorption processes have been proposed. Two of them are most frequently used to model adsorption columns, the HSDM and the DFPSDM. They differ in how they handle intraparticle mass transport and whether they include axial dispersion for flow down the column. The dispersed flow pore and surface diffusion model

(DFPSDM), includes both pore diffusion and surface diffusion, as well as axial dispersion. However, Crittenden et al. (1987) noted that under many conditions these constraints can be relaxed and simpler models can be used. The homogeneous surface diffusion model (HSDM) considers surface diffusion while neglecting pore diffusion and axial dispersion.

The transport of arsenic onto porous adsorbent is considered intraparticle diffusion limited. Intraparticle diffusion occurs either within the pore space (Dp) or along the adsorbent surface within the pores (Ds). Surface diffusivity has been established as dominating transport mechanisms for organic and/ inorganic adsorption onto porous adsorbents (Komiyama & Smith, 1974; Noll et al., 1992). The mass transport models applied for metal adsorption onto porous hydrous ferric oxides demonstrate that pore diffusion accounted for only 3% of total adsorption sites (Axe & Anderson, 1997). So it can be assumed that the internal mass transfer is governed by surface diffusion only and is modeled using the Homogenous Surface Diffusion Model (HSDM) (Hand et al., 1983; Sontheimer et al., 1988).

4.2.1 Homogeneous Surface Diffusion Model (HSDM)

The HSDM has been successfully used to predict the performance of activated carbon fixed-bed (Crittenden and Weber, 1978a; b; Sontheimer et al., 1988) and was also used to model arsenic removal in iron-based adsorbent columns (Sperlich et al., 2005; Vaughan et al., 2007). The model mathematically correlates the different ways of mass transfer in the adsorbents for example by means of advection, dispersion, film diffusion, pore and surface diffusion.

Two partial differential equations (PDE) are used to describe the homogeneous surface diffusion model (HSDM); they are for the mass transport through the adsorbents (filter equation) and into the adsorbent grain (intraparticle equation). For the HSDM model to be valid, some assumptions are made: plug-flow conditions in the bed, linear driving liquid-phase mass transfer, solid phase mass transfer only by surface diffusion, constant hydraulic loading rate and diffusion coefficients, spherical adsorbent grains, and the use of the Freundlich isotherm to describe the adsorption equilibrium.

In HSDM the fixed bed adsorbent is considered as a combination of multiple layers of infinitesimal elements. The mass balance over such an infinitesimal element of the filter bed leads to equation (4.1), where the first term represents the mass in the void fraction (pores), the second term reflects solute entering and exiting the element by advective transport, and the last term represents the sink, i.e., the mass of solute adsorbed by the adsorbent grains:

$$\varepsilon \frac{\partial c}{\partial t} + v \frac{\partial c}{\partial z} + 3(1 - \varepsilon) \frac{k_f}{r_p} (c - c^*) = 0 \qquad (4.1)$$

where ε is the bed porosity, ν is the superficial velocity (cm/s), k_f is the film transfer coefficient (cm/s), r_p is the adsorbent radius (cm), c is the liquid-phase concentration (μg/L), and c* is the liquid-phase concentration at the exterior adsorbent surface.

Intraparticle transport is described according to Fick's second law and is given in radial coordinates by

$$\frac{\partial q}{\partial t} = D_s \left(\frac{\partial^2 q}{\partial r^2} + \frac{2 \partial q}{r \partial r} \right) \qquad (4.2)$$

where D_s is the surface diffusion coefficient (cm^2/s), q is the solid phase concentration (μg/g), and r is the radial coordinate (cm).

Equations (4.1) and (4.2) can be transformed into a dimensionless form by introducing X, Y, Z, R, and T, dimensionless variables for the liquid-phase and solid-phase concentration, the axial position in the filter, the radial position in the adsorbent grain, and the time, respectively. The resulting dimensionless PDE for the fixed-bed filter is

$$\frac{1}{D_g}\frac{\partial X}{\partial T}+\frac{\partial X}{\partial Z}+3\,St(X-X^{*})=0, \quad (4.3)$$

where St is the dimensionless modified Stanton number, St= $k_f m/r_p\rho_p Q$, and Dg is the dimensionless solute distribution parameter, Dg= $\rho_B q_e/\varepsilon c_0$, X is the liquid-phase concentration, X = c/c_0, X* is the liquid-phase concentration at exterior adsorbent surface, dimensionless time coordinate, T = t/(EBCTεDg), Z is the axial coordinate, Z = z/L.

As an initial condition, the concentration at the beginning of operation is zero:

$$X_{T=0,Z}=0 \quad (4.4)$$

A constant influent concentration serves as a boundary condition:

$$X_{T,Z=0}=1 \quad (4.5)$$

The dimensionless intraparticle PDE is written as:

$$\frac{\partial Y}{\partial T}=\frac{St}{Bi}\left(\frac{\partial^2 Y}{\partial R^2}+\frac{2\partial Y}{R\partial R}\right), \quad (4.6)$$

where Bi is the dimensionless Biot number, Bi= $k_f r_p C_0/D_s\rho_p q_e$, Y is the solid-phase concentration, Y= q/q_e, and R is the dimensionless radial coordinate, R = r/r_p.

Initially the solid-phase concentration is zero:

$$Y_{T=0,Z,R}=0 \quad (4.7)$$

As there is no flux at the particle center, the boundary condition is:

$$\left.\frac{\partial Y}{\partial R}\right|_{R=0}=0 \quad (4.8)$$

At the exterior adsorbent grain surface, the mass transported into the grain equals the mass transported through the stagnant liquid film. The resulting boundary condition for the particle surface is

$$\left.\frac{\partial Y}{\partial R}\right|_{R=1} = Bi(X - X^*), \tag{4.9}$$

which includes the description of the adsorption equilibrium by the Freundlich (1906) equation:

$$Y_{R=1} = X^{*\,1/n}, \tag{4.10}$$

where 1/n is the dimensionless Freundlich exponent.

4.2.1.1 Numerical Solutions to the HSDM

Solutions to the HSDM for batch reactor systems are provided so that surface diffusion coefficients, which are required for fixed-bed predictions, can be determined by comparing these solutions to batch reactor data. Two methods for the solution of HSDM developed by Hand et al. (1983, 1984) include (l) user-oriented approximate solutions and (2) numerical solutions. The user-oriented solutions to the HSDM have many limitations and constraints (Hand, 1983). For example, the final equilibrium concentration from the rate study must fall near 50% of the initial concentration, the value of the Freundlich isotherm parameter 1/n must be known to the nearest tenth, the Biot number must be over a certain number depending on 1/n, and the dimensionless concentrations are only valid within a specific range. Development of computer programs for the numerical solutions provided fewer constraints on the input (Friedman, 1984; Hand, 1984; Sperlich, 2008). The software FAST (Fixed-bed Adsorption Simulation Tool) used in this study is a numerical solution, based on a finite differences method, to the PDEs for the HSDM; the details can be found elsewhere (Sperlich et al., 2008). The resulting explicit calculation scheme for the dimensionless liquid-phase and solid-phase concentrations are shown in Eq. (4.11) and (4.12) respectively:

$$X_{i+1,j} = X_{i,j} - \alpha[X_{i,j} - X_{i,j-1}] - \beta[X_{i,j} - X^*_{i,j}] \tag{4.11}$$

$$Y_{i+1,k} = Y_{i,k} + \gamma \left[\left(1 + \frac{1}{R}\right) Y_{i,k+1} - 2Y_{i,k} + \left(1 - \frac{1}{R}\right) Y_{i,k-1} \right], \qquad (4.12)$$

where α is the Courant number of filter PDE 4.3, β is the numerical stability number of filter PDE 4.3, and γ is the Courant number of intraparticle PDE 4.6. Mathematically,

$\alpha = D_g \Delta T / \Delta Z$, $\beta = 3\, St D_g \Delta T$, and $\gamma = Ed \Delta T / \Delta R^2$

where D_g is the solute distribution parameter, $D_g = \rho_B q_e / \varepsilon c_0$, Ed is the diffusivity modulus, Ed = St/Bi, ΔT is the discretization grid width for dimensionless time coordinate, ΔZ is the discretization grid width for dimensionless axial coordinate, and ΔR is the discretization grid width for dimensionless radial coordinate.

To guarantee the stability and consistency of the numerical solution, the following criteria have to be met: $\alpha < 1.0$, $\beta < 0.3$, and $\gamma < 0.5$. The output data (bed volume vs. C/C_o) provided by the software were used to generate the breakthrough curves (BTC) which were compared to the experimental values.

4.2.1.1.1 Parameter Estimation (HSDM Parameters)

To predict breakthrough of fixed-bed systems, the model input parameters have to be known. These values are either easily accessible (outer model parameters) or must be determined indirectly from accordingly designed experiments (inner model parameters). Since the parameters do not act independently to influence adsorber performance, they can be summarized in dimensionless groups (essential model parameters) to reduce the number of influencing parameters.

4.2.1.1.1.1 Outer Model Parameters

Outer model parameters, in contrast to inner model parameters, are usually known or can be determined easily. They represent operational conditions and/or adsorber geometry. Outer model parameters include the grain size, grain density, volumetric flow rate, influent concentration, adsorbent mass, and density of the adsorber bed. Although these parameters can be measured easily, some of them are not constant over the adsorber column. Hence, average values have to be used.

4.2.1.1.1.2 Inner Model Parameters

Inner model parameters cannot be easily measured but have to be determined in especially designed experiments. They can also be determined by empirical correlations from the literature or derived from column data. Adsorption equilibrium parameters, Freundlich 1/n and K_F, the liquid-phase mass transfer coefficient k_f, and the surface diffusion coefficient D_s fall in this category. Adsorption equilibrium parameters were derived from batch equilibrium isotherms data as described by the Freundlich (1906) equation. Film diffusion coefficients were estimated by the correlation provided by Wakao & Funazkri (1978). Surface diffusion coefficient was found from DCBR test. A best-fit D_s was determined by comparing HSDM simulations to experimental data.

4.2.1.1.1.3 Essential Model Parameters/dimensionless numbers

The influence of the dimensionless groups on the form of the BTC has been thoroughly investigated (Sontheimer et al., 1988). Hand et al. (1984) successfully applied the HSDM for over 100 adsorbate-adsorbent (organic pollutant-activated carbon) systems. The 10 inner and outer input parameters defining the shape of the BTC can be transformed into four remaining dimensionless groups, Bi, St, Dg, and 1/n. Therefore, these parameters are decisive when discussing model attributes or shortcomings.

4.2.1.2 Determination of Surface Diffusion Coefficient

The intraparticle diffusion coefficient was determined based on the experiment using differential column batch reactor (DCBR) as described by Sontheimer et al. (1988). In a DCBR, the adsorbate solution is passed through a thin layer of adsorbent packed in a small column, and the effluent is circulated back to the solution. The layer of the adsorbent needs to be thin enough so that the concentration gradient in the bed is very small. Under this condition, the change in concentration can be modeled as in a completely mixed batch reactor (CMBR). The film transfer coefficient k_f can be determined using empirical correlations (Wakao & Funazkri, 1978). This k_f value is then fed to the HSDM and only D_s is determined from fitting the adsorbate concentration profile.

4.3 Development of Scaling Relationships for RSSCT

The scaling equations for RSSCT are derived from the dimensionless groups in the Pore-Surface Diffusion Model (PSDM), an extended form of the HSDM to include pore diffusion. When pore diffusion is not important compared to surface diffusion, it can be neglected and HSDM is assumed.

Mass transfer models lead to the development of dimensionless parameters, which are equated to define similitude between the small and large-scale columns. Subsequent to determining similitude, the RSSCTs can be scaled up to evaluate the performance of full-scale treatment systems. Similarity of operation between small and large-scale adsorbers is assured by properly selecting the particle size, hydraulic loading, and EBCT for the RSSCT. Theoretical similarity can be achieved if the large and small systems have equal equilibrium capacities, bulk densities, operating temperatures, and influent concentrations. Crittenden et al. (1986) found that the adsorbent particle size determines the relationships between hydraulic loading and EBCT for small and full-scale columns. The scaling equations are also based upon the surface diffusion coefficient's dependence on particle size. Crittenden et al. (1986, 1987, 1991) developed scaling equations for both constant and non-constant diffusivities with respect to particle size. The scaling laws ensure that the RSSCT and the full-scale system will have identical breakthrough profiles. By equating the modulus of surface diffusivity, Ed, a relationship between EBCTs for small- and large-scale columns is determined:

$$\frac{EBCT_{SC}}{EBCT_{LC}} = \left(\frac{R_{SC}}{R_{LC}}\right)^2 \frac{D_{s,LC}}{D_{s,SC}} = \frac{t_{SC}}{t_{LC}} \qquad (4.13)$$

The dependence of the surface diffusion coefficient on particle radius is defined by the diffusivity factor, x, as follows:

$$\frac{D_{s,SC}}{D_{s,LC}} = \left(\frac{R_{SC}}{R_{LC}}\right)^X \qquad (4.14)$$

Combining equations (4.13) and (4.14) yields:

$$\frac{EBCT_{SC}}{EBCT_{LC}} = \left(\frac{R_{SC}}{R_{LC}}\right)^{2-X} = \frac{t_{SC}}{t_{LC}} \qquad (4.15)$$

where $EBCT_{SC}$ and $EBCT_{LC}$ are EBCTs for the small and large columns, respectively; R_{SC} and R_{LC} are GAC particle radii for the small and large columns, respectively; t_{SC} and t_{LC} are operating times for the small and large columns, respectively. The above relationship is valid when either pore diffusion or surface diffusion (or both) controls intraparticle mass transfer. When the diffusivity is independent of particle size (i.e. constant diffusivity-CD), then X= 0 and Eq. 4.15 becomes:

$$\frac{EBCT_{SC}}{EBCT_{LC}} = \left(\frac{R_{SC}}{R_{LC}}\right)^2 = \frac{t_{SC}}{t_{LC}} \qquad (4.16)$$

When diffusivity is linearly dependent of particle size (i.e. proportional diffusivity-PD), then X= 1 and Eq. 4.15 becomes:

$$\frac{EBCT_{SC}}{EBCT_{LC}} = \left(\frac{R_{SC}}{R_{LC}}\right) = \frac{t_{SC}}{t_{LC}} \qquad (4.17)$$

Considering similar breakthrough spreading for small and large columns, the Reynolds number of a small column would be equal to that of a large column along with other dimensionless parameters such as Stanton number (St) and Peclet number (Pe). Consequently, the following operational design equation for the RSSCT can be developed:

$$\frac{v_{SC}}{v_{LC}} = \frac{R_{LC}}{R_{SC}} \qquad (4.18)$$

where v_{SC} and v_{LC} are hydraulic loading rates of the small and large columns respectively. In the PD-RSSCT, the above equation can be also used for selecting the hydraulic loading. However, this may lead to a small column with a long bed and high head loss. The hydraulic loading in the small column can be reduced by the ratio of the product of the Reynolds and Schmidt number in equation 4.18 as long as dispersion is not the main mass transport mechanism in the column. Berrigan (1985) showed that dispersion was not important if the product of the Reynolds and Schmidt numbers was in the mechanical dispersion range of 200-200,000. The modified form of equation 4.18 can be expressed as:

$$\frac{v_{SC}}{v_{LC}} = \frac{R_{LC}}{R_{SC}} * \frac{Re_{SC}.Sc}{Re_{LC}.Sc} \qquad (4.19)$$

4.3.1 An Example of using Scaling relationship/ Scale up

A 1 min EBCT was mainly used for the media of 100×140 (median: 125 μm) and 80×140 (median: 136 μm). In accordance with the proportional diffusivity similitude (Parette and Cannon 2005), the mini-column tests with 1 min EBCT (100×140 mesh) simulated an EBCT of 8.4 minutes for US mesh #12×40 (1700-425 μm; median 1060 μm) full-scale media, or 3.5 minutes for US mesh #20×50 (850-300 μm; median 440 μm).

Table 4.1 Example of scaling relationship

Parameters	Small column	Large/Full-scale column
Particle diameter, d_p, mm	0.165	0.725 (12x30 mesh)
EBCT, min	1.0	19.31 for CD→ using equation 4.16 4.39 for PD → using equation 4.17

After determining the EBCT, the velocity in the large column, v_{LC} is calculated by using equation 4.19.

The height of the full-scale column, h_{LC} is determined as:

$h_{LC} = v_{LC} \text{ x } EBCT_{LC}$

The bed volume, BV_{LC} required is:

$BV_{LC} = h_{LC}\ X\ \frac{\pi}{4}(d_{id})^2$, where d_{id} is the internal diameter of the full-scale column.

The flow rate for the full-scale column is then calculated as:

$$Q_{LC} = v_{LC}\ X\ \frac{\pi}{4}(d_{id})^2$$

A single RSSCT simulates one set of full-scale operating conditions from which it can be completely designed using Equations 4.13 to 4.19. For full-scale operation diffusivity factor plays an important role. The diffusivity factor is determined from the DCBRs with different particle sizes. Once the diffusivity factor is found the pilot scale column can be run to validate the RSSCT data and subsequently the full-scale column can be operated.

Chapter 5

Materials and Methods

5.1 Chemicals

All chemicals were of reagent grade and the solutions were prepared in Milli-Q water (Q-H_2O, Millipore Corp.). Sodium arsenate ($Na_2HAsO_4.7H_2O$,99%) and arsenic trioxide (As_2O_3, 99%) were bought from Anachemia Science (Quebec, Canada). All other chemicals including sodium borohydride ($NaBH_4$) and ferric nitrate [$Fe(NO_3)_3.9H_2O$] were purchased from Fisher Scientific (Ontario, Canada).

5.2 Synthesis of nZVI/GAC

Acid washed granular activated carbon (GAC 12X30, Siemens Water Technology Inc.) derived from coconut shells was prepared as the support material for nZVI (Choi et al., 2008) with modification. The GAC was washed with deionized water and dried at 110°C overnight. Iron was incorporated into the GAC via an incipient wetness impregnation method, where 20.61 g of $Fe(NO_3)_3.9H_2O$ (Fisher) was melted at 55-60°C with a small quantity of water (30 mL) and then mixed with 15 g of GAC for 10 min. For total incorporation of Fe to the GAC, the slurry was shaken at room temperature for 4 h and then dried in a hot water bath at 70^0C for 5 h. The sample was then dried in an oven at 90^0C for 12 h. It was further calcined in a furnace at 150^0C for 1 h to remove any solvent and moisture. By this protocol, the Fe oxide precipitation inside the pore structure of the GAC occurred at elevated temperature in the acidic condition. Finally, to remove nitrate ions, the temperature was increased to 300^0C, held for 4 h, and allowed to cool down to room temperature. Unincorporated free Fe was removed using a no. 20 sieve (USA Standard Testing Sieve). Now this material is termed as Fe/GAC (here Fe is Fe_2O_3). To reduce Fe(III) to elemental Fe, 1.6 g of $NaBH_4$ (Fisher) were prepared in 20 mL DI water. Fe/GAC weighing 4 g was resuspended in 50 mL of ethanol/DI water (30/70, v/v). A 5N NaOH solution was added to the Fe/GAC suspension drop by drop to bring the pH above 6.5. Then, $NaBH_4$ solution was added slowly to the pH adjusted Fe/GAC suspension with continuous N_2 purging, and the mixture was stirred until no significant H_2 production was observed (~2 h). As a result of the reaction between Fe/GAC and $NaBH_4$, the iron oxides were reduced to elemental Fe (Liu et al., 2005).

$$4Fe^{3+} + 3BH_4^{-} + 9H_2O \rightarrow 4Fe^{0} + 3H_2BO_3^{-} + 12H^{+} + 6H_2 \qquad (5.1)$$

Since the acidic pH of the Fe/GAC has an adverse effect on the reduction of Fe, pH adjustment of Fe/GAC to above 6.5 was needed before the reduction of Fe/GAC. This reduction procedure should be performed very carefully because of the production of explosive H_2. Then the GAC composite was recovered by filtering the slurry with a no. 20 sieve, washed with copious amounts of ethanol to remove free ZVI and other impurities, and then dried at 70^{0}C with continuous N_2 purging. The nano scale zero-valent iron incorporated GAC is termed as nZVI/GAC and was used in the experiments.

5.3 Characterization of nZVI/GAC

5.3.1 Scanning Electron Microscopy (SEM)

The surface morphology of the pristine GAC and the zero-valent iron modified carbon (nZVI/GAC) was analyzed by scanning electron microscopy (SEM) using a Hitachi S3400N microscope (at 15kV). The samples were placed on a carbon conductive tape attached with an aluminum holder. The images were taken with a backscattered electron detector. The experiment was done in the laboratory of the Department of Mechanical and Industrial Engineering , Concordia University, Montreal.

5.3.2 EDS

The elemental composition of the pristine GAC and the arsenic loaded nZVI/GAC were determined by Energy Dispersive Spectroscopy (EDS). The experiment was conducted with the same samples for SEM analysis where the microscope (Hitachi S3400N) was equipped with an EDS detector. The EDS analysis was done on certain areas of the samples to find the distribution of elements across different zones. The analyses were done at the Department of Mechanical and Industrial Engineering laboratory, Concordia University, Montreal.

5.3.3 BET Surface Area Determination

The specific surface area and mean pore size of the adsobents were measured by BET (Brunauer-Emmett-Teller) method. The BET isotherm is the basis for determining the extent of nitrogen adsorption on a given surface. A Micromeritics TriStar 3000 V6.07A surface area analyzer was used in this work. For both pristine and nZVI/GAC, 1.0 g of sample was vacuum-degassed at 473K for four hours. The sample was contained in a glass tube, cooled to cryogenic temperature (77.3K), then exposed to nitrogen gas at a series of precisely controlled pressures. With each incremental pressure, the number of nitrogen molecules on the surface increased. The pressure at which adsorption equilibrium occurs was measured and the universal gas law was applied to determine the quantity of gas molecules adsorbed. As adsorption proceeded, the thickness of the adsorbed nitrogen film increased with the surface pores being filled. The process continued until the point of bulk condensation of the nitrogen and then the reverse sequence of desorption occurred. The systematic sorption and desorption of nitrogen provided the fundamental information on the surface characteristics (www.micromeritics.com). The analysis was performed by the technician at the mining and materials engineering laboratory, McGill University, Montreal.

5.3.4 X-ray Diffraction (XRD) Studies

The crystallographic properties of the mineral phases present in nZVI/GAC were determined using Philips PANalytical X'PertPro system, which was equipped with CuKα radiation (45 kV, 40 mA) with a 0.02º step size and 2.0 second step time over the range $20^{\circ} < 2\theta < 80^{\circ}$. The iron modified samples were reduced to a fine powder in an agate mortar before placing them in the XRD sample port. The analyses of the samples were carried out using X'Pert HighScore Plus Rietveld analysis software in combination with the Pearson's crystal database (Villars, 1997).

5.3.5 FTIR Analysis

Attenuated Total Reflectance-Fourier Transform Infra Red (ATR-FTIR) spectra were recorded on a Thermo Nicolet, Nexus 470 FTIR Spectrophotometer with Omnic 6.0 software. The spectrometer was equipped with a KBr beam splitter and a DTGS detector. The spectra were collected for both liquid and solid samples. Spectra of 1.33 mM As(V) solutions were measured at various pH values like 5, 7, and 9. The arsenate loaded adsorbent was made into powder form for analysis. The samples were placed on a germanium crystal and a pressure probe was placed in position to apply consistent pressure on the sample. An average of 64 scans was used at a resolution of 1 cm^{-1}. Data analysis of the collected spectrum was performed with the Omnic software package (Version 6.0, Thermo Scientific).

5.3.6 Bulk Density

Bulk density was determined by weighing a graduated cylinder with uncompacted media that occupied a 5 mL volume, then subtracting the weight of the graduated cylinder. The bulk density was then determined by dividing the weight of the adsorbent by the occupied volume (5 mL). This gives bulk density of the media in units of g/mL or g/cm^3.

5.3.7 Determination of Iron Content

The iron content of the synthesized nZVI/GAC was determined according to the procedure described in literature (Lu, 1995). In short, 100 mg of adsorbent were mixed with 30 mL of 1:1 HCl, followed by shaking at 25 °C for 2 h and heating in a water bath at 90°C for 20 min. The supernatant was collected by filtration with 0.2 µm syringe filter and analyzed by ICP-MS (Agilent 7700x) to determine total iron.

5.3.8 Stability of Impregnated Iron

The stability of impregnated iron was determined from the batch adsorption test at pH range 2-11. The experiments were performed by adding 40 mg of nZVI/GAC in 40 mL arsenic solution (equivalent to 1 g/L) in 50-mL polypropylene centrifuge tubes. The tubes were shaken on an end-over-end shaker for 12 hours at room temperature (22±1^{0}C). After shaking, the supernatant solution was filtered through a 0.20 µm syringe filter and analyzed for dissolved iron along with arsenic by ICP-MS (Agilent Model 7700x).

5.3.9 Zero Point Charge (pHzpc) Determination

A 0.1M solution of NaCl having different pH values (3-11) was prepared by using deionized water that was bubbled with nitrogen to stabilize the pH by preventing the dissolution of CO_2. Modified carbon samples (150 mg) were put in contact with 50 ml of each solution, and stirred for 24 h in sealed vials. The final pH was measured, and plotted as a function of the initial pH of the solution. The pH at zero point charge, pHzpc, was determined as the pH of the NaCl solution that did not change after the contact with the samples (Sontheimer et al., 1988; Newcombe et al., 1993).

5.4 Batch Sorption Studies

Batch sorption studies were done separately, following the same experimental procedure, for arsenate and arsenite. For the adsorption study, stock solutions of 100 mg/L, 20 mg/L and 10 mg/L were prepared by dissolving appropriate amounts of $Na_2HAsO_4.7H_2O$ and As_2O_3 in deionized (DI) water. Batch experiments were performed by adding 40 mg of nZVI/GAC in 40 mL arsenic solution (equivalent to 1 g/L) in 50-mL polypropylene centrifuge tubes. As an inert electrolyte 0.1M NaCl was placed in the tubes. The tubes were shaken on an end-over-end shaker for different time periods at room temperature (22±1^{0}C). After shaking, the supernatant solution was filtered through a 0.20 µm membrane filter with a disposable syringe and analyzed for total arsenic by ICP-MS (Agilent Model 7700x) with a detection limit of 0.1 µg/L. Each sample was analyzed in triplicate and only those results were produced with the RSD (relative standard deviation) values of less than 5%. Relative standard deviation is a quantitative measurement that shows how far a particular data deviates from the mean value and is mathematically expressed in percentage as [% RSD = (standard deviation / mean) * 100]. The adsorption capacity was calculated by using the following equation:

$q = (C_0 - C_e)/m$

Where q is the adsorption capacity (µg/g), C_o is the initial As concentration (µg/L), C_e is the equilibrium As concentration (µg/L), and m is the mass of adsorbent (g/L).

Adsorption isotherms were produced at pH 4.5 with a nZVI/GAC dose of 1 g/L and different initial As(V) concentrations ranging from 500 µg/L to 15000 µg/L. The adsorption envelopes were generated with a fixed As(V) concentration (5000 µg/L) and varying the pH. The solution pH was adjusted using 0.1 M NaOH or HCl to the desired pH value, measured by Accumet (model AR25) pH meter. The pH of the solution was monitored during the experiment and was controlled every 4 hours. In some cases, 0.01M acetate buffer was used for pH control. The buffer was prepared by mixing appropriate amounts of sodium acetate, glacial acetic acid, and sodium chloride in DI water. The effluent pH was also measured to determine any possible changes of pH. It was found by preliminary experiments that 12h of shaking was enough to reach equilibrium. To check the adsorption of arsenic on the glass/plastic ware walls, an adsorbent free control experiment with a known arsenic concentration was performed with every set of experiments.To show the effect of reaction time on adsorption, nZVI/GAC was kept in contact with the arsenic solution in different time periods with fixed pH and adsorbent dose.

The influence of possible competitive ions present (PO_4^{3-}, SO_4^{2-}, NO_3^-, F^-, SiO_3^{2-}, Ca^{2+}, Mg^{2+}, Mn^{2+}) in water on arsenic adsorption was examined at their nominal and maximal values (1 mM and 10 mM). The experiment was done at two different pH levels (pH 4.5 and 6.5) as the adsorption was higher at acidic pH while keeping the arsenic concentrations and adsorbent doses constant.

5.5 Desorption

A desorption test was performed to investigate the reusability of the adsorbent. After adsorption reaction of 40 mg adsorbent with 40 mL of 5 mg/L arsenate solution for 12 h, the arsenate-loaded nZVI/GAC was separated and washed with distilled water to remove residual arsenic solution. The nZVI/GAC was mixed with 40 mL of 0.1M NaOH at pH 13 or NaH_2PO_4 solution at pH 4.5 or 6.5 and agitated for 12 h. The extracted arsenic in the solution was then analyzed to find out the desorption rate.

5.6 Solid Waste Leaching Procedure (TCLP)

The exhausted adsorbent was evaluated for arsenic leachability using the Toxicity Characteristic Leaching Procedure (TCLP) to determine whether it was hazardous (USEPA, 1992). In the TCLP, the solid waste is mixed with an acidic extraction liquid (dilute acetic acid) that is supposed to simulate the acid fluid at the bottom of a landfill. The solid sample should weigh at least 100 grams and the extraction liquid equal to 20 times the weight of the solid sample. This sample and the extraction fluid are then placed into a tumbler and mixed for at least 18 hours. This tumbling simulates the leaching action of water seeping through waste in a landfill. After tumbling, the mixture is filtered and the filtrate/extract is analyzed. If it contains arsenic at or greater than 5 mg/L, the waste is hazardous (USEPA, 1992).

The leaching solution was prepared by adding 5.7 mL of 0.1 M glacial acetic acid (CH_3COOH) and 64.3 mL of 1 M NaOH and bringing the mixture up to 1000 mL with deionized water, resulting in a pH of 4.93 ± 0.05. Twenty mL of leaching solution were added to a 25 mL polyethylene vial containing 1 g of spent adsorbent. The vial was capped and tumbled for 18 h. After agitation, the mixture was filtered using a 0.2 µm syringe filter. The aliquot was acidified by 0.1 M nitric acid to pH <2 and analyzed for arsenic by an Inductively Coupled Plasma-Mass Spectrometer (ICP-MS) (USEPA, 1992).

5.7 Determination of Surface Diffusion Coefficients

A differential column batch reactor (DCBR) was used to measure internal transport processes, specifically surface diffusion . A ten liter, pH 4.5 (controlled by 0.010 M acetate buffer), 100 µg/L As(V) batch reactor solution was prepared using deionized water. The volume of the batch reactor was chosen to be ten liters because it was required that no more than 5% of its volume can be withdrawn during all sampling and at least ten concentration measurements should be made throughout the duration of the rate test. The initial concentration was chosen to be the same as that used in the RSSCT column studies due to the fact that the surface diffusion coefficient may have some concentration dependence (Hand, 1983). The adsorbent dose (D_0) used was that which made the equilibrium concentration approximately 50% of the initial concentration as determined by Equation (5.2).

$$D_0 = \frac{0.5C_0}{K_F(0.5C_0)^{1/n}} \qquad (5.2)$$

where C_0 is the initial arsenic concentration (µg/L), K_F is the Freundlich constant, and 1/n is the dimensionless Freundlich exponent.

The film transfer coefficient for a fixed-bed differential column can then be calculated based as follows (Wakao & Funazkri, 1978)

$$\frac{2k_f r_p}{D_l} = 2 + 1.1Re^{0.6}Sc^{\frac{1}{3}} \tag{5.3}$$

where D_l is the liquid phase diffusivity (cm^2/s), k_f is the film transfer coefficient (cm/s), r_p is the adsorbent radius (cm), Re is the Reynolds number, and Sc is the Schmidt number. The Reynolds and Schmidt numbers for fixed bed reactors are given as:

$$Re = \frac{2\rho_l r_p v}{\varepsilon\mu} \tag{5.4}$$

$$Sc = \frac{\mu}{\rho_l D_l} \tag{5.5}$$

where ρ_l is the density of water (g/cm^3), ε is the bed porosity, ν is the superficial velocity (cm/s), and μ is the dynamic viscosity (g/cm.s).

The liquid phase diffusivity, as determined from properties of both water and arsenate, is given by (Hayduk & Laudie, 1974):

$$D_l = \frac{13.26x10^{-5}}{\mu^{1.14}{V_b}^{0.589}} \tag{5.6}$$

where V_b is the molal volume of arsenate (cm^3/mole).

Equation 5.6 is valid only if $15 < V_b < 500$ cm^3/g-mole (Crittenden et al., 1987). The value of V_b for arsenate was found to be 56 cm^3/g-mole based on Schroeder's (1949) additive method. This equation gives the liquid phase diffusivity in units of cm^2/s when the viscosity is given in centipoise and the molal volume in cm^3/g-mole.

The batch solution was pumped to the upflow direction through a 0.70 cm diameter column. The bed volume was 1.8 cm^3 corresponding to a bed height of 5 cm; the 12x30 mesh adsorbent media (0.8g) was sandwiched by glass beads in the bed as shown in Figure 5.1. The bed porosity was 0.48. A flow rate of 10 mL/min through the columns was sufficient to ensure a high Biot number.

Tubing was connected from the batch reactor, through the pump, to the influent end of the column. Effluent tubing was run back into the batch reactor, since the solution is recycled. Sample aliquots (10 mL) were collected over time from the sampling port until C(t) = C_e.

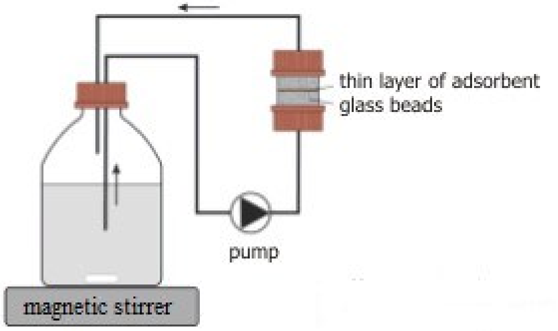

Figure 5.1 Schematic of the differential column batch reactor setup. Volume = 10 L, Q= 10 mL/min, BV= 1.8 cm^3, Bed height= 5 cm, Media= (12x30) 0.8 g, pH 4.5

5.8 Rapid Small Scale Column Test (RSSCT)

The mini column was 0.7 cm in diameter and 20 cm in length with Teflon end caps. Teflon tubing and Peristaltic pumps (Masterflex®) were connected with flow meters. The columns were packed in sequence from bottom to top: borosilicate glass beads, glass wool, nZVI/GAC, glass wool, and borosilicate glass beads; this packing technique suitably holds the nZVI/GAC in-place and ensures the uniform distribution of the influent flow. The columns were operated in upflow mode to minimise the problems that might arise due to the entrapment of air bubbles in the column. The experimental setup is shown in Figure 5.2.

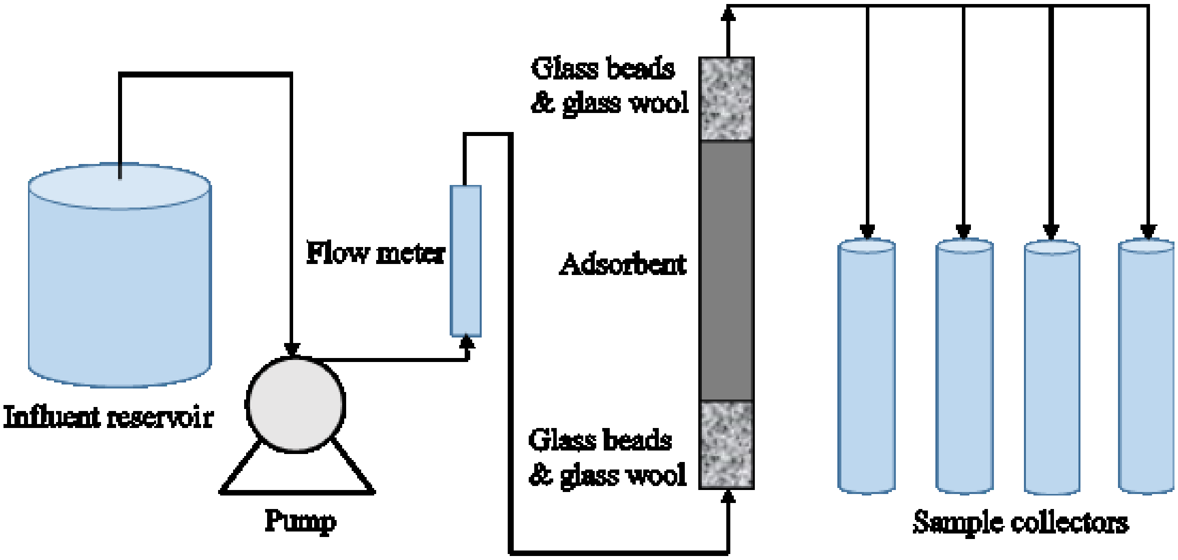

Figure 5.2 Schematic of the Rapid Small Scale Column Test (RSSCT) setup.

The 80x100-mesh nZVI/GAC used in the mini column was obtained by crushing the 12x30-mesh nZVI/GAC and sieving it to 80x100-mesh. Sieved nZVI/GAC was added to the column using a funnel and DI water to flush the material down into the column. Columns were backwashed to remove fines by operating the column in downflow mode with DI water until the effluent ran clear. The bed volume (BV) of the RSSCT was chosen as 5 cm^3 corresponding to a bed height of 13 cm and an nZVI/GAC mass of 3.44 g. Different EBCTs of 0.5, 1, and 2 min (corresponding flow rates of 2.5, 5, and 10 mL/min) were used to examine their effects on the column breakthrough. Three initial concentrations of 100, 50, and 20 µg/L were chosen to investigate their effects on adsorption in the fixed-bed column. The pH of the feed solution was adjusted to 4.5 by using 0.1M HCl. Ionic strength of the solution was maintained as 0.1M NaCl. The effluent was collected every 500 to 1000 bed volumes depending on the experiment. An appropriate amount of aliquot was filtered with 0.20 µm syringe (Corning) filters, diluted, and acidified with 1:2 ratio of trace metal grade

HCl and HNO_3. Effluent samples were collected until the media reached exhaustion. The RSSCT parameters are shown in Table 5.1.

Table 5.1 RSSCT parameters

Parameters	**Values**
Particle size (mesh)	80x100
Particle diameter (mm)	0.18 - 0.15
Porosity	0.24
Column diameter (cm)	0.70
pH	4.5
Ave. influent As conc. (µg/L)	20-100
Bed height (cm)	13
Flow rate (mL/min)	2.5-10
Surface loading (m/h)	4-16
EBCT (min)	0.5-2

5.9 Arsenic Analysis

The samples were analyzed for arsenic at the environmental lab, Department of Building, Civil, and Environmental Engineering, Concordia University, Montreal, using ICP-MS (Agilent 7500x). The samples were acidified with trace metal grade 1% HNO_3 and 0.5% HCl (2:1 v/v) before analysis. The ICP-MS is commonly used in arsenic analysis because of its low detection limit. The Agilent 7500x ICP-MS, specifically, is powered by a pneumatic nebulizer, which utilizes the mechanical forces of an argon gas flow to generate an aerosol sample. The aerosol sample then passes through a chamber, where it is separated according to size, allowing for only finer droplets to continue through to the sample injector of the plasma torch. In the plasma torch, the sample is converted from a droplet to ions via collisions with energetic argon electrons. These ions are transported through an interface and then focused through ion optics into a mass spectrometer, where the ions generate a detectable electrical signal. When compared with the latest technologies for arsenic analysis, these mass spectrometers provide high precision results, as well as exceptional trace element measurement capabilities; and were considered reliable for this work.

Chapter 6

Results and Discussion

6.1 Characterization of nZVI/GAC

6.1.1 SEM

The scanning electron micro images of the pristine GAC and the synthesized nZVI/GAC loaded with arsenic are shown in Figure 6.1. It can be seen that the surface of the pristine GAC is rough and full of visible cracks and pores (images A & B). The supported nZVI particles in the pores of the GAC are more or less spherical in shape (images C & D). The majority of the nZVI particles are within 150 nm in diameter. However, an agglomeration phenomenon of some particles is observed. It is comparable to the round-shaped clusters of zero-valent iron synthesized in solution with the diameter <100 nm (Kanel et al., 2005). It can also be seen that most of the zero-valent iron particles were loaded into the pores and cracks rather than onto outer surfaces. This is very important for repeated use in water treatment facilities without loss of the iron particles. The analysis ensures that the performed synthesis effectively generates targeted nZVI-GAC.

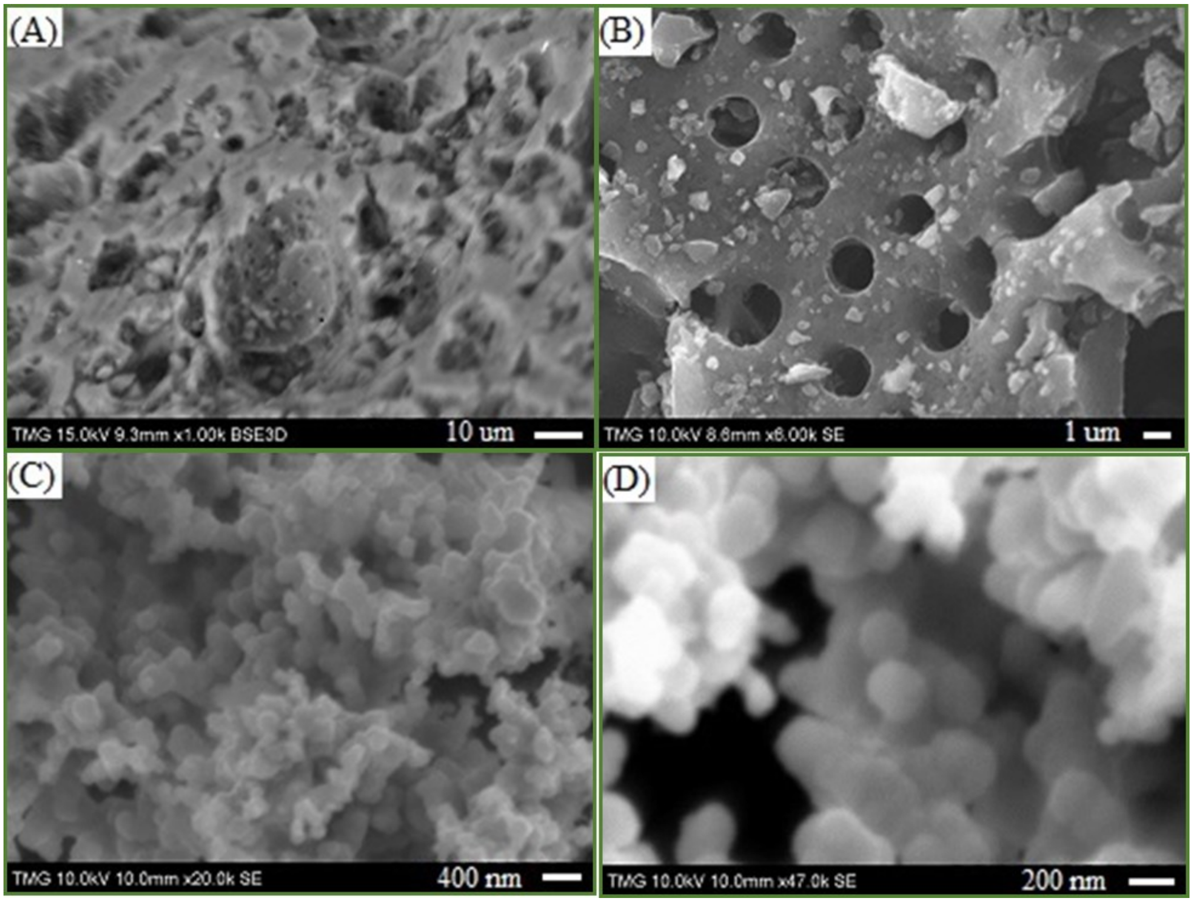

Figure 6.1. SEM of pristine GAC: (A) and (B), and As(V) loaded nZVI/GAC: (C) and (D)

6.1.2 Energy Dispersive Spectroscopy (EDS)

The elemental composition of arsenic loaded nZVI/GAC as determined by Energy Dispersive Spectroscopy (EDS) confirms the presence of carbon, oxygen, iron and trace amounts of sodium, silicon and arsenic as shown in Figure 6.2. In comparison, the EDS of pristine GAC contains only carbon, oxygen and trace amounts of aluminum. The analysis confirms that the synthesis procedure is effective at precipitating iron onto the GAC surface. The presence of arsenic on nZVI/GAC validates the adsorption phenomenon of the adsorbent.

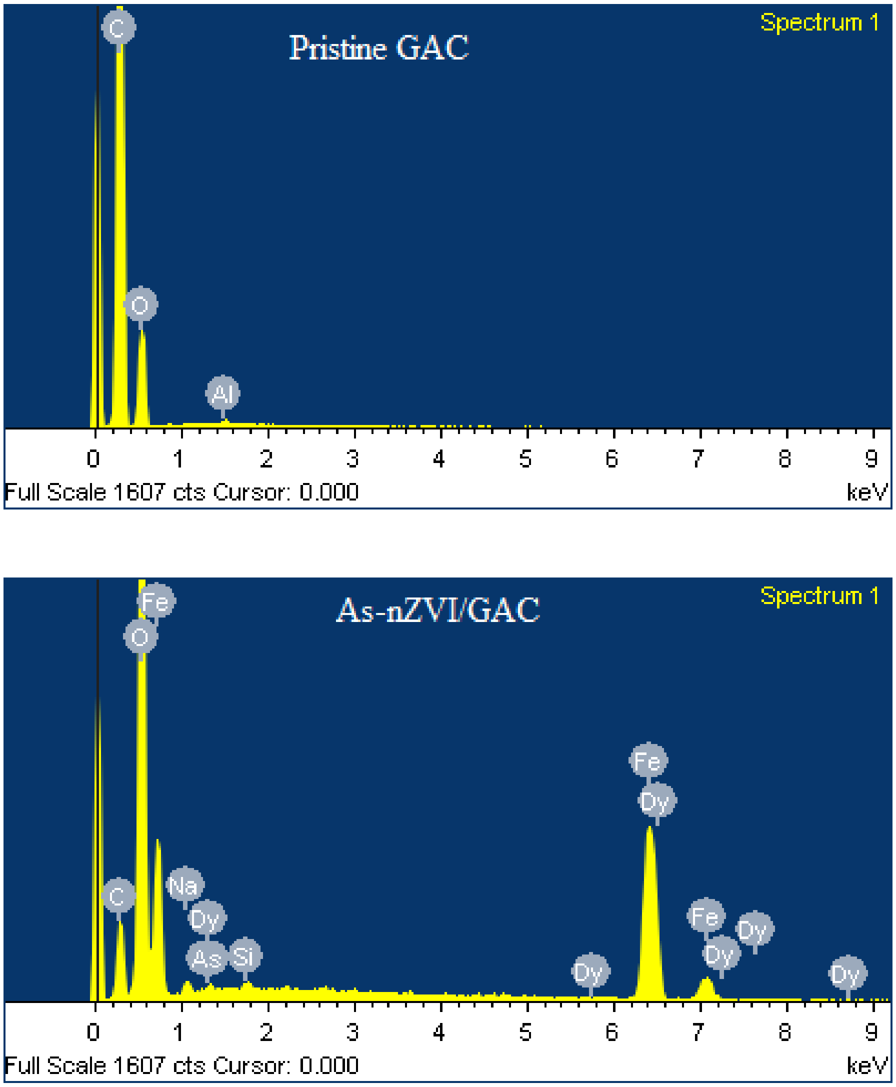

Figure 6.2. Energy Dispersive Spectroscopy (EDS) of pristine and arsenic loaded nZVI/GAC

6.1.3 BET

BET analyses were conducted in order to compare the surface area and pore size distribution of the pristine and systhesized nZVI/GAC. Data collected from BET surface analyses include pore size distribution, pore volume, and pore surface area of the adsorbent media. The results clearly indicate the reduction of surface area (from 952 to 654 m^2/g) and pore volume (from 0.455 to 0.328

cm^3/g) of the nZVI/GAC in comparison to the pristine GAC. The average pore width also reduced from 47 to 43 Å. It appears that a fraction of pores in the GAC is blocked due to the modification, leading to a lower specific surface area. Similar results were found for GAC-based iron containing adsorbent for arsenic removal. The BET surface areas of iron modified GACs decreased from 541 to 380 m^2/g and from 528 to 350 m^2/g for Darco 20x50 and Darco 20x40LI respectively (Gu et al., 2005).

6.1.4 XRD

To confirm the elemental state of iron on the synthesized nZVI/GAC, XRD analysis was performed. Figure 6.3 displays XRD patterns of nZVI/GAC prepared by adsorbing 10 g/L of sample with 100 mg/L of arsenate. The intensity peaks at $2\Theta = 44.7^0$ and 65.02^0 are characteristics of elemental iron, Fe(0) (Hoch et al., 2008). The weakly diffracted peak of Fe(0) indicates that the synthesized nano-scale ZVI is poorly crystalline. The peaks were found to have low intensity because of the presence of an amorphous iron phase (Ponder et al., 2000). Despite the weak peaks, the XRD result confirms the presence of ZVI on the surface of GAC and that the nZVI/GAC synthesis procedure successfully reduced ferric iron to its zero-valent state. In addition to the ZVI intensity peaks identified on the plots, several peaks are also visible in the scan. These peaks are attributed to the crystalline structure of iron oxides like maghemite (γ-Fe_2O_3), and magnetite (Fe_3O_4) which is indicative of the protective oxide shell casting the ZVI core formed during the post-synthesis nitrogen passivation. From the XRD pattern it can be surmised that the adsorbent surface also contains poorly crystalline iron oxides/hydroxides (amorphous oxides). The ZVI and iron oxides take part in removal of arsenic from water (Leupin et al., 2005; Manning et al., 2002).

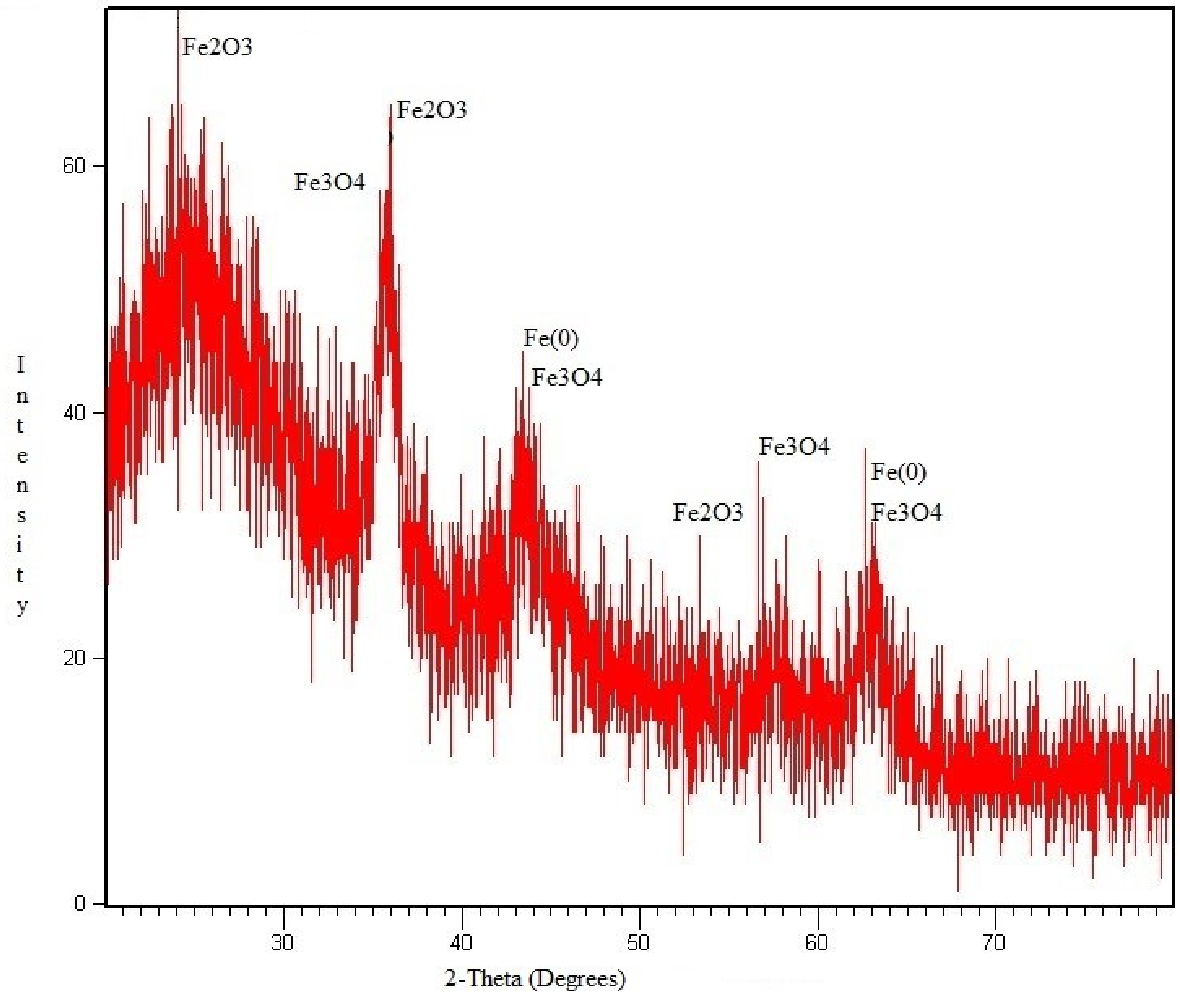

Figure 6.3. XRD analysis of nZVI/GAC

6.1.5 FTIR Spectroscopy

6.1.5.1 FTIR Study of Dissolved As(V) Species:

Dissolution of arsenic oxide in water produces different species of arsenic oxoanion depending on the pH of the solution. The degree of protonation has an influence on symmetry and vibrations of

IR spectra: T_d, tetrahedral symmetry (AsO_4^{3-}) is reduced to C_{3v} ($HAsO_4^{2-}$), C_{2v} ($H_2AsO_4^-$), and C_{3v} (H_3AsO_4) with decreasing pH value. This can be observed in shifts at stretching vibrations of $\nu_{as/s}$(As-OH) and $\nu_{as/s}$(As-O) (Myneni et al., 1998).

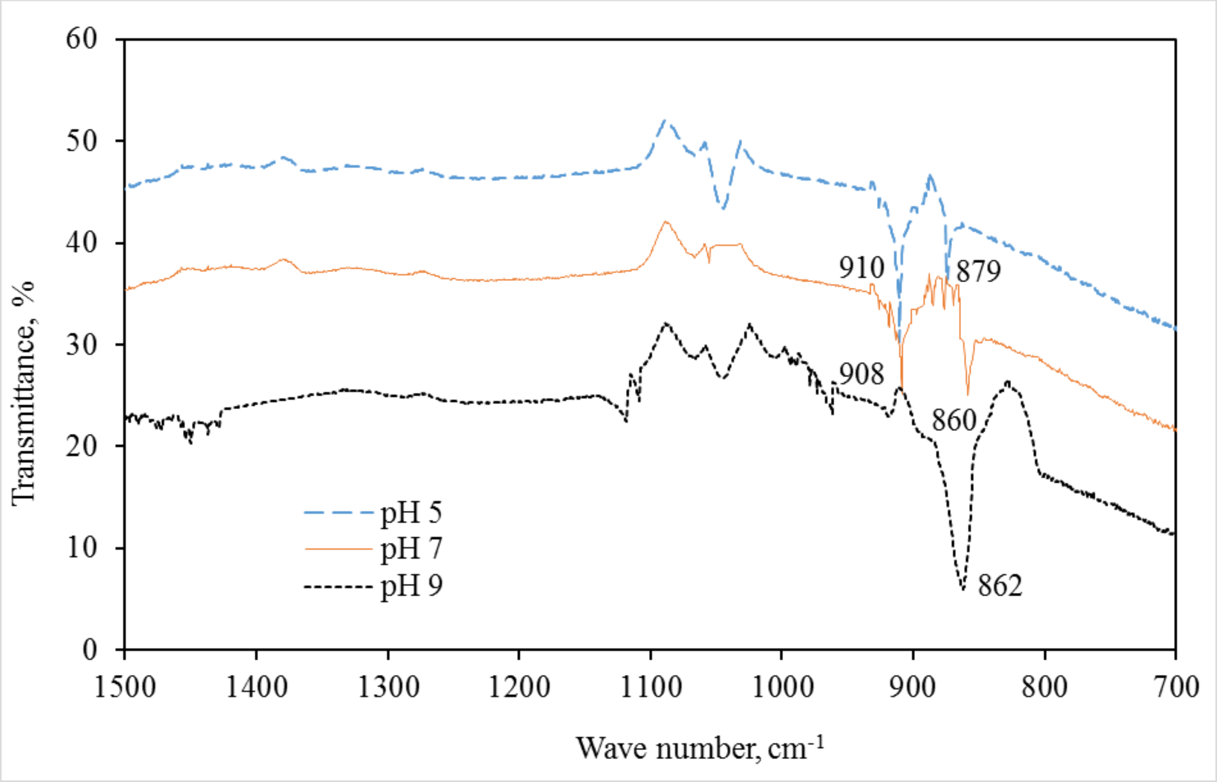

Figure 6.4. FTIR spectra of 1.33 mM As(V) species at pH 5, 7, and 9

Figure 6.4 shows the vibrational spectra of As(V) with different protonations. A spectrum of $HAsO_4^{2-}$ (pH 9) shows a single vibration at 862 cm^{-1} corresponding to the $\nu_{as(}$As-O). The arsenate solution at pH 7 consists presumably of a mixture of $HAsO_4^{2-}/H_2AsO_4^-$ species, which is detectable also in the spectrum: a single peak at 860 cm^{-1} and a shoulder at wave number of 908 cm^{-1}. The peak at 860 cm^{-1} is the same as pH 9 vibration while vibration at 908 cm^{-1} is ν_{as}(As-O) of $H_2AsO_4^-$. At pH 5, the $H_2AsO_4^-$ is split into two peaks, where 879 cm^{-1} corresponds to ν_s(As-O) and 910 cm^{-1} is the same as in pH 7, but with a stronger absorption. Measured spectra of As(V) species are in agreement with previous studies and protonated As(V) spectrum at pH 3 is identical to spectra at pH 5 (Roddick-Lanzilotta et al., 2002; Goldberg & Johnston 2001; Myneni et al., 1998; Pena et al., 2006).

6.1.5.2 FTIR Study of Adsorbed As(V) Species

Figure 6.5 shows the spectra of As(V) adsorbed onto nZVI/GAC at various pH values. The peak positions of the adsorbed samples were significantly different from those of the dissolved As species, which is attributable to symmetry reduction arising from the oxyanion adsorption. If the symmetry reduction were caused by protonation, as would be the case for outer-sphere adsorption, the peak positions would be similar as the corresponding dissolved As species. Therefore the band shift observed in this study indicated the formation of inner-sphere complexes. Due to the similarities of phosphate and arsenate sorption properties, the band assignments of adsorbed As(V) spectra are comparable to those of $(MO)_2PO_2$ surface complexes having C_{2v} symmetry (Tejedor-Tejedor & Anderson, 1990; Gong, W., 2001; Guan et al., 2008; Pena et al., 2006). Because metal ions are not as strongly coordinated to oxygen as protons (Myneni et al., 1998a; Tejedor-Tejedor & Anderson, 1990; Gong, W., 2001; Guan et al., 2008), the O atom binding with Fe has an empty orbit that partially participates in electron delocalization and in turn the strength of the As-O bond is reduced. Therefore, the As-O bond in $(FeO)_2AsO_2$ would be weaker than that in $(HO)_2AsO_2^-$ and the As-O bond in $(FeO)AsO_3^-$ would be weaker than that in $(HO)AsO_3^{2-}$. Consequently, red-shifts in the IR stretch frequencies would be predicted as a result of arsenate complexation to the corrosion products of nZVI on the surface of nZVI/GAC. The spectra of arsenate adsorbed on nZVI/GAC exhibited two bands at 886-893 and 833-836 cm^{-1}. However, the band at 886-893 cm^{-1} was only observed in the spectra at pH 7 when $HAsO_4^{2-}$ began to appear in aqueous solution. The peak at 833-836 cm^{-1}, red-shifted relative to ν_{as}(As-O) in $HAsO_4^{2-}$ is assigned to ν(As-O) in the monodentate complex $(FeO)AsO_3^-$.The higher frequency band at 886-893 cm^{-1} is assigned to ν(As-O) in $(FeO)_2AsO_2$ complexes (bidentate complexes) as the frequency of this band is lower than ν(As-O) in $(HO)_2AsO_2^-$ and higher than that in $HAsO_4^{2-}$.

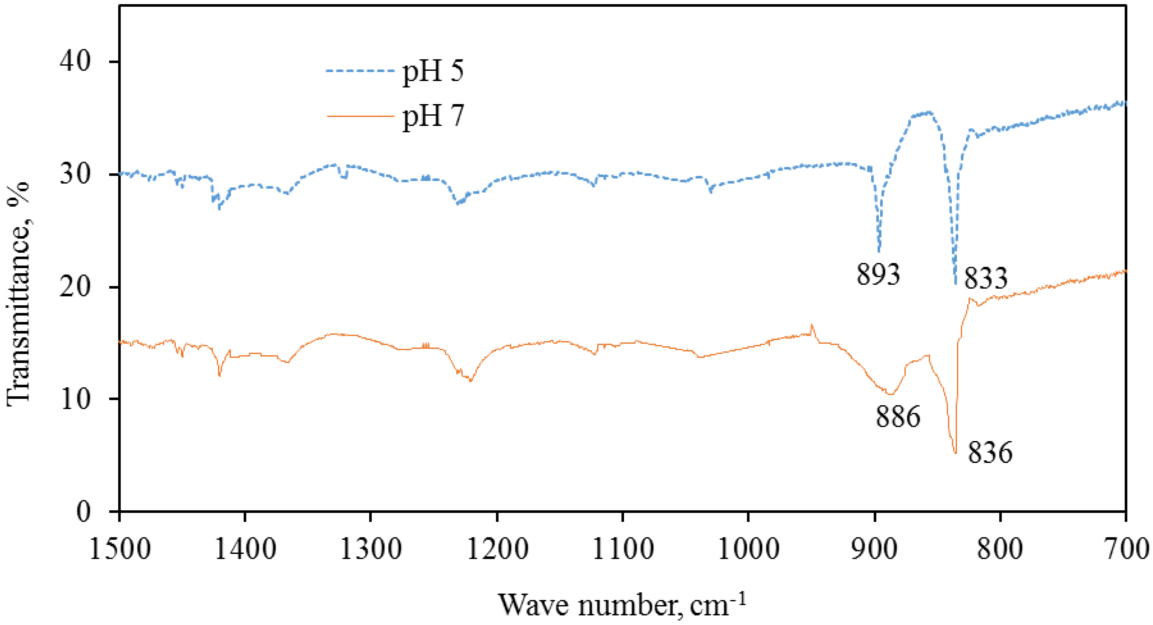

Figure 6.5. FTIR spectra of adsorbed As(V) species at pH 5 and 7.

nZVI/GAC dose =10 g/L, As(V) = 100 mg/L

6.1.6 Bulk Density

The bulk density of the adsorbent was determined as 0.44 g/cm^3. Gu et al. (2005) found similar results in their experiments of GAC-based iron-containing adsorbents for arsenic removal. They found the bulk densities of GACs from American Norit Co. Inc. i.e. Darco 20x40LI (0.4 g/cm^3), GAC 1240+ (0.51 g/cm^3), Darco 12x20LI (0.39 g/cm^3). The bulk density was used as an input parameter for surface diffusion calculations and modeling. Also it is required to determine the volume of the reactors in column operation.

6.1.7 Iron Content

Iron content depends on the impregnation method as well as the heterogeneity of pore sizes and the morphologies of GAC itself. The amount of impregnated iron has an impact on arsenic adsorption capacity. When a small amount of iron is impregnated in GAC, the iron is expected to distribute in a single layer on the internal surface of GAC. Therefore, the adsorption capacity remains relatively low. When more iron is loaded on the GAC, more surface area of GAC is covered by iron which contributes to increased adsorption capacity. However, high amounts of iron may cause blockages in GAC pores as well, resulting in decline of the specific surface area. The relationships between the iron content and maximum adsorption capacity and iron use efficiency were evaluated (Chang et al., 2010). It was found that arsenate adsorption capacity increased with increasing iron content and reached a peak adsorption capacity of 1.95 mg/g when the iron content increased to 4.22%. Further increase of iron content resulted in a gradual decrease in adsorption capacity. An optimum amount of iron impregnation is expected for the maximum adsorption capacity. The iron content found in this study for nZVI/GAC was ~6.5% by weight. This is comparable with the iron contents of 8.52% and 4.22% for Norit RX3 EXTRA and Darco 20x50 Fe-GACs respectively (Chang et al., 2010).

6.1.8 Stability of Impregnated Iron

The stability of impregnated iron plays an important role for effective adsorption. It can be seen from Figure 6.6 that impregnated iron dissolved below pH 3. The maximum concentration of dissolved iron was 15 mg/L observed at pH 2.0. This amount is equivalent to 23% of total impregnated iron. At the pH range 3-11 the impregnated iron was very stable. So, the stability of iron is not a matter of concern within the normal pH range.

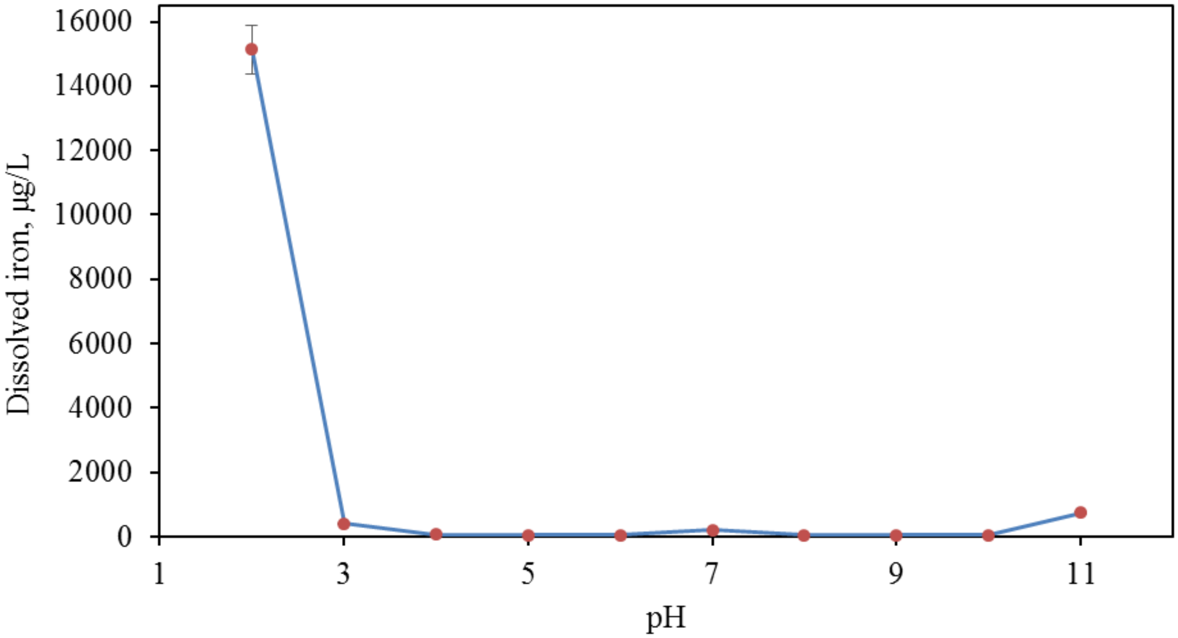

Figure 6.6. Stability of impregnated iron on nZVI/GAC with 6.5% iron.

6.1.9 Zero Point Charge (pH_{ZPC})

The point at which the pH does not change i.e. the initial and final pH is the same is defined as the media's pH of zero point charge (pH_{ZPC}). In Figure 6.7, the red line has been drawn at 45^0 inclined to the X-axis so that any point on it represents the equal value of initial and final pH. The blue curve represents the experimental values. The intersection point of the two curves is the zero point charge (pH_{ZPC}) which was found for the nZVI/GAC at pH 8.2. The zero point charge of an adsorbent is a significant parameter which contributes to the types and intensity of adsorption. An example of the use of pHzpc values was shown in studies with activated alumina. The optimum pH for arsenic adsorption onto activated alumina ranges from 5.5 to 6 (Chwirka et al., 2000;

Clifford 1999; Jekel, 1994). At lower pH, the activated alumina begins to dissolve, thus losing adsorptive capacity. At higher pH, activated alumina loses its positive charge, limiting electrostatic attraction between the positive surface and negative arsenate. Also at higher pH, there is an increase in OH^- in solution, which competes with arsenate for adsorption sites. The concept of pH dependent adsorption of arsenate onto nZVI/GAC is discussed in detail in the arsenate sorption mechanism section (section 6.8).

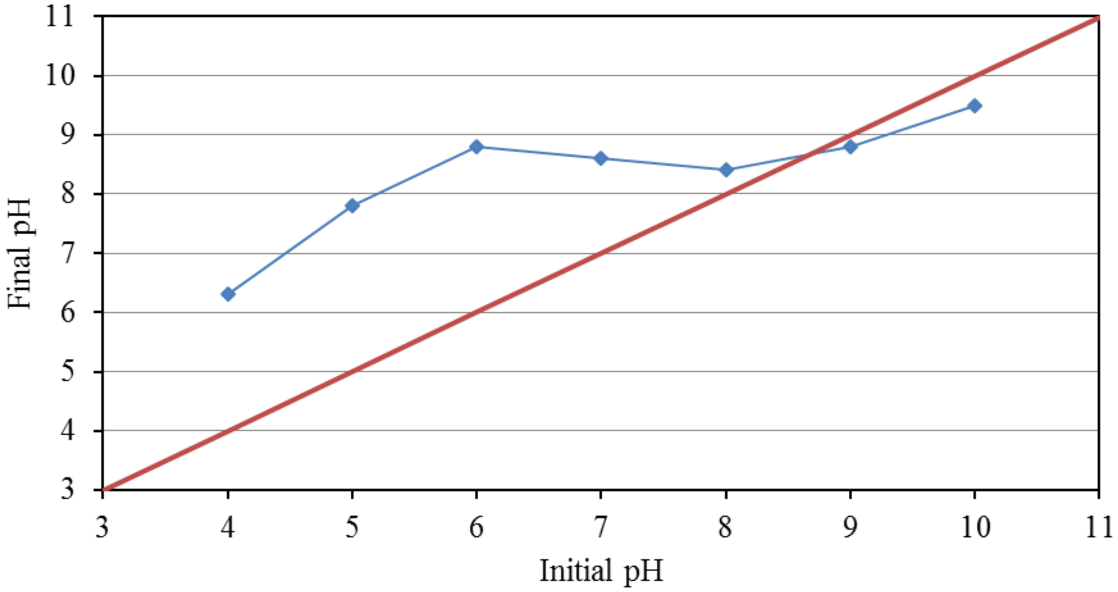

Figure 6.7. Zero point charge determination, initial pH vs. final pH

6.2 Batch experiment/ Controlling factors

6.2.1 Effect of pH

The adsorption studies of arsenate and arsenite are presented in Figures 6.8 through 6.11 at pH 2-11 with the virgin GAC or nZVI/GAC dose of 1 g/L and arsenic concentrations of 5000 µg/L. The comparison of arsenite adsorption capacity of virgin and modified GAC are illustrated in Figure

6.8. It is shown in Figure 6.8 that the adsorption of arsenite on the virgin and the modified GAC is insensitive to pH range of 2-11 although the adsorption capacity of modified GAC is higher than that of the virgin GAC (~1400 μg/g vs. ~170 μg/g). Figure 6.9 indicates that the arsenate adsorption on nZVI/GAC is pH sensitive whereas that on virgin GAC is not and the capacity of nZVI/GAC is much higher than that of the virgin GAC. Figure 6.10 compares the adsorption capacity of nZVI/GAC for arsenite and arsenate. It is obvious that arsenate is much better removed than arsenite by nZVI/GAC. Hence, all further experiments were done only with arsenate. If arsenite is present in water, an additional oxidation step is required for better removal. Some effective oxidants are free chlorine, hypochlorite, ozone, permanganate, and hydrogen peroxide (Jekel, 1994).

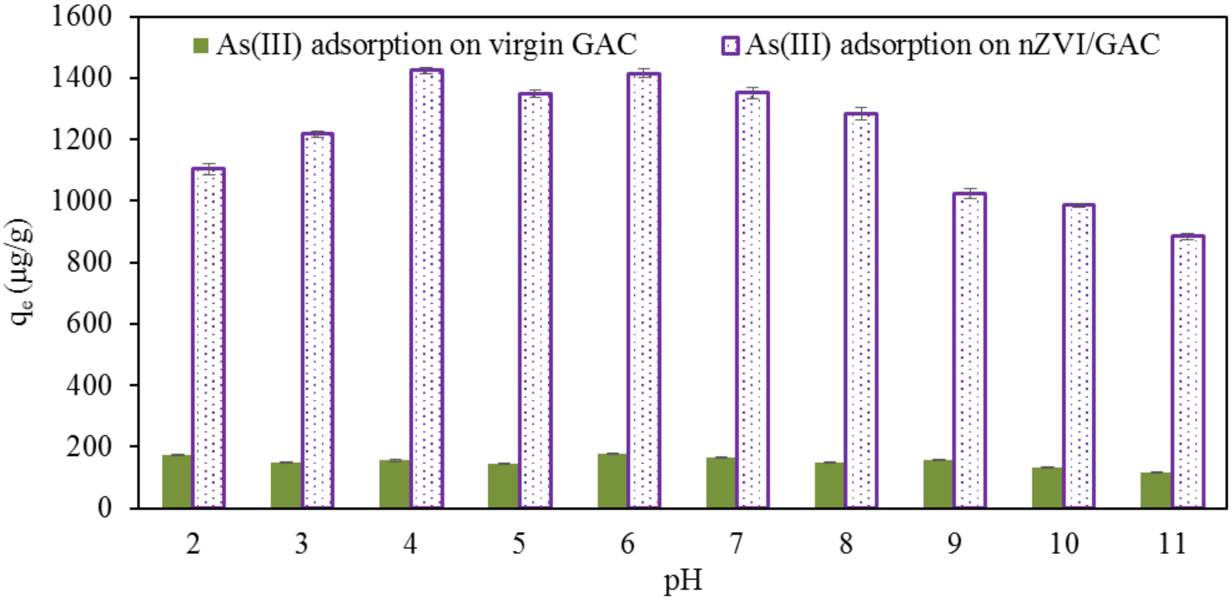

Figure 6.8. Adsorption of As(III) on virgin GAC and nZVI/GAC. Initial As(III) conc.: 5000 μg/L, virgin GAC or nZVI/GAC: 1g/L in 0.1M NaCl , equilibrium time: 12 h.

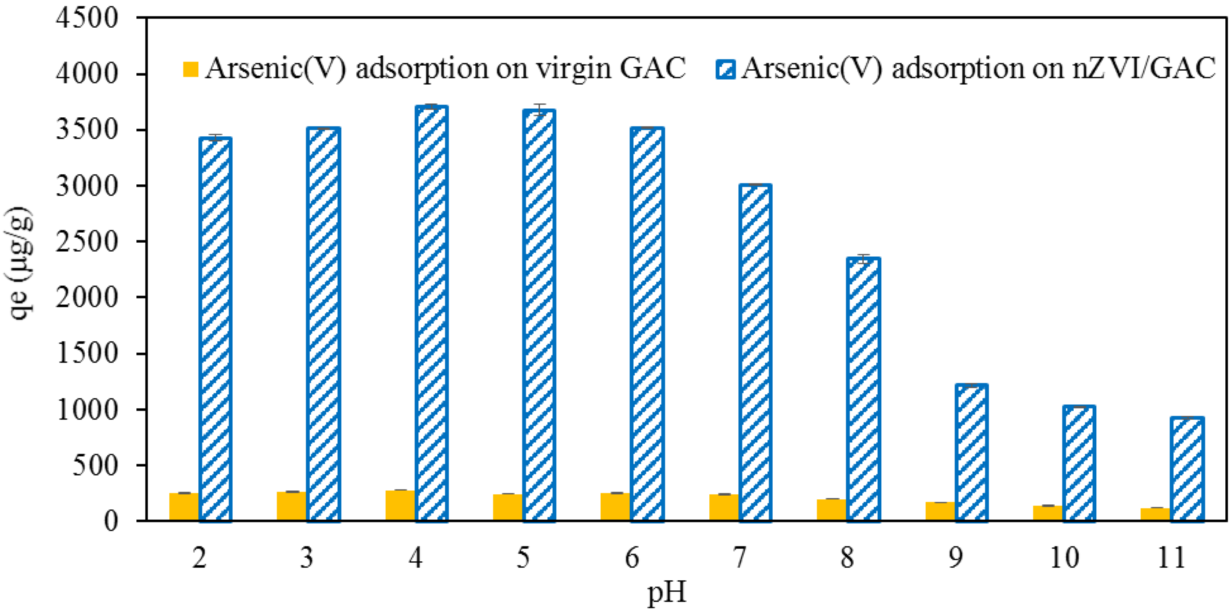

Figure 6.9. Adsorption of As(V) on virgin GAC and nZVI/GAC. Initial As(V) conc.: 5000 µg/L, virgin GAC or nZVI/GAC: 1g/L in 0.1M NaCl, equilibrium time: 12 h.

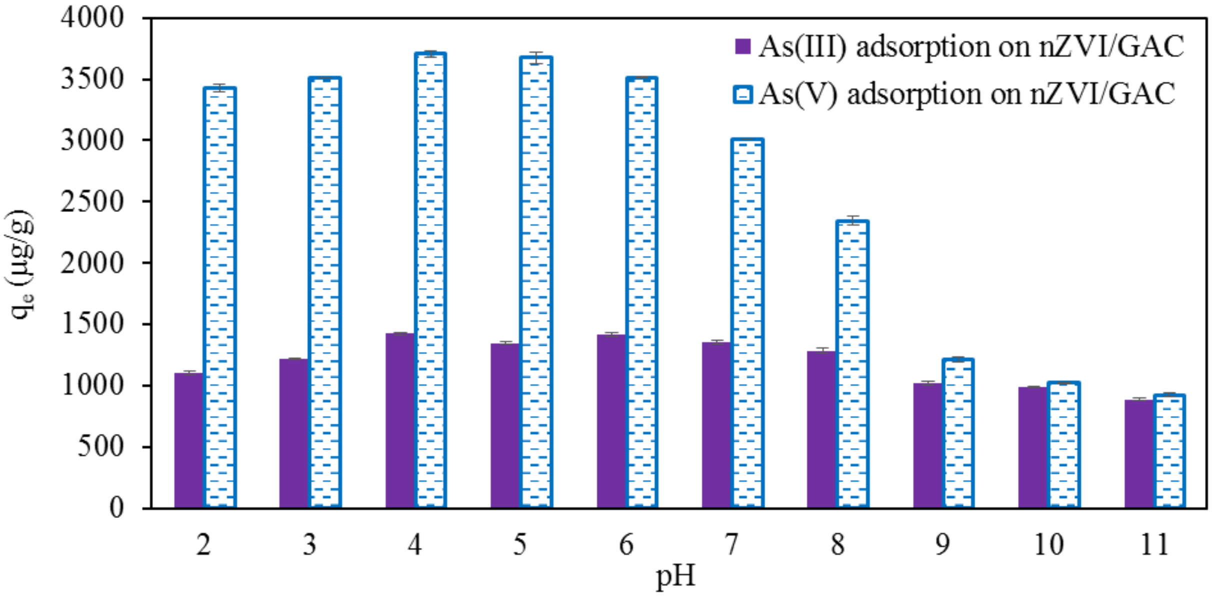

Figure 6.10. Adsorption of As(III) and As(V) on nZVI/GAC. Initial As(III)/As(V) concentration: 5000 µg/L, nZVI/GAC: 1g/L in 0.1M NaCl , Equilibrium time: 12 h.

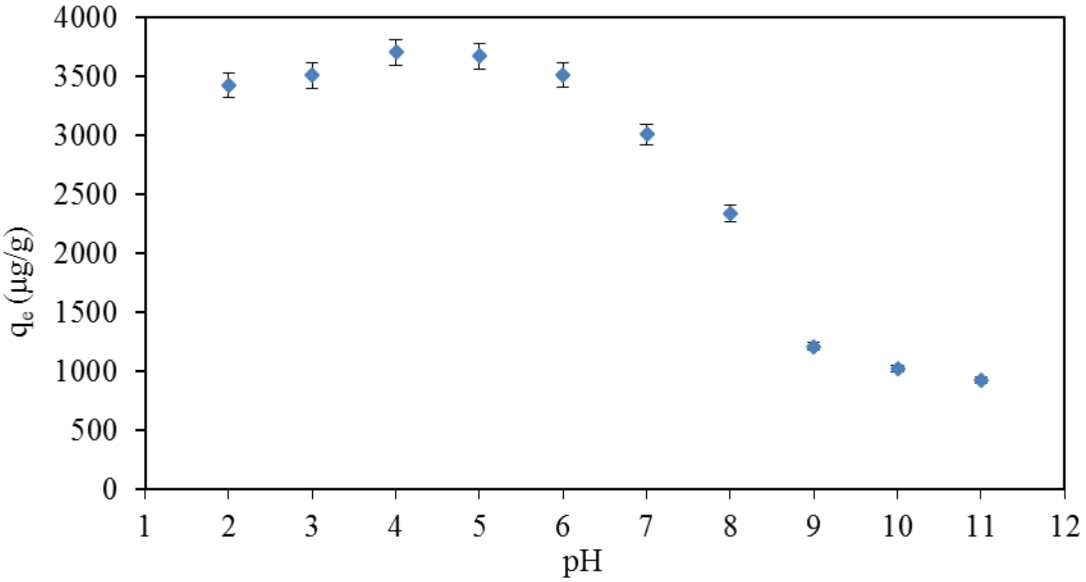

Figure 6.11. Adsorption of As(V) on nZVI/GAC. Initial As(V) concentration: 5000 µg/L, nZVI/GAC: 1g/L in 0.1M NaCl , Equilibrium time: 12 h.

It is seen from Figure 6.11 that the adsorption changes little over the pH 2~6.5 range and there is sharp decrease from pH 7.5~11. The pH dependent behaviour of arsenate adsorption onto nZVI/GAC is a consequence of interaction of the aqueous arsenic species with the charged surface of the nZVI/GAC. The speciation of arsenic is a function of pH and the charge on the nZVI/GAC surface is a function of pH at its zero point charge (pH_{zpc}), at which the net surface charge is zero. The species of arsenate exist as $H_2AsO_4^-$, $HAsO_4^{2-}$, and AsO_4^{3-} when the pH shifts from acidic to alkaline condition corresponding to their dissociation constants: $pKa_1 = 2.3$, $pKa_2 = 6.8$, $pK_{a3} = 11.6$ (Goldberg & Johnston, 2001). It is well known that the adsorbent surface is positively charged at a pH below pH_{ZPC} and negatively charged at a pH above pH_{ZPC}, resulting in increased electrostatic attraction or repulsion with anionic species. The pH_{ZPC} of the synthesized nZVI/GAC was determined to be pH 8.2 (Figure 6.7), below which the surface is positively charged and favorable for the adsorption of anionic arsenic species. The surface of the adsorbent becomes less positively charged when pH increases and thus shows less attraction towards anionic arsenate species. Therefore, the adsorption of arsenate shows a decreasing trend with increasing pH and this has been well documented in previous work of arsenate adsorption on ferrihydrite and nano zero-valent iron (Guo & Chen, 2005; Kanel et al., 2006; Raven et al., 1998; Jia & Demopoulos, 2005).

6.2.2 Effect of Initial Arsenate Concentration

To find out the influence of initial arsenate concentration on adsorption behaviour, a batch experiment at a pH of 4.5 and an nZVI/GAC dose of 1 g/L with varying initial arsenate concentration from 500 µg/L to 15000 µg/L was performed as shown in Figure 6.12. The adsorption increased from 480 to 6124 µg/g with the increase of initial concentration from 500 to 15000 µg/L. In the case of low initial concentration, a relatively slower transport due to a decreased diffusion coefficient and decreased mass transfer coefficient was observed previously (Aksu & Gönen, 2004).

It was found that biosorption of arsenate with *Lessonia nigrescens*, and anaerobic biomass increased with the increase of initial arsenate concentration (Hansen et al., 2006; Chowdhury & Mulligan, 2011). The removal efficiency depends on the number of active sites present on the adsorbent surface. At higher initial concentration, the interaction of arsenic species with the available sites on the adsorbent surface could be higher due to increased diffusion and mass transfer. This may contribute to more rapid sorption at higher initial concentrations.

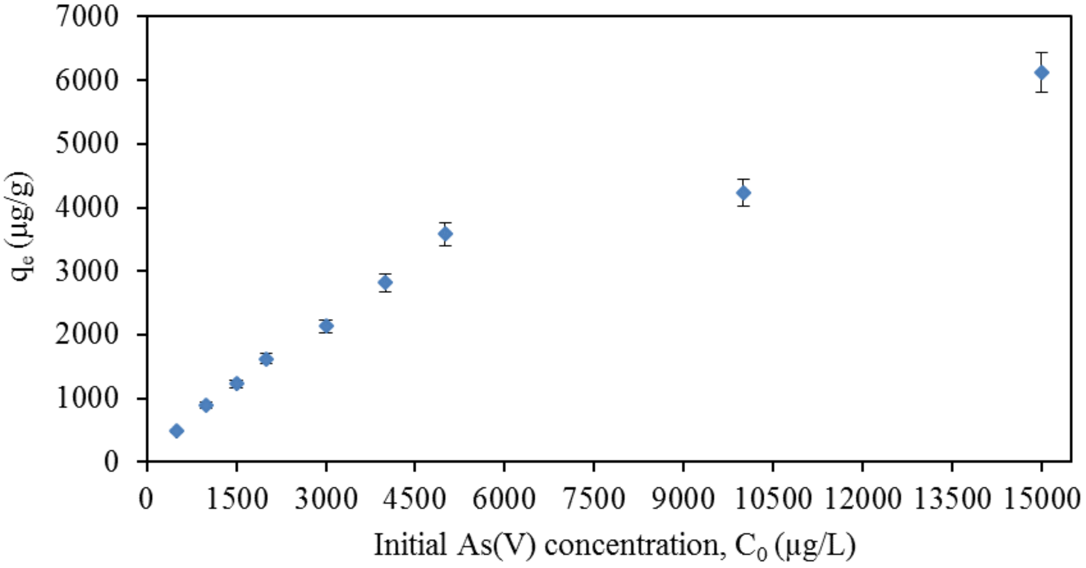

Figure 6.12. Adsorption effect of initial As(V) concentration. pH 4.5 controlled by a 0.010 M acetate buffer, nZVI/GAC: 1g/L in 0.1M NaCl , equilibrium time: 12 h.

6.2.3 Effect of Contact Time

Adsorption of As(V) on nZVI/GAC is shown in Figure 6.13 at pH 4.5 with the nZVI/GAC dose of 1 g/L and arsenate concentration of 5000 µg/L while varying the contact time from 15 to 720 minutes. It was found that 66% adsorption was achieved in 15 min and 72% in 120 min. The adsorption on nZVI/GAC seems to take place in two phases. The first phase involved rapid adsorption because of the easiness of accessibility to the adsorption sites. The second slower phase could be due to the retarded accessibility to micro pores or less energetic sites that leads to a long period to reach equilibrium.

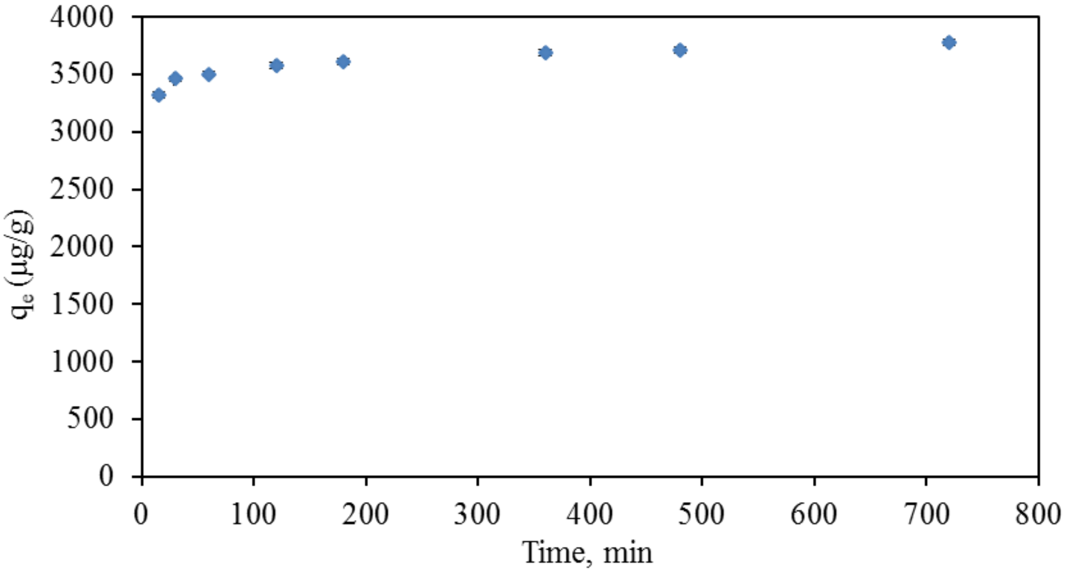

Figure 6.13. Effect of reaction time on As(V) adsorption. Initial As(V) concentration: 5000 µg/L, pH 4.5 controlled by a 0.01M acetate buffer, nZVI/GAC: 1g/L in 0.1M NaCl.

6.2.4 Adsorption Rate Expression

The rate of adsorption was determined at pH 4.5 with the nZVI/GAC dose of 1 g/L and arsenate concentration of 5000 µg/L with different contact time periods from 15 to 720 minutes. The adsorption kinetic data followed the pseudo-second order kinetic model based on the correlation coefficients (R^2= 0.99); the kinetic model is shown in Figure 6.14. The initial sorption rate (h), determined from the pseudo-second order kinetic model, was 666 µg/g.min. This value is higher than those found in the literature as presented in Table 6.1. Arsenate removal rates depend on the continuous generation of iron oxide adsorption sites (corrosive rate). The higher sorption rate can be attributed to the reaction taking place between arsenate and the corrosion products of Fe(0). Materials with fast sorption rates are suitable for column operation as they need less residence time for sorption.

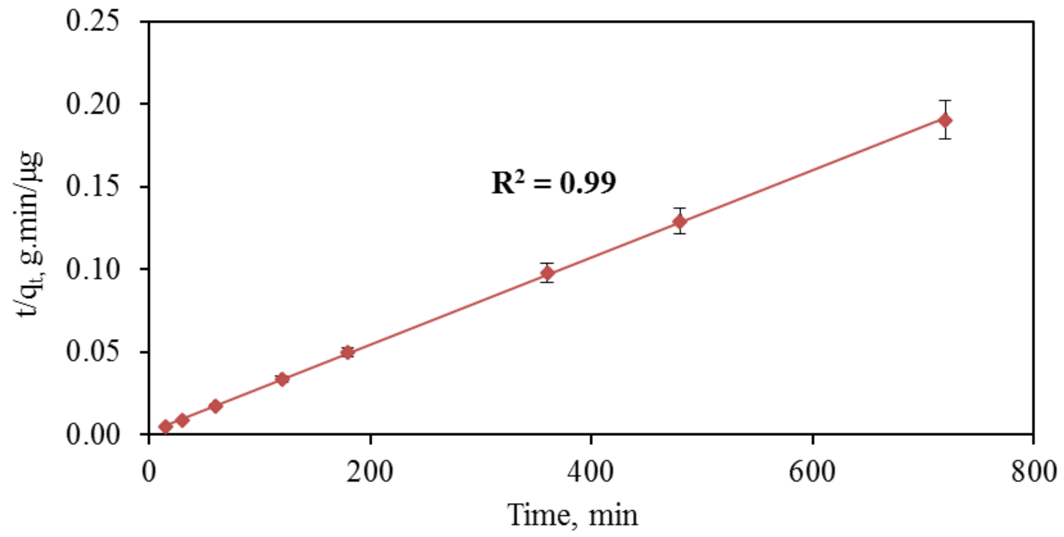

Figure 6.14. Adsorption rate of As(V) onto nZVI/GAC by pseudo-second order kinetic model. Initial As(V): 5000 µg/L, nZVI/GAC: 1 g/L in 0.1M NaCl, pH 4.5 controlled by a 0.01M acetate buffer.

Table 6.1 Comparison of initial sorption rates of nZVI/GAC and other materials

Name of materials	**Initial As(V) concentration, C_0 (µg/L)**	**Initial sorption rates, h (µg/g.min)**	**References**
Nanosized iron oxide-coated perlite	1000	447	Mostafa et al., 2011
Anion exchanger derived from coconut coir pith	5000	98	Anirudhan & Unnithan, 2007
Iron-doped activated carbon	300	38	Fierro et al., 2009
Activated carbon with iron hydro(oxide) nanoparticles	50	4	Vitela-Rodriguez & Rangel-Mendez, 2013
Untreated powdered eggshell	1500	10	Oke et al., 2008
Synthetic siderite	10000	179	Guo et al., 2010
nZVI/GAC	5000	666	This study

6.2.5 Effect of Co-existing Ions

The effect of common coexisting ions in contaminated drinking water on arsenate removal by nZVI/GAC at pH 4.5 and 6.5 is shown in Figures 6.15 and 6.16. Initial arsenate concentration was 5000 μg/L and the concentrations of competitive ions were 0.1 mM and 10 mM. It is seen from Figures 6.15 and 6.16 that 10 mM of phosphate has the maximum negative impact on arsenate adsorption followed by silicate. The effects of sulphate, nitrate, and fluoride, even in 10 mM concentration were minimal under experimental conditions. Arsenate, phosphate, and silicate can form inner-sphere complexes with the surfaces of iron oxides (Manning & Goldberg, 1996; Swedlund & Webster, 1999); iron (hydro)/oxide is a corrosion product of nZVI present on the adsorbent, nZVI/GAC. They would compete for similar binding sites and hence decreased the sorption of arsenic. Sulfate ions can be sorbed both specifically and non-specifically. Their bonding strength with iron (hydr)/oxide is much weaker than that of arsenate (Jia & Demopoulos, 2005). Common divalent metal cations such as Ca^{2+}, Mg^{2+}, Mn^{2+} were found to have co-operative behaviour on arsenate adsorption as was reported for iron (hydr)oxides (Jia & Demopoulos, 2005; Wilkie & Hering, 1996). The presence of metal cations could shift the adsorbent surface to a more positively charged nature, which might enable the adsorbent to show higher affinity for arsenate anions. In the present studies, these cations had a very little impact on arsenate adsorption. It can be surmised that the cations possess neither competitive nor co-operative behaviour on adsorption.

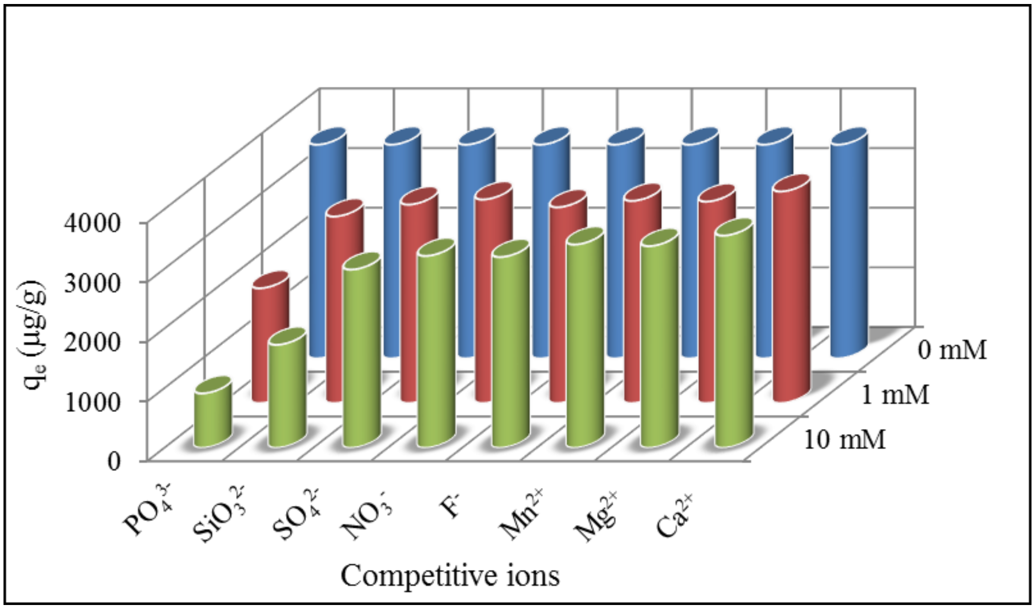

Figure 6.15. Effect of coexisting ions on arsenate adsorption. Initial As(V) concentration: 5000 μg/L, nZVI/GAC: 1 g/L in 0.1M NaCl, pH 4.5 adjusted by 0.1M HCl or NaOH.

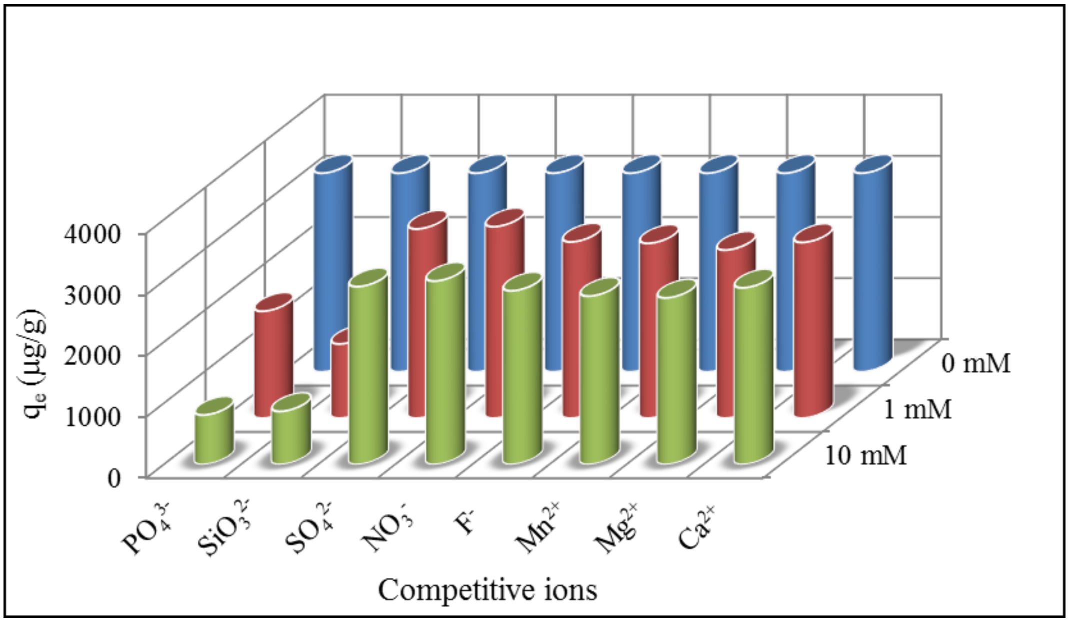

Figure 6.16. Effect of coexisting ions on arsenate adsorption. Initial As(V): 5000 μg/L, nZVI/GAC: 1 g/L in 0.1M NaCl, pH 6.5 adjusted by 0.1M HCl or NaOH.

6.3 Adsorption Isotherms

The adsorption data were fitted with the two popular isotherm models, Langmuir and Freundlich isotherm equations, to identify the most appropriate adsorption parameters to be used for future design purposes. The Langmuir model assumes monolayer adsorption onto a homogeneous surface with a finite number of identical sites, while the Freundlich is an empirical model assumes adsorption onto heterogeneous surfaces. Although, the correlation coefficients of the isotherms using linear regression analysis for As(V) adsorption at pH 4.5 were found to fit well with both Langmuir and Freundlich isotherm models , the Freundlich isotherm could be a better choice based on the higher root mean square value. The isotherms are shown in Figures 6.17 and 6.18.

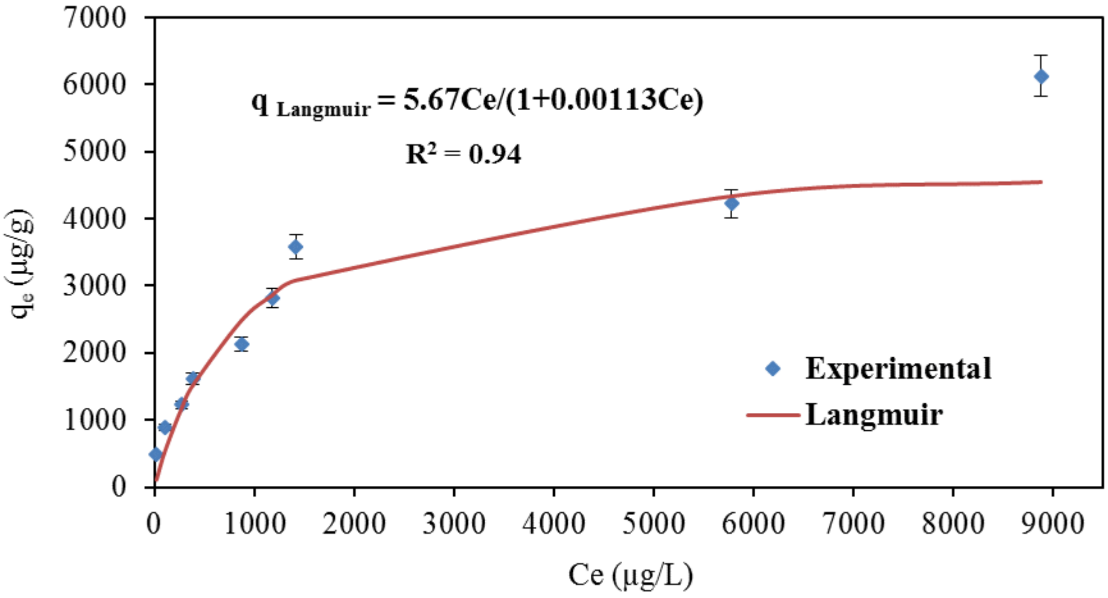

Figure 6.17. Langmuir adsorption isotherm of As(V) by nZVI/GAC. pH 4.5 controlled by a 0.01M acetate buffer, Equilibrium time: 12 h.

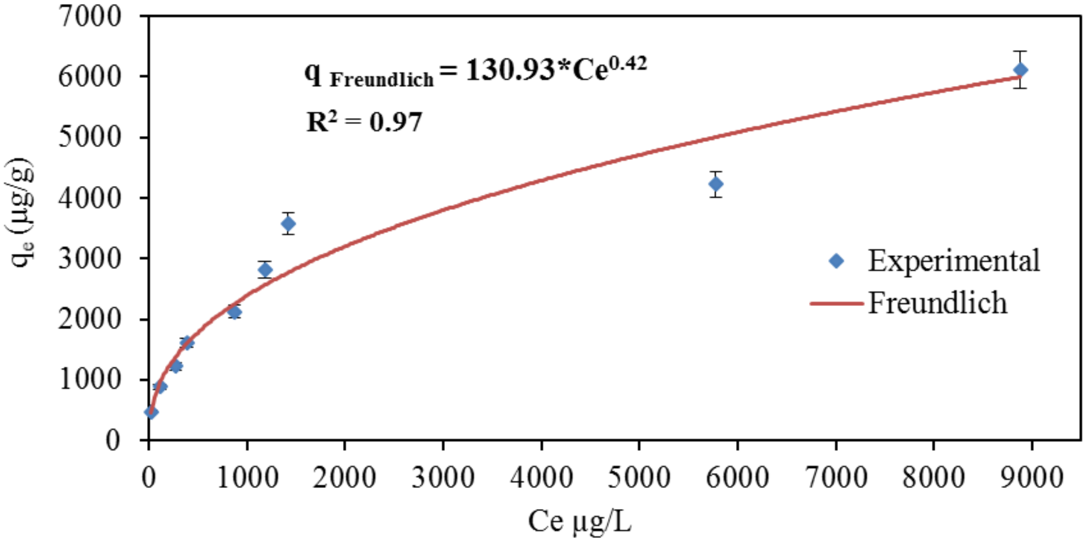

Figure 6.18. Freundlich adsorption isotherm of As(V) by nZVI/GAC. pH 4.5 controlled by a 0.01M acetate buffer, Equilibrium time: 12 h.

The magnitude of n also gives an indication of the favorability and capacity of the adsorbent/adsorbate system. The value of n (n=2.38) lies between 1 and 10 indicating a favorable Freundlich pattern of adsorption (Slejkop, 1985). The isotherm parameters are listed in Table 6.2.

Table 6.2 Isotherm parameters for As(V) adsorption on nZVI/GAC

Langmuir isotherm	Value	Freundlich isotherm	Value
q_{max} (µg/g)	5000	K_F (µg/g)(L/µg)$^{1/n}$	131
b (L/µg)	0.0011	n	2.38
R^2	0.94	R^2	0.97

The maximum adsorption capacity of nZVI/GAC determined from Langmuir and Freundlich isotherm models were 5000 µg/g and 6000 µg/g respectively at pH 4.5. This adsorption capacity of arsenate is comparable to the reported adsorbents: iron oxide-coated sand (43 µg/g)

(Thirunavukkarasu et al., 2003), nano iron (hydr)oxide impregnated granulated activated carbon (263 µg/g) (Hristovski et al., 2009), iron-containing ordered meso-porous carbon (7000 µg/g) (Gu et al., 2007), granular ferric hydroxide (GFH) (2300 µg/g) (Daus et al., 2004), Fe(III) oxide-impregnated GAC840 (4500 µg/g) (Reed et al., 2000). The higher adsorption capacity of nZVI/GAC could be due to the nano scale dispersion of iron oxides in the porous GAC structure that can create a large number of active sites for arsenate adsorption.

6.4 Desorption/Regeneration

The spent nZVI/GAC was regenerated by shaking the arsenic loaded adsorbent in 0.1M NaOH at room temperature. Approximately 87% of adsorbed arsenic was desorbed by the alkaline solution in 12 h. In comparison, desorption using phosphate at pH 4.5 and 6.5 only achieved a stripping efficiency of 32% and 47%, respectively (Figure 6.19). Similarly, it was reported that more than 90% of loaded arsenic on bead cellulose supported iron oxyhydroxide was desorbed with strong alkaline solutions (Guo & Chen, 2005). The desorption trend of arsenate from the spent adsorbent might be a result of the formation of stronger As-Fe complexes. The decreased amount of phosphate-extractable arsenate suggests either that the arsenate sorbed on the surface of the nZVI corrosion products forming stronger complexes (Grossl et al., 1997), or that part of it diffused into the interior sites of the nZVI corrosion products in the process of chemical transformation (Reinsch et al., 2010), making it less susceptible to phosphate displacement. It is possible to reuse the adsorbent after regeneration with NaOH.

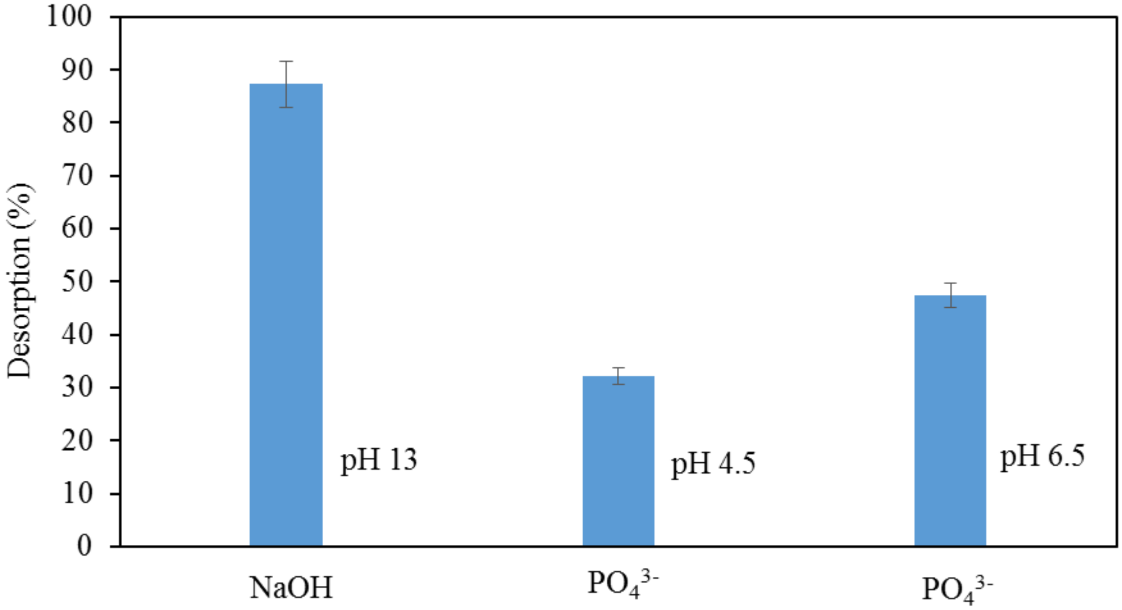

Figure 6.19. Desorption of As(V) by 0.1M NaOH and 0.1M PO_4^{3-} at different pHs

6.5 Disposal of Solid Waste (TCLP)

To safely dispose of the solid waste, the exhausted adsorbent was evaluated for arsenic leachability using the Toxicity Characteristic Leaching Procedure (TCLP) to determine whether it was hazardous. The current TCLP limit for arsenic is 5 mg/L (USEPA, 2003). Because the amount of adsorbent used in the experiment was small, only 1 g of the spent adsorbent was used in the test instead of 100 g as stated in the standard procedure. The spent adsorbent (1 g) was mixed with 20 mL of extraction liquid. After agitation, the filtrate was analyzed. The result showed that the concentration of leached arsenate in the filtrate was 2.15 mg/L which is much lower than the regulatory limit of 5 mg/L. Hence, the adsorbent can be safely disposed of without any treatment in a sanitary landfill.

6.6 Determination of Surface Diffusion Coefficients

The surface diffusion coefficient was determined from the differential column batch reactor (DCBR) rate study data. Solutions to the homogeneous surface diffusion model (HSDM) for batch reactors and fixed-beds were published by Hand et al. (1983). These solutions can be used to determine surface diffusion coefficients based on Freundlich isotherm parameters and other dimensionless parameters, such as the Biot number.

In this study the software FAST (Sperlich 2008) was used for the numerical solutions of HSDM for batch reactors to determine the surface diffusion coefficient. Initially the software needs, with other input parameters, a "guess" surface diffusion coefficient; this diffusion coefficient is varied and recorded when the experimental values vs. model prediction yields the smallest standard deviation. The DCBR experimental and the best fit simulation data are presented in Figure 6.20.

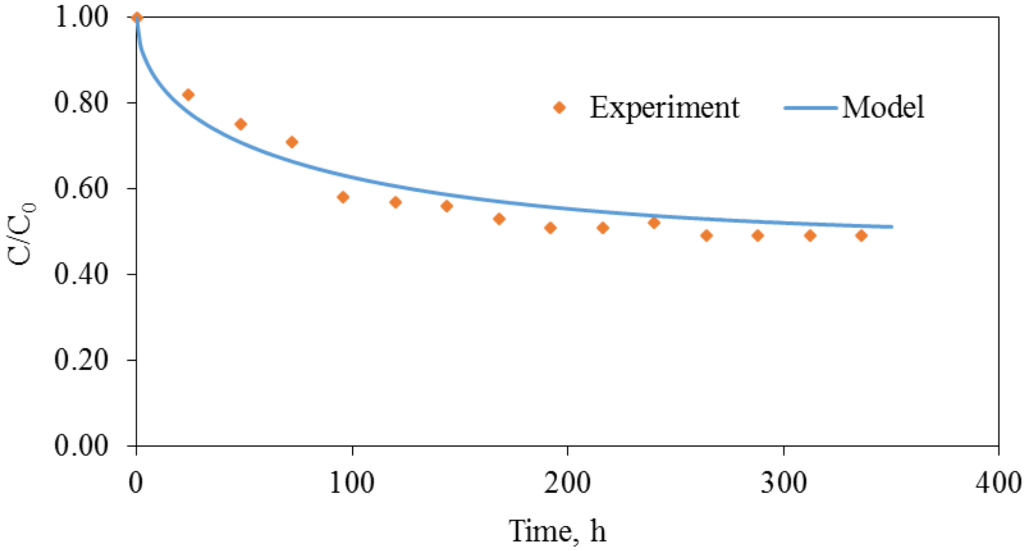

Figure 6.20. DCBR data and HSDM prediction (D_s =2.2x10^{-14} m^2/s)

The input data fed into the program are provided in Table 6.3. The determined value ($2.2\text{x}10^{-14}$ m^2/s) fits in the range of surface diffusivities from 10^{-16} to 10^{-10} m^2/s reported in the literature (Axe & Trivedi, 2002).

Table 6.3 DCBR input parameters for FAST

Parameters	**Value**	**Units**
Adsorbent mass, m	0.80	g
Particle density, ρ_p	0.85	g/cm^3
Particle diameter, d_p	0.0725	cm
Initial concentration, C_0	100	µg/L
Volume of reactor, V	10	L
Freundlich isotherm exponent,1/n	0.42	-
Freundlich isotherm coefficient, k_F	131	$(\mu g/g)(L/\mu g)^{1/n}$
Liquid-phase mass transfer coefficient, k_f	$5.723\text{x}10^{-05}$	m/s

Although surface diffusivity is assumed to be constant in the equations of the transport models, it has been shown that D_s is a function of adsorbate concentration and also particle size (Sontheimer et al., 1988). If D_s proved to be constant with particle size, the scaling equation 4.16 would be applicable for design. If the surface diffusion coefficients were linearly proportional to particle size, then the scaling equation 4.17, with a diffusivity factor of unity, would be applicable for design.

6.7 RSSCT

The dynamic behaviour of the columns was predicted by the HSDM model using the software FAST 2.0. The results of the mini column experiments are presented as breakthrough curves which are a plot of the normalized effluent arsenic concentration (C/C_0) versus the number of bed volumes of water treated. Comparison of experimental and HSDM predicted breakthrough curves are shown in Figures 6.21 through 6.26.

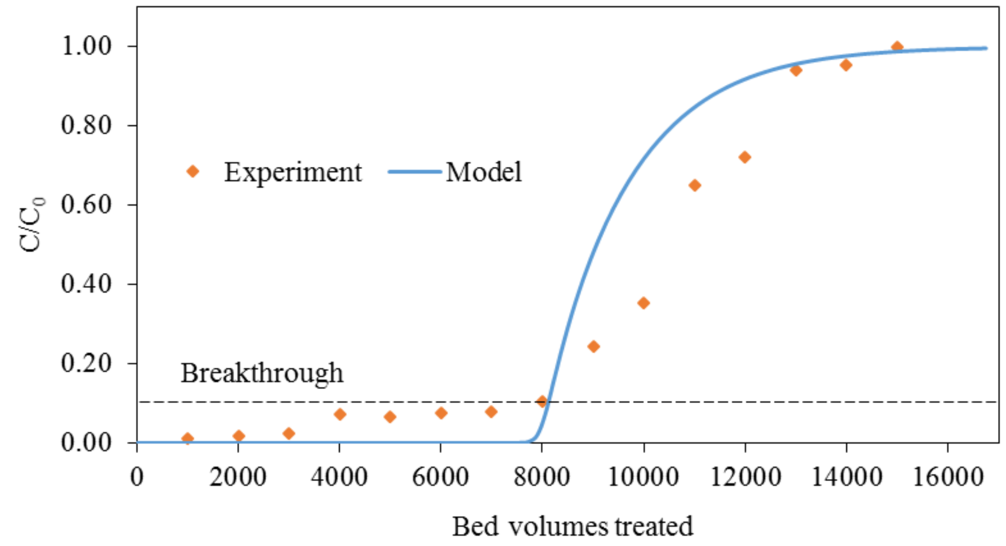

Figure 6.21. Experimental and HSDM predicted breakthrough curve for EBCT= 0.5 min

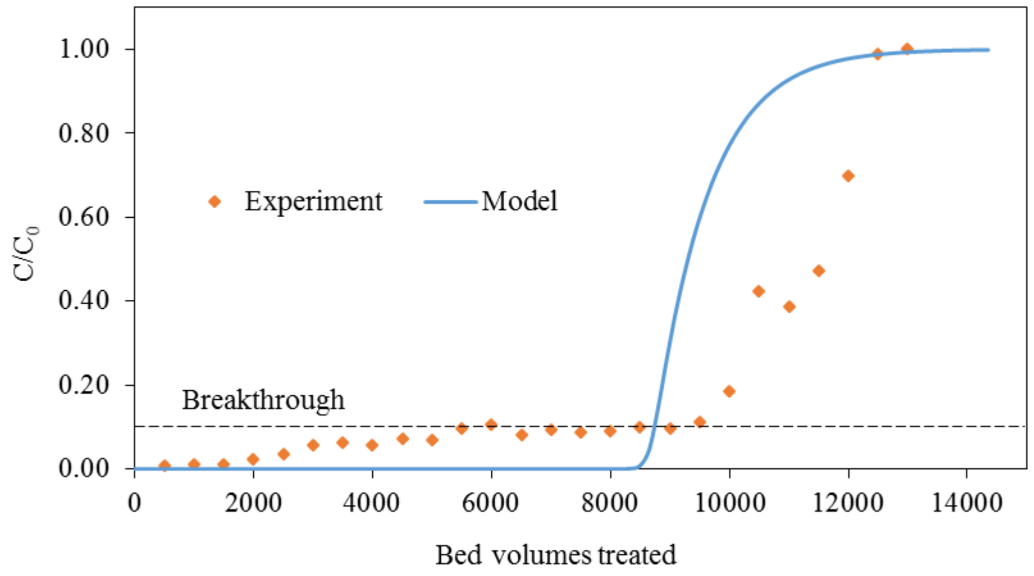

Figure 6.22. Experimental and HSDM predicted breakthrough curve for EBCT= 1.0 min

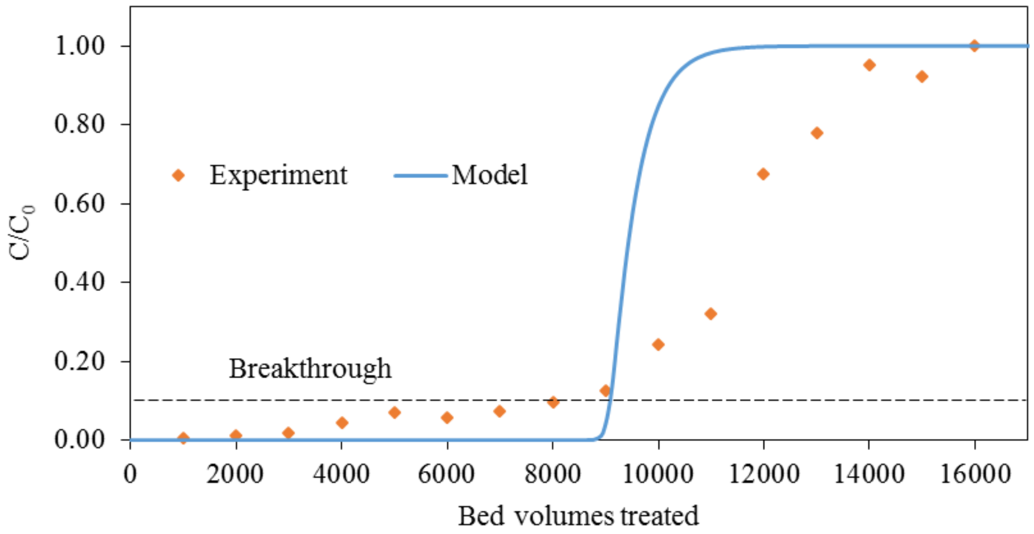

Figure 6.23. Experimental and HSDM predicted breakthrough curve for EBCT= 2.0 min

Figures 6.21-6.23 illustrate the effect of different EBCTs on the column performance. The EBCTs were selected as 0.5, 1.0, and 2.0 minutes by varying the flow rates to 10, 5, and 2.5 mL/min respectively while maintaining a constant influent concentration of 100 µg/L. From Figures 6.21-6.23 and Table 6.4, it can be seen that the number of bed volumes (BVs) treated increased with the increase of empty bed contact time (EBCT). As the EBCT increased from 0.5 minute to 1 minute and 2 minutes, the bed volumes at a breakthrough of 10 µg/L (BV_{10}) increased to 6.7% and 9.3% respectively. Sufficient contact time facilitates more mass transfer onto the surface and into the pores so that more arsenic can be removed at a longer EBCT.

Table 6.4 RSSCT performance based on EBCTs

Initial conc. (μg/L)	EBCT (min)	BVs at breakthrough of 10 μg/L (BV_{10})	BVs at saturation (BV_{sat})	Run time up to saturation (days)
100	0.5	7,500	14,000	4.86
100	1.0	8,000	13,000	9.02
100	2.0	8,200	16,000	22.22

Three different initial concentrations of 100, 50, and 20 μg/L were used to examine their effect on the breakthrough curve (Figures 6.24-6.26). These columns were run by keeping a constant EBCT of one minute i.e. a constant flow rate of 5 mL/min.

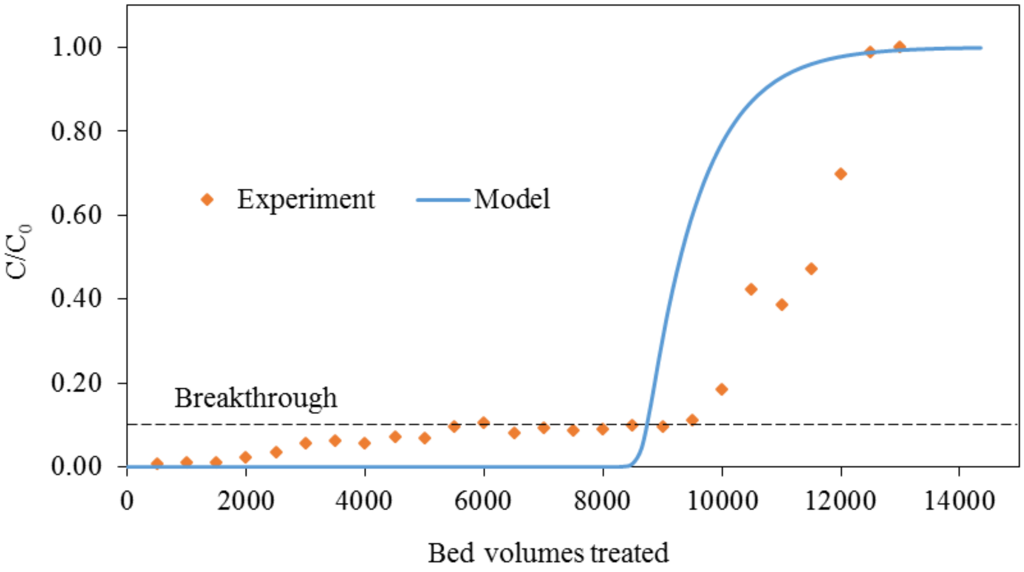

Figure 6.24. Experimental and HSDM predicted breakthrough curves for C_0 = 100 μg/L

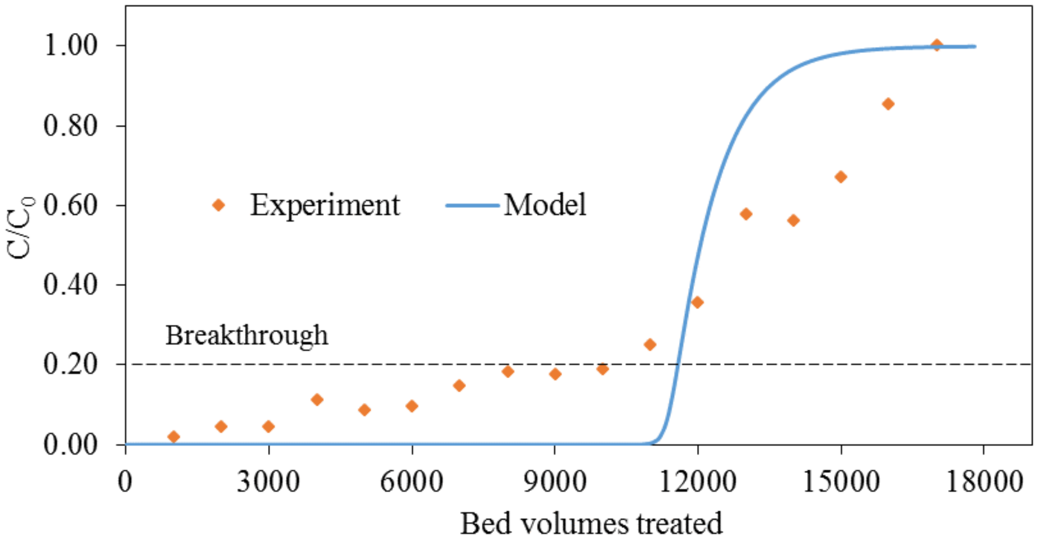

Figure 6.25. Experimental and HSDM predicted breakthrough curves for C_0 = 50 µg/L

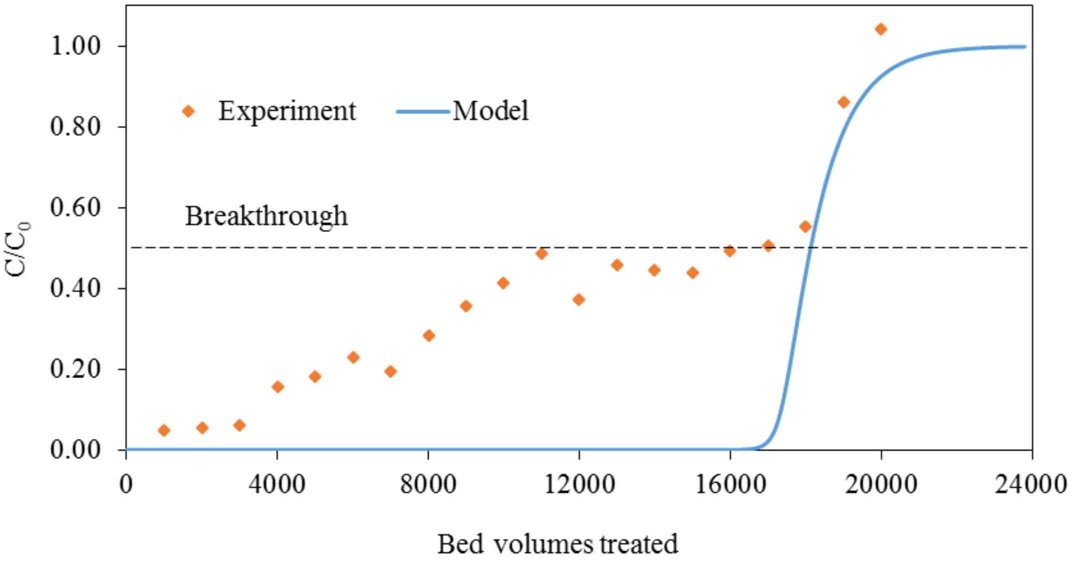

Figure 6.26. Experimental and HSDM predicted breakthrough curves for C_0 = 20 µg/L

Table 6.5 clearly demonstrates that the treated bed volumes increase with decreased initial concentration. The treated bed volumes increased to 25% and 112% when the initial concentration decreased from 100 µg/L to 50 µg/L and 20 µg/L respectively. Similar results were observed by Nguyen et al. (2011) when the arsenic concentration was decreased from 55 µg/L to 15 µg/L the bed volumes (BV_{10}) increased from 17,800 to 44,200 (148%) in GFH, from 10,700 to 25,100 9 (134%) in E33, and from 7,400 to 19,500 (163%) in Metsorb. With decreased arsenic concentration, it takes more time to cover the active sites present on the adsorbent yielding a delayed saturation of the bed; this translates to an extended breakthrough time that eventually leads to an increased number of bed volumes treated (Han et al., 2007).

Table 6.5 RSSCT performance based on initial concentrations

Initial conc. (µg/L)	EBCT (min)	BVs at breakthrough of 10 µg/L (BV_{10})	BVs at saturation (BV_{sat})	Run time up to saturation (days)
100	1.0	8,000	13,000	9.02
50	1.0	10,000	17,000	11.81
20	1.0	17,000	20,000	13.89

According to Hand et al. (1984), three categories of breakthrough curves were defined corresponding to different Biot numbers. Category (1): when $Bi \leq 0.5$, liquid-phase mass transfer rate controls the adsorption process and the effluent concentration profile curves sharply upward to $C/C_0 = 1.0$. Category (2): when $0.5 < Bi \leq 30$, both liquid- and solid-phase mass transfer rate controls the adsorption process and the effluent concentration profile tends to be S-shaped or sigmoidal. Category (3): when $Bi > 30$, solid-phase mass transfer rate controls the adsorption process and the effluent concentration profile will be concave downward, and it will asymptotically approach C_0. BTCs in categories 1 and 2 show sigmoidal breakthrough profiles and are most commonly found in organic pollutants adsorption onto activated carbon. The Biot numbers found for all RSSCTs were more than 30 (Bi = 43-88) except for the one examined to show the effect of initial concentration of 20 µg/L (Bi = 26). So the breakthrough characteristics should follow category 3 which is typical for arsenic as found by Aragon (2002).

However, the HSDM simulation exhibits some divergence from the monitored BTC, but correctly describes the initial phase. The ending phases of the BTCs specifically after the breakthrough do not perfectly follow the simulation data due to more than one type of bonding mechanism responsible for arsenic removal. Initially, the primary bond between the adsorbent and solute is due to electrostatic attraction between the anionic arsenic ions and the cationic iron oxide present on the nZVI/GAC. A strictly electrostatic mechanism would be expected to yield steep breakthrough curves similar to those from an ion exchange column. With time, mono- and bi-dentate covalent bonds form which are stronger. Fendorf et al. (1997) and other investigators have described the nature of these bonds. The presence of a second, slower but stronger adsorption mechanism, such as covalent bonding, contributes to the breakthrough curve in which internal diffusion and attachment effectively extend the length of the mass transfer zone. Another justification of dissimilarity in breakthrough curves can be explained by the fundamental assumptions incorporated in the HSDM. In HSDM, plug flow through the bed was assumed. This assumption is invalid due to advection, dispersion, diffusion, and adsorption taking place within the column. This is apparent in the breakthrough curves.

6.8 Arsenic Sorption Mechanism

It is proposed that adsorption of arsenic onto the surface of nZVI/GAC proceeds in three steps: (1) migration to the surface; (2) dissociation (or deprotonation) of complexed aqueous arsenic; (3) surface complexation (Myneni et al., 1998a; Jia et al., 2006; 2007; Raven et al., 1998; Wilkie &

Hering, 1996). Step 1 is the prerequisite of the adsorption reaction and largely controlled by electrostatic attraction or repulsion of the aqueous arsenate species with the surface of the adsorbent (Raven et al., 1998; Wilkie & Hering, 1996). Hence, the pH of zero point charge (pH_{ZPC}) of the adsorbent and the speciation of aqueous arsenate are governing factors. The degree of protonation of arsenate anions in aqueous solution is a function of pH. The dissociation constants of aqueous arsenate are $pK_{a1} = 2.2$, $pK_{a2} = 6.97$ and $pK_{a3} = 11.53$ (David & Allison, 1999), resulting in arsenate species varying from $H_2AsO_4^-$, $HAsO_4^{2-}$, to AsO_4^{3-} when pH increases from acidic to alkaline region. In the presence of water, iron oxide surface is generally covered with surface hydroxyl groups (Fe-OH). The oxide surface is protonated ($Fe\text{-}OH_2^+$) or deprotonated ($Fe\text{-}O^-$) when the pH is lower or higher than the zero point charge (pH_{ZPC}) respectively (Stumm and Morgan 1992). Interaction of an adsorbent surface functional group with an adsorbate ion or molecule creates a surface complex: inner sphere or outer sphere. The outer-sphere surface complex is formed when water layer exists between the adsorbate ion or molecule and the adsorbent surface functional groups. Then adsorption is solely based on electrostatic interactions and van der Waals forces. While inner-sphere surface complexation, either ionic or covalent bonds, are formed between adsorbate and adsorbent surface functional groups, no water layer exists between them. Outer- and inner-sphere surface complex can, and often do, occur simultaneously (Sparks, 2003) with one complex formed being predominant.

The pH_{ZPC} of the synthesized nZVI/GAC was determined to be pH 8.2, below which the surface is positively charged and favorable for the adsorption of anionic species. The surface of the adsorbent becomes less positively charged when the pH increases and hence shows less attraction towards anionic arsenate species. Therefore, the adsorption of arsenate decreased significantly all the way with increasing pH and this has been well documented in previous work of arsenate adsorption on ferrihydrite and nano zero-valent iron (Guo & Chen, 2005; Kanel et al., 2006; Raven et al., 1998; Jia & Demopoulos, 2005).

It is believed that the electrostatic attraction readily occurs at the initial stage of adsorption. As with time it turns into an inner-sphere surface complexation reaction. The inner-sphere surface complexation can be explained by FTIR data associated with the experimental results from XRD and SEM analyses. The XRD results reveal that the surface of the nZVI/GAC is composed of ZVI as well as different types of iron oxides. From the SEM image it is seen that the surface of the nZVI/GAC is heterogeneous in nature, full of cracks and micro/macro pores, which is filled with the iron oxides/hydroxides and iron nano-particles. The higher efficiency of arsenic removal is due to the enhanced adsorption on the reactive nZVI or on the corrosion products of nZVI i.e. the surface oxide shell. The adsorption can proceed via ligand exchange/surface complex reactions between arsenate anions and surface OH or other groups. The ligand exchange mechanism was confirmed by the increasing solution pH with the increase in reaction time during the batch experiment. The FTIR spectra of As(V)-adsorbed nZVI/GAC (Figure 6.5) revealed that the band shift observed attributed to the formation of inner-sphere complexes. The peak positions of the dissolved arsenate species were different from those of the adsorbed ones, which were an indication of forming complex and contributed to symmetry reduction. The lower desorption rate by phosphate can be related to the result of complex formation between As(V) and nZVI corrosion products.

The adsorption of As(V) on nZVI/GAC was ascribed as either monodentate [$(FeO)AsO_3^-$] and or bidentate complexes [$(FeO)_2AsO_2$)] (Dong et al., 2012). This is in good agreement with the results of FTIR characterization of As-adsorbing ferrihydrite and ferric oxide reported by Jia et al. (2007) and Goldberg and Johnston (2001). The EXFAS studies also indicated that As(V) was predominantly adsorbed on goethite (O'Reilly et al., 2001) and on green rust (Randall et al., 2001) as inner-sphere bidendate binuclear surface complexes.

The removal of As(III) could be due to the partial oxidation of As(III) to As(V) on nano scale zero-valent iron (nZVI). The oxidation of As(III) to As(V) was found during ZVI batch and column experiments (Sasaki et al., 2009). They proposed the oxidants could be the ZVI corrosion products. Kanel et al. (2005) also found that As(III) was partially oxidized to As(V) on the surface of nano scale ZVI after 12 hours incubation. A simultaneous process of iron corrosion and As(III) oxidation were reported by Noubactep (2008). The lower adsorption rate of As(III) can be related to its partial oxidation on nZVI; complete oxidation of As(III) to As(V) can ensure better removal of arsenite. The authors proposed a schematic of the arsenic adsorption mechanism on nZVI/GAC as shown in Figure 6.27.

In summary, the composite material nZVI/GAC contains the nZVI which has a core-shell structure. The core consists of mainly zero valent iron and the shell is largely iron oxide/hydroxides formed due to the oxidation of ZVI. The shell provides the sites for adsorption. At acidic pH, arsenate anions and positively charged adsorbent surface (adsorbent's pH_{zpc} 8.2) favoures arsenate adsorption. Hence, the arsenate removal is maximum in the pH range of 2-6.5. At pH 6.8~8, the positive charge on the adsorbent surface reduces and as a result, the arsenate removal declines. At a higher pH range of 8.5~11, the adsorption sharply decreases as the negatively charged adsorbent surface repels the arsenate anions.

In the case of arsenite, a partial oxidation occurs while the nZVI corrodes. At a pH below 9.2, arsenite exists as a non-ionic form which exerts little interaction with the positively charged adsorbent surface. This is why arsenite removal is lower at a wider pH range of 2-11.

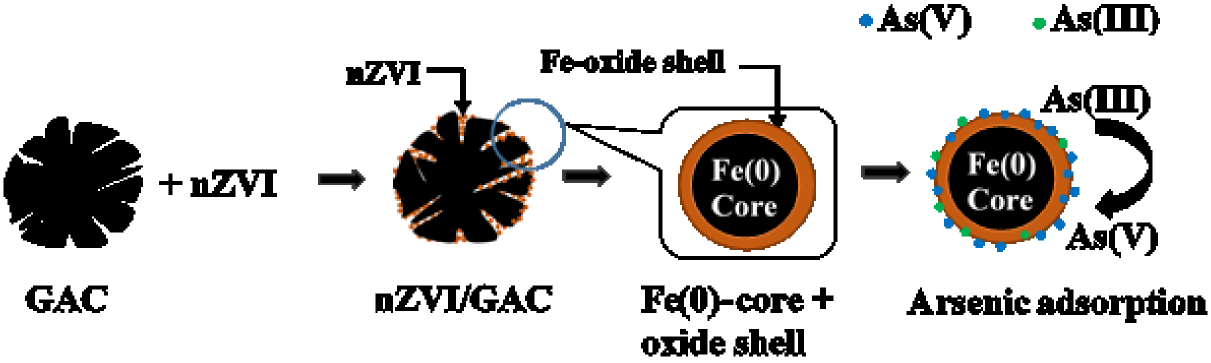

Figure 6.27. Schematic of the proposed arsenic adsorption mechanism on nZVI/GAC

Chapter 7

Conclusions, Contributions, and Recommendations for Future Work

7.1 Conclusions

Granular activated carbon was modified by incorporating nano scale zero-valent iron (nZVI/GAC) and its performance for arsenic removal from drinking water was investigated by batch and rapid small scale column test (RSSCT). The RSSCT data were simulated by the HSDM model using the software FAST 2.0. The synthesized adsorbent, nZVI/GAC was characterized by SEM/EDS, BET, XRD, and FTIR. Based on the experimental results, the following conclusions can be drawn.

- It was found that virgin GAC is not suitable for arsenite or arsenate removal due to its low adsorption capacity (~170 μg/g); the adsorption is insensitive to a pH range of 2-11. Arsenite adsorption on nZVI/GAC varies a little with the capacity range 800~1400 μg/g depending on pH in the range of 2-11.
- The study also shows that the removal of arsenate depends on pH, initial arsenate concentration, and contact time.
- The pH dependent arsenate adsorption was found higher (3000-3700 μg/g) over the acidic pH range 2-6.5 and relatively lower (1350-885 μg/g) in the pH range 7.5-11.
- The maximum adsorption capacity of nZVI/GAC determined from Langmuir and Freundlich isotherm models were 5000 μg/g and 6000 μg/g respectively at pH 4.5.

- The initial concentration affected the adsorption capacity as it increased from 480 to 6124 µg/g with the increase of initial concentration from 500 to 15000 µg/L.
- The effect of contact time on adsorption showed that 66% adsorption was achieved in 15 min and 72% in 120 min.
- The effect of common ions present in drinking water on adsorption of arsenate was examined. Arsenate adsorption efficiency was markedly decreased in the presence of phosphate or silicate, while the effects of sulfate, nitrate, chloride, fluoride, manganese, magnesium and calcium were insignificant. This is because anions like phosphate, silicate, and sulfate showed competitive while cations like manganese, magnesium and calcium showed neither competitive nor cooperative behaviour with arsenate for sorption. The rate of adsorption was relatively fast and followed a pseudo-second order kinetics model. The initial sorption rate (h) calculated from pseudo-second order kinetic model was 666 µg/g.min.
- SEM micro image analyses confirmed that the loaded zero-valent iron in the pores was spherical in shape.
- The elemental composition of pristine GAC and arsenic loaded nZVI/GAC by Energy Dispersive Spectroscopy (EDS) revealed the presence of arsenic on nZVI/GAC. This ensures the bonding between the adsorbent and arsenic.
- BET surface area analyses showed the reduction of surface area (from 952 to 654 m^2/g) and pore volume (from 0.455 to 0.328 cm^3/g) of the nZVI/GAC in comparison to the pristine GAC. These reductions were due to the deposition of iron oxide/ZVI onto the pores of the GAC.
- XRD reveals that the surface of the nZVI/GAC is a mixture of nZVI corrosion products including amorphous iron(III) oxide/hydroxide, magnetite (Fe_3O_4), and/or maghemite (γ-

Fe_2O_3). These oxide surfaces provide the potential of forming spontaneous complexes with arsenic species.

- The complex formation was supported by the FTIR analyses of the dissolved and solid phase arsenate species. The symmetry reduction arising from the arsenic oxyanion adsorption was attributable to the formation of inner-sphere complexes. The studies confirmed the formation of monodentate [$(FeO)AsO_3^-$] and bidentate [$(FeO)_2AsO_2$] complexes.
- The regeneration of spent nZVI/GAC using alkaline solution of 0.1M NaOH was effective as it desorbed 87% of adsorbed arsenic. Desorption using phosphate at pH 4.5 and 6.5 was not effective as it only achieved the efficiency of 32% and 47%, respectively.
- It was determined by the TCLP that the concentration of leached arsenate in the filtrate was 2.145 mg/L which is much lower than the regulatory limit of 5 mg/L. Hence the solid waste can be safely disposed of in a sanitary landfill without any treatment.
- To predict the performance of full-scale column, rapid small-scale column test (RSSCT) was performed. The dynamic behaviour of the columns was predicted by the HSDM model using the software FAST 2.0. In comparison of experimental and HSDM predicted breakthrough curves there were some divergence between them. The initial phases of the breakthrough curves were correctly described but the ending phases of the BTCs specifically after the breakthrough did not follow the simulation data likely due to more than one type of bonding mechanism responsible for arsenic removal.
- From the RSSCT results it was found that the number of bed volumes treated depends on the empty bed contact time (EBCT) as well as the initial arsenate concentration. The number of bed volumes increased with increasing EBCTs and decreasing initial concentration. As the EBCT increased from 0.5 minute to 1 minute and 2 minutes the bed volumes at breakthrough

of 10 µg/L (BV_{10}) increased to 6.7% and 9.3% respectively. The bed volumes (BV_{10}) increased to 25% and 112% when the initial concentration decreased from 100 µg/L to 50 µg/L and 20 µg/L respectively.

From the experimental results and discussion it can be concluded that nZVI/GAC is a promising adsorbent for removing arsenate from contaminated drinking water.

7.2 Contributions

The original contribution of the research based on the experimental findings can be summarized as follows.

- A novel type of adsorbent, loaded with nano scale zero-valent iron, was introduced to effectively remove arsenic from contaminated water. The adsorbent was characterized by SEM/EDS, XRD, BET surface area, and FTIR analyses.
- The investgation revealed that the removal efficiency is affected by these factors: pH, initial concentration, and contact time.
- It was found that some of the common ions present in drinking water had an adverse impact while the others had insignificant impact on the removal efficieny.
- The studies confirmed that the regeneration of the adsorbent is possible and the spent adsorbent can be safely disposed of as a non-hazardous material.
- It was found from the rapid small-scale column test (RSSCT) that the empty bed contact time (EBCT) and the initial arsenic concentration had a significant impact on the column performance.
- The complex reactions between arsenic anions and the corrosion products of the zero valent iron were evidenced as the removal mechanism of arsenic from water.

7.3 Recommendations for Future Work

Drinking water contamination by arsenic is a huge concern to the scientific community all over the world. In a single research work it is not possible to consider all the facets of the problem. This study focused and clearly explained some of the aspects of the problem. Based on the results found in this study the modified adsorbent material seems promising in removing arsenate from drinking water. To find a comprehensive solution in removing arsenic the following points should be considered for future work.

- Arsenic speciation needs to be done in the solid phase (spent adsorbent) to examine the redox reaction. The speciation can better help explain the adsorption mechanism.
- The column operation needs to be performed with different particle size to verify whether the breakthrough curve follows the CD or PD pattern. In the case of the PD pattern, also it is required to identify whether the diffusivity varies linearly or nonlinearly with regard to the particle size.
- A pilot-scale column should be run to validate the RSSCT data. This will ensure the extent of discrepancy, if any, of the scaling procedure between the pilot and large-scale columns. Also the column needs to be operated with real contaminated water to find out the effect of other impurities on adsorption.
- The change of adsorption capacity and desorption behaviour, if any, needs to be verified due to the aging of the modified adsorbent materials.
- To find the best match of the experimental data other mathematical models need to be examined or developed.
- The cost analysis needs to be done in order to justify the economic feasibility of the adsorption process.

References

Aksu, Z., & Gönen, F. (2004). Biosorption of phenol by immobilized activated sludge in a continuous packed bed: prediction of breakthrough curves. *Process Biochemistry*, *39*(5), 599-613.

Al-Duri, B. & McKay, G. 1995. (eds), Adsorption Modeling and Mass Transfer, CRC, Boca Raton, FL, USA, pp 133-173.

Alowitz, M. J., & Scherer, M. M. (2002). Kinetics of nitrate, nitrite, and Cr (VI) reduction by iron metal. *Environmental Science & Technology*, *36*(3), 299-306.

American Water Works Association Research Foundation (AWWARF). (2000). Arsenic Treatability Options and Evaluation of Residuals Management Issues, Amy, G.L., M. Edwards, P. Brandhuber, L. McNeill, M. Benjamin, F. Vagliasindi, K. Carlson, and J. Chwirka., Denver, CO.

Andreae, M. O. (1978). Distribution and speciation of arsenic in natural waters and some marine algae. *Deep Sea Research*, *25*(4), 391-402.

Anirudhan, T. S., & Unnithan, M. R. (2007). Arsenic (V) removal from aqueous solutions using an anion exchanger derived from coconut coir pith and its recovery. *Chemosphere*, *66*(1), 60-66.

Appelo, C. A. J., Van der Weiden, M. J. J., Tournassat, C., & Charlet, L. (2002). Surface complexation of ferrous iron and carbonate on ferrihydrite and the mobilization of arsenic. *Environmental Science & Technology*, *36*(14), 3096-3103.

Aragon, A. R. (2004). Ph.D dissertation: Development of Small-Scale Column Testing Procedure for the Evaluation of Arsenic Adsorption Media, University of New Mexico.

Azcue, J. M. and Nriagu, J. O. 1994. Arsenic: Historical perspectives, in: Nriagu, J.O. (editor), *Arsenic in the Environment, Part1: Cycling and Characterization*, John Wiley & Sons, New York, NY, USA.

Azcue, J. M., & Nriagu, J. O. (1995). Impact of abandoned mine tailings on the arsenic concentrations in Moira Lake, Ontario. *Journal of Geochemical Exploration*, *52*(1), 81-89.

Badruzzaman, M., & Westerhoff, P. (2005). "The Application of Rapid Small Scale Column Tests (RSSCTs) In Iron-based Pakecd Bed Arsenic Treatment Systems." Advances in arsenic research: Integration of experimental and observational studies and implications for mitigation, ACS symposium series, New York City, NY, 146.

Ballantyne, J. M., & Moore, J. N. (1988). Arsenic geochemistry in geothermal systems. *Geochimica et Cosmochimica Acta, 52*(2), 475-483.

Banerjee, K., Helwick, R. P., & Gupta, S. (1999). A treatment process for removal of mixed inorganic and organic arsenic species from groundwater. *Environmental Progress*, *18*(4), 280-284.

Bang, S., Johnson, M. D., Korfiatis, G. P., & Meng, X. (2005). Chemical reactions between arsenic and zero-valent iron in water. *Water Research*, *39*(5), 763-770.

Belton, J. C., Benson, N. C., Hanna, M. L., & Taylor, R. T. (1985). Growth inhibitory and cytotoxic effects of three arsenic compounds on cultured Chinese hamster ovary cells. *Journal of Environmental Science & Health Part A*, *20*(1), 37-72.

Benefield, L. D., Judkins, J. F., & Weand, B. L. (1982). *Process Chemistry for Water and Wastewater Treatment*. Prentice Hall Inc.

Berg, M., Tran, H. C., Nguyen, T. C., Pham, H. V., Schertenleib, R., & Giger, W. (2001). Arsenic contamination of groundwater and drinking water in Vietnam: a human health threat. *Environmental Science & Technology*, *35*(13), 2621-2626.

Bhumbla, O. K. & Keefer, R. F. (1994). Arsenic Mobilization and Bioavailability in Soils. In: Arsenic in the Environment, Part I: Cycling and Characterization. 10. Nriagu (Ed.). New York: Wiley-Interscience, 51-82.

Borum, D. R. & Abernathy, C.O. (1994). In: Arsenic Exposure and Health Effects*,* Chappel, W.R., Abernathy, C.O., Cothern, C.R., Eds. *Science and Technology Lett*. Northwood, U.K.

Boyle, D. R., Turner, R. J. W., & Hall, G. E. M. (1998). Anomalous arsenic concentrations in groundwaters of an island community, Bowen Island, British Columbia. *Environmental Geochemistry and Health*, *20*(4), 199-212.

Buche, B. D., & Owens, L. P. (1996). Removal of arsenic from ground water using granular activated carbon. In *North American Water and Environment Congress & Destructive Water* (pp. 1173-1177). ASCE.

Budinova, T., Petrov, N., Razvigorova, M., Parra, J., & Galiatsatou, P. (2006). Removal of arsenic (III) from aqueous solution by activated carbons prepared from solvent extracted olive pulp and olive stones. *Industrial & Engineering Chemistry Research*, *45*(6), 1896-1901.

Caly, L., & LR, R. (1994). Interfacial chemistry and electrochemistry of carbon surfaces. *Chemistry and Physics of Carbon*, *24*, 213-310.

Campbell, C. T., & Parker, S. C. (2002). The effect of size-dependent nanoparticles energetics on catalyst sintering. *Science, 298*, 811-814.

Cao, J., Wei, L., Huang, Q., Wang, L., & Han, S. (1999). Reducing degradation of azo dye by zero-valent iron in aqueous solution. *Chemosphere*, *38*(3), 565-571.

Capek, I. (2004). Preparation of metal nanoparticles in water-in-oil (w/o) microemulsions. *Advances in Colloid and Interface Science*, *110*(1), 49-74.

Ćavar, S., Klapec, T., Grubešić, R. J., & Valek, M. (2005). High exposure to arsenic from drinking water at several localities in eastern Croatia. *Science of the Total Environment*, *339*(1), 277-282.

Chang, Q., Lin, W., & Ying, W. C. (2010). Preparation of iron-impregnated granular activated carbon for arsenic removal from drinking water. *Journal of Hazardous Materials*, *184*(1), 515-522.

Chen, H. W., Frey, M. M., Clifford, D., McNeill, L. S., & Edwards, M. (1999). Arsenic treatment considerations. *Journal-American Water Works Association*, *91*(3), 74-85.

Chen, W., Parette, R., Zou, J., Cannon, F. S., & Dempsey, B. A. (2007). Arsenic removal by iron-modified activated carbon. *Water Research*, *41*(9), 1851-1858.

Choi, H., Al-Abed, S. R., Agarwal, S., & Dionysiou, D. D. (2008). Synthesis of reactive nano-Fe/Pd bimetallic system-impregnated activated carbon for the simultaneous adsorption and dechlorination of PCBs. *Chemistry of Materials*, *20*(11), 3649-3655.

Chowdhury, M. R. I., & Mulligan, C. N. (2011). Biosorption of arsenic from contaminated water by anaerobic biomass. *Journal of Hazardous Materials*, *190*(1), 486-492.

Chwirka, J., Thompson, B. M., & Stomp III, J. M. (2000). Removing arsenic from groundwater. *Journal of the American Water Works Association*, *92*(3), 79-88.

Clifford, D., & Ghurye, G. (2001). Oxidizing arsenic III to arsenic V for better removal. *Water Quality Products*, *3,* 28-29.

Clifford, D. (1999). Ion Exchange and Inorganic Adsorption. Water Quality and Treatment: A Handbook of Community Water Supplies. R. D. Letterman. New York, McGraw-Hill, Inc.

Coumans, C. (2003). Mining in Canada: the bigger picture. Presentation for Philippine delegation to Ottawa, Canada.

Crittenden, J. C., Reddy, P. S., Arora, H., Trynoski, J., Hand, D. W., Perram, D. L., & Summers, R. S. (1991). Predicting GAC performance with rapid small-scale column tests. *Journal-American Water Works Association*, *83*(1), 77-87.

Crittenden, J. C., Berrigan, J. K., Hand, D. W., & Lykins, B. (1987). Design of rapid fixed-bed adsorption tests for nonconstant diffusivities. *Journal of Environmental Engineering*, *113*(2), 243-259.

Cullen, W. R., & Reimer, K. J. (1989). Arsenic speciation in the environment. *Chemical Reviews*, *89*(4), 713-764.

Daus, B., Wennrich, R., & Weiss, H. (2004). Sorption materials for arsenic removal from water: a comparative study. *Water Research*, *38*(12), 2948-2954.

David, S. B., & Allison, J. D. (1999). Minteqa2, an equilibrium metal speciation model: User's manual 4.01. Environmental Research laboratory, US Environmental Protection Agency: Athens, GA.

Davis, J. A., James, R. O., & Leckie, J. O. (1978). Surface ionization and complexation at the oxide/water interface: I. Computation of electrical double layer properties in simple electrolytes. *Journal of Colloid and Interface Science*, *63*(3), 480-499.

Demirbaş, O., Alkan, M., & Doğan, M. (2002). The removal of Victoria blue from aqueous solution by adsorption on a low-cost material. *Adsorption*, *8*(4), 341-349.

Deng, B., Caviness, M. & Gu, Z. (2005). Arsenic removal by activated carbon-based materials. In *Advances in Arsenic Research: Integration of Experimental and Observational Studies and Implications for Mitigation*, Vlassopoulos, D., Benning, L., Meng, X., O'Day, P., Eds.; ACS Symposium Series; American Chemical Society: Washington, DC, USA.

Dixon, H. B. (1996). The biochemical action of arsonic acids especially as phosphate analogues. *Advances in Inorganic Chemistry*, *44*, 191-227.

Domenico, P. A., & Schwartz, F. W. (1998). Physical and chemical hydrogeology (Vol. 44). New York: Wiley.

Domingo, J. L. (1994). Metal-induced developmental toxicity in mammals: A review. *Journal of Toxicology and Environmental Health, Part A Current Issues*,*42*(2), 123-141.

Dong, H., Guan, X., & Lo, I. M. (2012). Fate of As (V)-treated nano zero-valent iron: determination of arsenic desorption potential under varying environmental conditions by phosphate extraction. *Water research*, *46*(13), 4071-4080.

Drever, J. I. (1997). *The Geochemistry of Natural Waters: Surface and Groundwater Environments*.

Driehaus, W., Jekel, M., & Hildebrandt, U. (1998). Granular ferric hydroxide-a new adsorbent for the removal of arsenic from natural water. *Aqua*, *47*, 30-35.

Edwards, M. (1994). Chemistry of arsenic removal during coagulation and Fe-Mn oxidation. *Journal-American Water Works Association*, *86*(9), 64-78.

Eguez, H. E., & Cho, E. H. (1987). Adsorption of arsenic on activated charcoal. *JOM*, *39*(7), 38-41.

Elliott, D. W., & Zhang, W. X. (2001). Field assessment of nanoscale bimetallic particles for groundwater treatment. *Environmental Science & Technology*, *35*(24), 4922-4926.

European Commission Directive**. (**1998). Related with drinking water quality intended for human consumption. 98/831EC*,* Brussels, Belgium.

Farrell, J., Wang, J., O'Day, P., & Conklin, M. (2001). Electrochemical and spectroscopic study of arsenate removal from water using zero-valent iron media. *Environmental Science & Technology*, *35*(10), 2026-2032.

Faust, S. D., & Aly, O. M. (1987). *Adsorption Processes for Water Treatment*. Boston: Butterworth.

Fendorf, S., Eick, M. J., Grossl, P., & Sparks, D. L. (1997). Arsenate and chromate retention mechanisms on goethite. 1. Surface structure. *Environmental Science & Technology*, *31*(2), 315-320.

Fields, K., Chen, A. S., Wang, L., & Sorg, T. J. (2000). Arsenic removal from drinking water by iron removal plants. National Risk Management Research Laboratory, Office of Research and Development, US Environmental Protection Agency.

Fierro, V., Muñiz, G., Gonzalez-Sánchez, G., Ballinas, M. L., & Celzard, A. (2009). Arsenic removal by iron-doped activated carbons prepared by ferric chloride forced hydrolysis. *Journal of Hazardous Materials*, *168*(1), 430-437.

Figueiredo, J. L., Pereira, M. F. R., Freitas, M. M. A., & Orfao, J. J. M. (1999). Modification of the surface chemistry of activated carbons. *Carbon*, *37*(9), 1379-1389.

Fowler, B. A. (1977). Toxicology of environmental arsenic, In: Toxicology of Trace Elements. *Advances in Modern Toxicology*, *Vol. 2, pp*. 79-122. Goyer, R.A. & Mehlman, M.A. (Eds.). Hemisphere, Washington, D.C.

Franzblau, A., & Lilis, R. (1989). Acute arsenic intoxication from environmental arsenic exposure. *Archives of Environmental Health: An International Journal*, *44*(6), 385-390.

Freundlich, H. (1906). Über die adsorption in lösungen. *Engelmann, Leipzig*.

Frey, M. M., Owen, D. M., Chowdhury, Z. K., Raucher, R. S., & Edwards, M. A. (1998). Cost to Utilities of a Lower MCL for Arsenic. *Journal-American Water Works Association*, *90*(3), 89-102.

Friedman, G., (1984). Mathematical modeling of multicomponent adsorption in batch and fixed-bed reactors. *Master's Thesis*. Michigan Technological University.

Gavaskar, A. R., Sass, N. N. M., Janoy, R. J., & O'Sullivan, D. (1998). Permeable Barriers for Goundwater Remediation-Design, Construction, and Monitoring, Battelle Memorial Institute, Columbus, OH.

Ghimire, K. N., Inoue, K., Yamaguchi, H., Makino, K., & Miyajima, T. (2003). Adsorptive separation of arsenate and arsenite anions from aqueous medium by using orange waste. *Water Research*, *37*(20), 4945-4953.

Ghurye, G. L., Clifford, D. A., & Tripp, A. R. (1999). Combined arsenic and nitrate removal by ion exchange. *Journal-American Water Works Association*, *91*(10), 85-96.

Gillham, R. W., & O'Hannesin, S. F. (1994). Enhanced degradation of halogenated aliphatics by zero-valent iron. *Ground Water*, *32*(6), 958-967.

Glavee, G. N., Klabunde, K. J., Sorensen, C. M., & Hadjipanayis, G. C. (1995). Chemistry of borohydride reduction of iron (II) and iron (III) ions in aqueous and nonaqueous media. Formation of nanoscale Fe, FeB, and Fe2B powders. *Inorganic Chemistry*, *34*(1), 28-35.

Goldberg, S., & Johnston, C. T. (2001). Mechanisms of arsenic adsorption on amorphous oxides evaluated using macroscopic measurements, vibrational spectroscopy, and surface complexation modeling. *Journal of Colloid and Interface Science*, *234*(1), 204-216.

Gong, W. (2001). A real time in situ ATR-FTIR spectroscopic study of linear phosphate adsorption on titania surfaces. *International journal of mineral processing*, *63*(3), 147-165.

Greenwood, N. N., Earnshaw, A. (1984). Chemistry of the elements. Pergamon Press, London.

Grossl, P. R., Eick, M., Sparks, D. L., Goldberg, S., & Ainsworth, C. C. (1997). Arsenate and chromate retention mechanisms on goethite. 2. Kinetic evaluation using a pressure-jump relaxation technique. *Environmental Science & Technology*, *31*(2), 321-326.

Gu, B., Liang, L., Dickey, M. J., Yin, X., & Dai, S. (1998). Reductive precipitation of uranium (VI) by zero-valent iron. *Environmental Science & Technology*, *32*(21), 3366-3373.

Gu, Z., Deng, B., & Yang, J. (2007). Synthesis and evaluation of iron-containing ordered mesoporous carbon (FeOMC) for arsenic adsorption. *Microporous and Mesoporous Materials*, *102*(1), 265-273.

Gu, Z., Fang, J., & Deng, B. (2005). Preparation and evaluation of GAC-based iron-containing adsorbents for arsenic removal. *Environmental Science & Technology*, *39*(10), 3833-3843.

Guan, X. H., Wang, J., & Chusuei, C. C. (2008). Removal of arsenic from water using granular ferric hydroxide: macroscopic and microscopic studies. *Journal of Hazardous Materials*, *156*(1), 178-185.

Guo, H., Li, Y., & Zhao, K. (2010). Arsenate removal from aqueous solution using synthetic siderite. *Journal of Hazardous Materials*, *176*(1), 174-180.

Guo, X., & Chen, F. (2005). Removal of arsenic by bead cellulose loaded with iron oxyhydroxide from groundwater. *Environmental Science & Technology*, *39*(17), 6808-6818.

Gupta, V. K., Saini, V. K., & Jain, N. (2005). Adsorption of As (III) from aqueous solutions by iron oxide-coated sand. *Journal of Colloid and Interface Science*, *288*(1), 55-60.

Hahn, H. (1997). Gas phase synthesis of nanocrystalline materials. *Nanostructured Materials*, *9*(1), 3-12.

Hall, K. R., Eagleton, L. C., Acrivos, A., & Vermeulen, T. (1966). Pore-and solid-diffusion kinetics in fixed-bed adsorption under constant-pattern conditions. *Industrial & Engineering Chemistry Fundamentals*, *5*(2), 212-223.

Han, R., Wang, Y., Yu, W., Zou, W., Shi, J., & Liu, H. (2007). Biosorption of methylene blue from aqueous solution by rice husk in a fixed-bed column. *Journal of Hazardous Materials*, *141*(3), 713-718.

Hand, D. W., Crittenden, J. C., & Thacker, W. E. (1984). Simplified models for design of fixed-bed adsorption systems. *Journal of Environmental Engineering*, *110*(2), 440-456.

Hansen, H. K., Ribeiro, A., & Mateus, E. (2006). Biosorption of arsenic (V) with *Lessonia nigrescens*. *Minerals Engineering*, *19*(5), 486-490.

Health Canada. (2006). “Guidelines for Canadian Drinking Water Quality: Guideline Technical Document”, Health Canada, Ottawa, Ontario.

Hem, J. D. (1985). Study and interpretation of the chemical characteristics of natural water. USGS Water-Supply Paper 2254. Washington, D.C., U.S. Government Printing Office.

Henning, F.A. and D.E. Konasewich. (1984). Characterization and assessment of wood preservation facilities in British Columbia. West Vancouver, BC, Canada: Environmental Protection Services, Pacific region, Environment Canada.

Hering, J. G., & Kneebone, P. E. (2002). Biogeochemical controls on arsenic occurrence and mobility in water supplies, chapter 7. In: Environmental Chemistry of Arsenic, ed. W.T. Frankenberger Jr, 155-181. New York, Marcel Dekker Inc.

Hindmarsh, J. T., McCurdy, R. F., & Savory, J. (1986). Clinical and Environmental Aspects of Arsenic Toxicity. *Critical Reviews in Clinical Laboratory Sciences*, *23*(4), 315-347.

Ho, Y. S., & McKay, G. (2000). The kinetics of sorption of divalent metal ions onto sphagnum moss peat. *Water Research*, *34*(3), 735-742.

Hoch, L. B., Mack, E. J., Hydutsky, B. W., Hershman, J. M., Skluzacek, J. M., & Mallouk, T. E. (2008). Carbothermal synthesis of carbon-supported nanoscale zero-valent iron particles for the remediation of hexavalent chromium. *Environmental science & technology*, *42*(7), 2600-2605.

Holm, T. R., & Curtiss, C. D. (1988). Arsenic contamination in east-central Illinois ground waters. ILENR/RE-W-88/16. Open-File Report. Champaign, Illinois: Illinois State Water Survey, Aquatic Chemistry Section.

Hounslow, A. W. (1980). Ground-Water Geochemistry: Arsenic in Landfills. *Ground Water*, *18*(4), 331-333.

Hristovski, K. D., Westerhoff, P. K., Möller, T., & Sylvester, P. (2009). Effect of synthesis conditions on nano-iron (hydr) oxide impregnated granulated activated carbon. *Chemical Engineering Journal*, *146*(2), 237-243.

Hsia, T. H., Lo, S. L., Lin, C. F., & Lee, D. Y. (1994). Characterization of arsenate adsorption on hydrous iron oxide using chemical and physical methods. *Colloids and Surfaces A: Physicochemical and Engineering Aspects*, *85*(1), 1-7.

Huang, C. P., & Fu, P. L. K. (1984). Treatment of arsenic (V)-containing water by the activated carbon process. *Journal (Water Pollution Control Federation)*, *56*(3), 233-242,

Huang, C. P., & Vane, L. M. (1989). Enhancing As^{5+} removal by a Fe^{2+}-treated activated carbon. *Research Journal of the Water Pollution Control Federation*, *61*(9), 1596-1603.

Hundal, L. S., Singh, J., Bier, E. L., Shea, P. J., Comfort, S. D., & Powers, W. L. (1997). Removal of TNT and RDX from water and soil using iron metal. *Environmental Pollution*, *97*(1), 55-64.

Ichinose, N. (1992). Superfine Particle Technology, Springer, Berlin, Germany.

Irgolic, K. J. (1982). Speciation of arsenic compounds in water supplies. USEPA report 600/1-82-010. pp-107.

Jain, C. K., & Ali, I. (2000). Arsenic: occurrence, toxicity and speciation techniques. *Water Research*, *34*(17), 4304-4312.

Jang, M., Min, S. H., Kim, T. H., & Park, J. K. (2006). Removal of arsenite and arsenate using hydrous ferric oxide incorporated into naturally occurring porous diatomite. *Environmental Science & Technology*, *40*(5), 1636-1643.

Jang, M., Chen, W., & Cannon, F. S. (2008). Preloading hydrous ferric oxide into granular activated carbon for arsenic removal. *Environmental Science & Technology*, *42*(9), 3369-3374.

Jekel, M. R. (1994). Removal of arsenic in drinking water treatment. *Advances in Environmental Science and Technology-New York*, *26*, 119-119.

Jia, Y., & Demopoulos, G. P. (2005). Adsorption of arsenate onto ferrihydrite from aqueous solution: influence of media (sulfate vs nitrate), added gypsum, and pH alteration. *Environmental Science & Technology*, *39*(24), 9523-9527.

Jia, Y., Xu, L., Fang, Z., & Demopoulos, G. P. (2006). Observation of surface precipitation of arsenate on ferrihydrite. *Environmental science & technology*,*40*(10), 3248-3253.

Jia, Y., Xu, L., Wang, X., & Demopoulos, G. P. (2007). Infrared spectroscopic and X-ray diffraction characterization of the nature of adsorbed arsenate on ferrihydrite. *Geochimica et Cosmochimica Acta*, *71*(7), 1643-1654.

Johnson, T. L., Scherer, M. M., & Tratnyek, P. G. (1996). Kinetics of halogenated organic compound degradation by iron metal. *Environmental Science & Technology*, *30*(8), 2634-2640.

Joshi, A., & Chaudhuri, M. (1996). Removal of arsenic from ground water by iron oxide-coated sand. *Journal of Environmental Engineering*, *122*(8), 769-771.

Kanel, S. R., Manning, B., Charlet, L., & Choi, H. (2005). Removal of arsenic (III) from groundwater by nanoscale zero-valent iron. *Environmental Science & Technology*, *39*(5), 1291-1298.

Kanel, S. R., Greneche, J. M., & Choi, H. (2006). Arsenic (V) removal from groundwater using nano scale zero-valent iron as a colloidal reactive barrier material. *Environmental Science & Technology*, *40*(6), 2045-2050.

Kanivetsky, R. (2000). Arsenic in Minnesota groundwater: Hydrogeochemical modeling of the Quaternary buried artesian aquifer and cretaceous aquifer systems. Report of Investigation 55. St. Paul, Minnesota: Minnesota Geological Survey.

Kartinen, E. O., & Martin, C. J. (1995). An overview of arsenic removal processes. *Desalination*, 103(1), 79-88.

Kim, H. C., Lee, C. G., Park, J. A., & Kim, S. B. (2010). Arsenic removal from water using iron-impregnated granular activated carbon in the presence of bacteria. *Journal of Environmental Science and Health Part A*, *45*(2), 177-182.

Kinniburgh, D. G., & Smedley, P. L. (2001). Arsenic contamination of groundwater in Bangladesh, vol. 2: Final report. BGS Technical Report WC/00/19. Keyworth, UK: British Geological Survey.

Koch, I., Feldmann, J., Wang, L., Andrewes, P., Reimer, K. J., & Cullen, W. R. (1999). Arsenic in the Meager Creek hot springs environment, British Columbia, Canada. *Science of the total environment, 236*(1), 101-117.

Korngold, E., Belayev, N., & Aronov, L. (2001). Removal of arsenic from drinking water by anion exchangers. *Desalination*, *141*(1), 81-84.

Korte, N. E., & Fernando, Q. (1991). A review of arsenic (III) in groundwater. *Critical Reviews in Environmental Science and Technology*, *21*(1), 1-39.

Krupa, N. E., & Cannon, F. S. (1996). GAC: pore structure versus dye adsorption. *Journal-American Water Works Association*, *88*(6), 94-108.

Lackovic, J. A., Nikolaidis, N. P., & Dobbs, G. M. (2000). Inorganic arsenic removal by zero-valent iron. *Environmental Engineering Science*, *17*(1), 29-39.

Lagergren, S. (1898). About the theory of so-called adsorption of soluble substances. *Kungliga Svenska Vetenskapsakademiens Handlingar*, *24*(4), 1-39.

Langmuir, I. (1918). The adsorption of gases on plane surfaces of glass, mica and platinum. *Journal of the American Chemical Society*, *40*(9), 1361-1403.

Lara, F., Cornejo, L., Yanez, J., Freer, J., & Mansilla, H. D. (2006). Solar-light assisted removal of arsenic from natural waters: effect of iron and citrate concentrations. *Journal of Chemical Technology and Biotechnology*, *81*(7), 1282-1287.

Lee, H., & Choi, W. (2002). Photocatalytic oxidation of arsenite in TiO2 suspension: kinetics and mechanisms. *Environmental Science & Technology*, *36*(17), 3872-3878.

Leist, M., Casey, R. J., & Caridi, D. (2000). The management of arsenic wastes: problems and prospects. *Journal of Hazardous Materials*, *76*(1), 125-138.

LeVan, M. D. (1996). Fundamentals of Adsorption. *Kluwer Academic Publishers,* Boston, USA.

Leyva-Ramos, R., Rangel-Mendez, J. R., Bernal-Jacome, L. A., & Mendoza, B. (2005). Intraparticle diffusion of cadmium and zinc ions during adsorption from aqueous solution on activated carbon. *Journal of Chemical Technology and Biotechnology*, *80*(8), 924-933.

Leupin, O. X., & Hug, S. J. (2005). Oxidation and removal of arsenic (III) from aerated groundwater by filtration through sand and zero-valent iron. *Water Research*, *39*(9), 1729-1740.

Li, S., Yan, W., & Zhang, W. X. (2009). Solvent-free production of nanoscale zero-valent iron (nZVI) with precision milling. *Green Chemistry*, *11*(10), 1618-1626.

Lien, H. L., & Wilkin, R. T. (2005). High-level arsenite removal from groundwater by zero-valent iron. *Chemosphere*, *59*(3), 377-386.

Liu, Y., Majetich, S. A., Tilton, R. D., Sholl, D. S., & Lowry, G. V. (2005). TCE dechlorination rates, pathways, and efficiency of nanoscale iron particles with different properties. *Environmental Science & Technology*, *39*(5), 1338-1345.

Lorenzen, L., Van Deventer, J. S. J., & Landi, W. M. (1995). Factors affecting the mechanism of the adsorption of arsenic species on activated carbon. *Minerals Engineering*, *8*(4), 557-569.

Loukidou, M. X., Matis, K. A., Zouboulis, A. I., & Liakopoulou-Kyriakidou, M. (2003). Removal of As (V) from wastewaters by chemically modified fungal biomass. *Water Research*, *37*(18), 4544-4552.

Maity, S., Chakravarty, S., Bhattacharjee, S., & Roy, B. C. (2005). A study on arsenic adsorption on polymetallic sea nodule in aqueous medium. *Water Research*, *39*(12), 2579-2590.

Majewski, P., & Thierry, B. (2007). Functionalized magnetite nanoparticles-synthesis, properties, and bio-applications. *Critical Reviews in Solid State and Materials Sciences*, *32*(3-4), 203-215.

Mandal, B. K., & Suzuki, K. T. (2002). Arsenic round the world: a review. *Talanta*, *58*(1), 201-235.

Manju, G. N., Raji, C., & Anirudhan, T. S. (1998). Evaluation of coconut husk carbon for the removal of arsenic from water. *Water Research*, *32*(10), 3062-3070.

Manning, B. A., & Goldberg, S. (1996). Modeling arsenate competitive adsorption on kaolinite, montmorillonite and illite. *Clays and Clay Minerals*,*44*(5), 609-623.

Manning, B. A., Fendorf, S. E., & Goldberg, S. (1998). Surface structures and stability of arsenic (III) on goethite: spectroscopic evidence for inner-sphere complexes. *Environmental Science & Technology*, *32*(16), 2383-2388.

Manning, B. A., Hunt, M. L., Amrhein, C., & Yarmoff, J. A. (2002). Arsenic (III) and arsenic (V) reactions with zero-valent iron corrosion products. *Environmental Science & Technology*, *36*(24), 5455-5461.

Mass, M. J. (1992). Human carcinogenesis by arsenic. *Environmental Geochemistry and Health*, *14*(2), 49-54.

Matheson, L. J., & Tratnyek, P. G. (1994). Reductive dehalogenation of chlorinated methanes by iron metal. *Environmental Science & Technology*, *28*(12), 2045-2053.

Matschullat, J. (2000). Arsenic in the geosphere-a review. *Science of the Total Environment*, *249*(1), 297-312.

Mauricio, A. V. (2010). Multi-tiered distributions of arsenic in iron nanoparticles: Observation of dual redox functionality enabled by a core-shell structure. *Chemical Communications*, *46*(37), 6995-6997.

Melitas, N., Wang, J., Conklin, M., O'Day, P., & Farrell, J. (2002). Understanding soluble arsenate removal kinetics by zerovalent iron media. *Environmental Science & Technology*, *36*(9), 2074-2081.

Miteva, E., Hristova, D., Nenova, V., & Maneva, S. (2005). Arsenic as a factor affecting virus infection in tomato plants: changes in plant growth, peroxidase activity and chloroplast pigments. *Scientia Horticulturae*, *105*(3), 343-358.

Mohan, D., & Pittman Jr, C. U. (2007). Arsenic removal from water/wastewater using adsorbents-a critical review. *Journal of Hazardous Materials*, *142*(1), 1-53.

Morel, F., & Hering, J. G. (1993). *Principles and applications of aquatic chemistry* (p. 588). New York etc: Wiley.

Morton, W. (1994). Health Effects of Environmental Arsenic. In: Arsenic in the Environment. J. O. Nriagu. New York. John Wiley & sons Inc.

Mostafa, M. G., Chen, Y. H., Jean, J. S., Liu, C. C., & Lee, Y. C. (2011). Kinetics and mechanism of arsenate removal by nanosized iron oxide-coated perlite. *Journal of Hazardous Materials*, *187*(1), 89-95.

Mulvaney, P. (2001). Metal nanoparticles: double layers, optical properties, and electrochemistry. In: *Nanoscale Materials in Chemistry*; Klabunde, K. J., Ed.; Wiley: NewYork, pp 121-167.

Muñiz, G., Fierro, V., Celzard, A., Furdin, G., Gonzalez-Sánchez, G., & Ballinas, M. L. (2009). Synthesis, characterization and performance in arsenic removal of iron-doped activated carbons prepared by impregnation with Fe (III) and Fe (II). *Journal of Hazardous Materials*, *165*(1), 893-902.

Myneni, S. C., Traina, S. J., Waychunas, G. A., & Logan, T. J. (1998). Experimental and theoretical vibrational spectroscopic evaluation of arsenate coordination in aqueous solutions, solids, and at mineral-water interfaces. *Geochimica et Cosmochimica Acta*, *62*(19), 3285-3300.

Myneni, S. C., Traina, S. J., Waychunas, G. A., & Logan, T. J. (1998a). Vibrational spectroscopy of functional group chemistry and arsenate coordination in ettringite. *Geochimica et Cosmochimica Acta*, *62*(21), 3499-3514.

National Nanotechnology Initiative. (2009). What Is Nanotechnology? Available online: Jan 22, 2013. (http://www.nano.gov/html/facts/whatIsNano.html).

Newcombe, G., Hayes, R., & Drikas, M. (1993). Granular activated carbon: importance of surface properties in the adsorption of naturally occurring organics. *Colloids and Surfaces A: Physicochemical and Engineering Aspects*, *78*, 65-71.

Nguyen, V. L., Chen, W. H., Young, T., & Darby, J. (2011). Effect of interferences on the breakthrough of arsenic: Rapid small-scale column tests. *Water Research*, *45*(14), 4069-4080.

NHMRC Australian Drinking Water Guidelines. (1996). National Health and Medical Council, Agriculture and Resource Management Council of Australia and New Zealand, Commonwealth of Australia. PF S93.

Nordstrom, D.K. (2002). Worldwide occurrence of arsenic in ground water, *Science,* 296, 2143-2145.

Noubactep, C. (2008). A critical review on the process of contaminant removal in Fe^0-H_2O systems. *Environmental Technology*, *29*(8), 909-920.

Nowack, B., & Stone, A. T. (2002). Homogeneous and heterogeneous oxidation of nitrilotrismethylene phosphonic acid (NTMP) in the presence of manganese (II, III) and molecular oxygen. *The Journal of Physical Chemistry B*, *106*(24), 6227-6233.

NSF International. (2001a). Environmental Technology Verification Report: Removal of Arsenic in Drinking Water-Hydranautics ESPA2-4040 Reverse Osmosis Membrane Element Module, NSF 0120EPADW395.

NSF International. (2001b). Environmental Technology Verification Report: Removal of Arsenic in Drinking Water-KOCH Membrane Systems TFC-ULP4 Reverse Osmosis Membrane Module, NSF 0125EPADW395.

Nurmi, J. T., Tratnyek, P. G., Sarathy, V., Baer, D. R., Amonette, J. E., Pecher, K., & Driessen, M. D. (2005). Characterization and properties of metallic iron nanoparticles: spectroscopy, electrochemistry, and kinetics. *Environmental Science & Technology*, *39*(5), 1221-1230.

Oke, I. A., Olarinoye, N. O., & Adewusi, S. R. A. (2008). Adsorption kinetics for arsenic removal from aqueous solutions by untreated powdered eggshell. *Adsorption*, *14*(1), 73-83.

Oliveira, L. C., Rios, R. V., Fabris, J. D., Garg, V., Sapag, K., & Lago, R. M. (2002). Activated carbon/iron oxide magnetic composites for the adsorption of contaminants in water. *Carbon*, *40*(12), 2177-2183.

Onishi, H. (1969). Arsenic. In: K.H. Wedepohl (Ed.), Handbook of Geochemistry, Vol. II, (Chapter 33), Springer-Verlag, New York.

O'reilly, S. E., Strawn, D. G., & Sparks, D. L. (2001). Residence time effects on arsenate adsorption/desorption mechanisms on goethite. *Soil Science Society of America Journal*, *65*(1), 67-77.

OSMONICS. (2002). Virden, Manitoba, Canada case study: arsenic. OSMONICS profiles of winning solutions, Minnetonka, MN, Canada.

Paige, C. R., Snodgrass, W. J., Nicholson, R. V., & Scharer, J. M. (1996). The crystallization of arsenate-contaminated iron hydroxide solids at high pH. *Water Environment Research*, 981-987.

Pakula, M., Biniak, S., & Swiatkowski, A. (1998). Chemical and electrochemical studies of interactions between iron (III) ions and an activated carbon surface. *Langmuir*, *14*(11), 3082-3089.

Pal, B. N. (2001). In: Technologies for Arsenic Removal from Drinking Water; Bangladesh University of Engineering and Technology, Dhaka, The United Nations University, Tokyo: Tokyo, pp 59-68.

Parette, R., & Cannon, F. S. (2005). The removal of perchlorate from groundwater by activated carbon tailored with cationic surfactants. *Water Research*, *39*(16), 4020-4028.

Payne, K. B., & Abdel-Fattah, T. M. (2005). Adsorption of arsenate and arsenite by iron-treated activated carbon and zeolites: effects of pH, temperature, and ionic strength. *Journal of Environmental Science and Health*, *40*(4), 723-749.

Pena, M., Meng, X., Korfiatis, G. P., & Jing, C. (2006). Adsorption mechanism of arsenic on nanocrystalline titanium dioxide. *Environmental science & technology*, *40*(4), 1257-1262.

Peryea, F. J., & Creger, T. L. (1994). Vertical distribution of lead and arsenic in soils contaminated with lead arsenate pesticide residues. *Water, Air, and Soil Pollution*, *78*(3-4), 297-306.

Pierce, M. L., & Moore, C. B. (1982). Adsorption of arsenite and arsenate on amorphous iron hydroxide. *Water Research*, *16*(7), 1247-1253.

Ponder, S. M., Darab, J. G., & Mallouk, T. E. (2000). Remediation of Cr (VI) and Pb (II) aqueous solutions using supported, nanoscale zero-valent iron. *Environmental Science & Technology*, *34*(12), 2564-2569.

Pontius, F. W. (1999). Complying with future water regulations. *Journal-American Water Works Association*, *91*(3), 46-58.

Prasad, G. (1994). Removal of arsenic (V) from aqueous systems by adsorption onto some geological materials. *Advances in Environmental Science and Technology-New York*, *26*, 133-133.

Rajaković, L. V. (1992). The sorption of arsenic onto activated carbon impregnated with metallic silver and copper. *Separation Science and Technology*, *27*(11), 1423-1433.

Randall, S. R., Sherman, D. M., & Ragnarsdottir, K. V. (2001). Sorption of As (V) on green rust (Fe_4 (II) Fe_2 (III)(OH) $12SO_4 \cdot 3H_2O$) and lepidocrocite (γ-FeOOH): Surface complexes from EXAFS spectroscopy. *Geochimica et Cosmochimica Acta*, *65*(7), 1015-1023.

Raven, K. P., Jain, A., & Loeppert, R. H. (1998). Arsenite and arsenate adsorption on ferrihydrite: kinetics, equilibrium, and adsorption envelopes. *Environmental Science & Technology*, *32*(3), 344-349.

Reed, B. E., Vaughan, R., & Jiang, L. (2000). As (III), As (V), Hg, and Pb removal by Fe-oxide impregnated activated carbon. *Journal of Environmental Engineering*, *126*(9), 869-873.

Reinsch, B. C., Forsberg, B., Penn, R. L., Kim, C. S., & Lowry, G. V. (2010). Chemical transformations during aging of zero-valent iron nanoparticles in the presence of common groundwater dissolved constituents. *Environmental science & technology*, *44*(9), 3455-3461.

Roddick-Lanzilotta, A. J., McQuillan, A. J., & Craw, D. (2002). Infrared spectroscopic characterisation of arsenate (V) ion adsorption from mine waters, Macraes mine, New Zealand. *Applied Geochemistry*, *17*(4), 445-454.

Ryker, S. J. (2003). Arsenic in ground water used for drinking water in the United States. In *Arsenic in Ground Water* (pp. 165-178). Springer US.

Sacre, J. A. (1997). Treatment walls: a status update. Ground water remediation technologies analysis center, TP-97-02, Pittsburgh, PA.

Saha, J. C., Dikshit, A. K., Bandyopadhyay, M., & Saha, K. C. (1999). A review of arsenic poisoning and its effects on human health. *Critical Reviews in Environmental Science and Technology*, *29*(3), 281-313.

Sasaki, K., Nakano, H., Wilopo, W., Miura, Y., & Hirajima, T. (2009). Sorption and speciation of arsenic by zero-valent iron. *Colloids and Surfaces A: Physicochemical and Engineering Aspects*, *347*(1), 8-17.

Scherer, M. M., Richter, S., Valentine, R. L., & Alvarez, P. J. (2000). Chemistry and microbiology of permeable reactive barriers for in situ groundwater clean up.*Critical Reviews in Microbiology*, *26*(4), 221-264.

Schroeder, E. D. (1977). *Water and Wastewater Treatment.* McGraw-Hill, NY, USA.

Selecky, M., Bill, W., & Gregg, G. (2003). Guidance Document: Arsenic Treatment for Small Water Systems. DOH Pub. # 331-210, Washington State Department of Health, Olympia, Wasington.

Sherman, D. M., & Randall, S. R. (2003). Surface complexation of arsenic (V) to iron (III)(hydr) oxides: structural mechanism from ab initio molecular geometries and EXAFS spectroscopy. *Geochimica et Cosmochimica Acta*, *67*(22), 4223-4230.

Slejko, F. L. (1985). *Adsorption technology. A step-by-step approach to process evaluation and application*. New York; Basel: Dekker.

Smedley, P. L., & Kinniburgh, D. G. (2002). A review of the source, behaviour and distribution of arsenic in natural waters. *Applied Geochemistry*, *17*(5), 517-568.

Snoeyink, V. L., & Summers, R. S. (1999). Adsorption of organic compounds. *AWWA Water Quality and Treatment-A Handbook of Community Water Supplies, 5th edition,* McGraw Hill, New York.

Sontheimer, H., Crittenden, J. C. & Summers, R. S. (1988). *Activated Carbon for Water Treatment*, DVGW Forschungsstelle, Engler-Bunte-Institut, Universitat Karlsruhe (TH), Germany.

Sparks, D. L. (2003). *Environmental Soil Chemistry*. Access Online via Elsevier.

Stumm, W. (1992). *Chemistry of the Solid-water Interface: Processes at the Mineral-water and Particle-water Interface in Natural Systems*. John Wiley & Son Inc.

Sturgeon, R. E., Siu, K. M., Willie, S. N., & Berman, S. S. (1989). Quantification of arsenic species in a river water reference material for trace metals by graphite furnace atomic absorption spectrometric techniques. *Analyst*, *114*(11), 1393-1396.

Su, C., & Puls, R. W. (2001). Arsenate and arsenite removal by zero-valent iron: kinetics, redox transformation, and implications for in situ groundwater remediation. *Environmental Science & Technology*, *35*(7), 1487-1492.

Subramanian, K. S., Viraraghavan, T., Phommavong, T., & Tanjore, S. (1997). Manganese Greensand for Removal of Arsenic in Drinking Water. *Water Quality Research Journal Canada*, *32*(3), 551-561.

Sullivan, K. A., & Aller, R. C. (1996). Diagenetic cycling of arsenic in Amazon shelf sediments. *Geochimica et Cosmochimica Acta*, *60*(9), 1465-1477.

Summers, R. S., Hooper, S. M., Solarik, G., Owen, D. M., & Seongho, H. (1995). Bench-scale evaluation of GAC for NOM control. *Journal-American Water Works Association*, *87*(8), 69-80.

Sun, X., & Doner, H. E. (1998). Adsorption and oxidation of arsenite on goethite. *Soil Science*, *163*(4), 278-287.

Suslick, K. S., Choe, S. B., Cichowlas, A. A., & Grinstaff, M. W. (1991). Sonochemical synthesis of amorphous iron. *Nature*, *353*(6343), 414-416.

Swedlund, P. J., & Webster, J. G. (1999). Adsorption and polymerisation of silicic acid on ferrihydrite, and its effect on arsenic adsorption. *Water Research*, *33*(16), 3413-3422.

Thirunavukkarasu, O. S., Viraraghavan, T., & Subramanian, K. S. (2003). Arsenic removal from drinking water using iron oxide-coated sand. *Water, Air, and Soil Pollution*, *142*(1-4), 95-111.

Thronton, R.C. and Fargo, M. (1997). The Geochemistry of Arsenic, *Arsenic: Exposure and Health Effects.* C.O. Abernathy, R.L. Calderon and W.R Chappell (Eds.) Chapman and Hall, New York.

US EPA. (1987). Volatile SOCs, Final rule, Fed. reg., 2:130:25690.

US EPA. (1992). Test Methods for Evaluating Solid Waste, Physical/Chemical Methods. Method

1311, SW-846, 3rd edition, Washington, DC.

US EPA. (2000). Arsenic Removal from Drinking Water by Ion Exchange and Activated Alumina Plants, Prepared by Battelle under contract 68-C7-0008 for EPA ORD.

US EPA. (2001a). National primary drinking water regulations: Arsenic and clarifications to compliance and new source contaminants monitoring, *Federal Register*, 66(14), 6975-7066.

US EPA. (2001b). Arsenic rule benefit analysis: An SAB review. [EPA-SAB-EC-01-008], Washington, DC.

US EPA. (2003). Arsenic treatment technology evaluation handbook for small systems, office of water (4606M), EPA 816-R-03-014.

Vahter, M. (2000). Genetic polymorphism in the biotransformation of inorganic arsenic and its role in toxicity. *Toxicology Letters*, *112*, 209-217.

Valberg, P. A., Beck, B. D., Bowers, T. S., Keating, J. L., Bergstrom, P. D., & Boardman, P. D. (1997). Issues in setting health-based cleanup levels for arsenic in soil. *Regulatory Toxicology and Pharmacology*, *26*(2), 219-229.

Vaughan, R. L., & Reed, B. E. (2005). Modeling As(V) removal by a iron oxide impregnated activated carbon using the surface complexation approach. *Water Research*, *39*(6), 1005-1014.

Villa-Lojo, M. C., Beceiro-Gonzalez, E., Alonso-Rodriguez, E., & Prada-Rodriguez, D. (1997). Arsenic speciation in marine sediments: effects of redox potential and reducing conditions. *International Journal of Environmental Analytical Chemistry*, *68*(3), 377-389.

Villars, Pierre. *Pearson's handbook: crystallographic data for intermetallic phases*. ASM international, 1997.

Viraraghavan, T., Subramanian, K. S., & Aruldoss, J. A. (1999). Arsenic in drinking water-problems and solutions. *Water Science and Technology*, *40*(2), 69-76.

Vitela-Rodriguez, A. V., & Rangel-Mendez, J. R. (2013). Arsenic removal by modified activated carbons with iron hydro (oxide) nanoparticles. *Journal of Environmental Management, 114,* 225-231.

Wakao, N., & Funazkri, T. (1978). Effect of fluid dispersion coefficients on particle-to-fluid mass transfer coefficients in packed beds: correlation of Sherwood numbers. *Chemical Engineering Science*, *33*(10), 1375-1384.

Wang, C. B., & Zhang, W. X. (1997). Synthesizing nanoscale iron particles for rapid and complete dechlorination of TCE and PCBs. *Environmental Science & Technology*, *31*(7), 2154-2156.

Welch, A. H., Lico, M. S., & Hughes, J. L. (1988). Arsenic in ground water of the western United States. *Ground Water*, *26*(3), 333-347.

Welch, A. H., & Stollenwerk, K. G. (Eds.). (2003). *Arsenic in ground water* (p. 475). Dordrecht: Kluwer Academic Publishers.

Westall, J. C. (1986). Reactions at the oxide-solution interface: Chemical and electrostatic models. *Geochemical Processes at Mineral Surfaces*, *323*, 54-78.

Westerhoff, P., Highfield, D., Badruzzaman, M., & Yoon, Y. (2005). Rapid small-scale column tests for arsenate removal in iron oxide packed bed columns. *Journal of Environmental Engineering*, *131*(2), 262-271.

WHO. (1993). Arsenic in drinking water, Fact Sheet No 210. Internet. Jan. 22, 2013. Available: https://apps.who.int/inf-fs/en/fact210.html.

WHO. (1996). Guidelines for drinking water quality. 2nd edition, Geneva

WHO. (1997). Guidelines for drinking water during coagulation, *Journal of Environmental Engineering*, 123:800-807.

Wilkie, J. A., & Hering, J. G. (1996). Adsorption of arsenic onto hydrous ferric oxide: effects of adsorbate/adsorbent ratios and co-occurring solutes. *Colloids and Surfaces A: Physicochemical and Engineering Aspects*, *107*, 97-110.

Wilkin, R. T., Su, C., Ford, R. G., & Paul, C. J. (2005). Chromium-removal processes during groundwater remediation by a zerovalent iron permeable reactive barrier. *Environmental Science & Technology*, *39*(12), 4599-4605.

Wong, H. K. T., Gauthier, A., Beauchamp, S., & Tordon, R. (2002). Impact of toxic metals and metalloids from the Caribou gold-mining areas in Nova Scotia, Canada. *Geochemistry: Exploration, Environment, Analysis*, *2*(3), 235-241.

www.micromeritics.com, visited October 15, 2014.

Yan, X. P., Kerrich, R., & Hendry, M. J. (2000). Distribution of arsenic (III), arsenic (V) and total inorganic arsenic in porewaters from a thick till and clay-rich aquitard sequence, Saskatchewan, Canada. *Geochimica et Cosmochimica Acta*, *64*(15), 2637-2648.

Yang, L., Wu, S., & Chen, J. P. (2007). Modification of activated carbon by polyaniline for enhanced adsorption of aqueous arsenate. *Industrial & Engineering Chemistry Research*, *46*(7), 2133-2140.

Yates, D. E., Levine, S., & Healy, T. W. (1974). Site-binding model of the electrical double layer at the oxide/water interface. *Journal of the Chemical Society, Faraday Transactions 1: Physical Chemistry in Condensed Phases*, *70*, 1807-1818.

Yates, D. E. (1975). *The Structure of the Oxide/Aqueous Electrolyte Interface* (Doctoral dissertation, University of Melbourne, Department of Physical Chemistry).

Yong, R. N., & Mulligan, C. N. (2003). *Natural Attenuation of Contaminants in Soils*. CRC Press, Boca Raton, Florida, USA.

Zhang, Q. L., Lin, Y. C., Chen, X., & Gao, N. Y. (2007). A method for preparing ferric activated carbon composites adsorbents to remove arsenic from drinking water. *Journal of Hazardous Materials*, *148*(3), 671-678.

Zhang, Q., Pan, B., Zhang, W., Pan, B., Zhang, Q., & Ren, H. (2008). Arsenate removal from aqueous media by nanosized hydrated ferric oxide (HFO)-loaded polymeric sorbents: effect of HFO loadings. *Industrial & Engineering Chemistry Research*, *47*(11), 3957-3962.

Zheng, J., H. Holger, D. Brian and D.M. Stephen. (2003). Speciation of arsenic in water, sediment, and plants of the Moira watershed, Canada, using HPLC coupled to high resolution ICP-MS. *Analytical and Bioanalytical Chemistry, 377,* 14-24.

Zhu, H., Jia, Y., Wu, X., & Wang, H. (2009). Removal of arsenic from water by supported nano zero-valent iron on activated carbon. *Journal of Hazardous Materials*, *172*(2), 1591-1596.

Appendix

A1. BET Analysis Data for Virgin GAC

Average pore width (Å)	Cumulative pore volume (cm^3/g)	Cumulative pore area (m^2/g)
1982	0.004	0.09
1775	0.017	0.38
728	0.030	1.10
395	0.031	1.20
265	0.032	1.27
201	0.032	1.32
162	0.032	1.36
137	0.032	1.39
125	0.032	1.41
114	0.032	1.44
90	0.033	1.59
76	0.033	1.72
65	0.033	1.97
56	0.034	2.39
49	0.035	3.02
43	0.036	3.99
38	0.042	10.78
34	0.045	13.98
30	0.048	17.98
27	0.050	21.32
25	0.054	27.69
22	0.060	37.56
19	0.072	63.74

A2. BET Analysis Data for nZVI/GAC

Average pore width (Å)	**Cumulative pore volume (cm^3/g)**	**Cumulative pore area (m^2/g)**
1747	0.006	0.14
1211	0.012	0.35
764	0.016	0.54
457	0.021	0.94
322	0.023	1.23
242	0.025	1.52
189	0.026	1.80
154	0.027	2.00
130	0.027	2.17
113	0.028	2.33
94	0.028	2.63
77	0.029	2.98
65	0.030	3.45
56	0.031	4.12
49	0.032	5.36
43	0.035	7.54
38	0.042	15.12
34	0.046	20.61
30	0.049	24.32
27	0.052	28.54
25	0.056	34.84
22	0.061	44.56
19	0.072	66.93

A3. Effect of pH on As(III) Adsorption on Virgin and nZVI/GAC

pH	As(III) adsorption on virgin GAC, (µg/g)	RSD (%)	As(III) adsorption on nZVI/GAC, (µg/g)	RSD (%)
2	175	2.35	1104	3.2
3	150	2.56	1218	1.58
4	155	3.58	1424	1.47
5	145	4.20	1347	1.87
6	178	3.21	1415	1.98
7	165	1.25	1351	2.57
8	147	2.45	1285	3.18
9	158	1.87	1022	3.2
10	134	2.54	987	1.21
11	115	3.12	885	2.35

A4. Effect of pH on As(V) Adsorption on Virgin and nZVI/GAC

pH	As(V) adsorption on virgin GAC, (µg/g)	RSD (%)	As(V) adsorption on nZVI/GAC, (µg/g)	RSD (%)
2	254	3.21	3425	1.67
3	265	1.25	3510	0.23
4	280	1.87	3705	1.23
5	247	2.54	3675	2.70
6	255	3.24	3515	0.33
7	242	2.54	3010	0.26
8	202	2.35	2345	2.97
9	171	1.22	1215	3.20
10	142	1.47	1024	1.06
11	124	2.65	925	2.50

A5. Effect of Initial Concentration on As(V) Adsorption on nZVI/GAC

Initial As(V) conc., C_0 (µg/L)	**As(V) adsorption, q (µg/g)**	**RSD (%)**
500	480	1.02
1000	890	1.10
1500	1224	1.24
2000	1616	1.78
3000	2130	2.41
4000	2820	2.72
5000	3580	3.21
10000	4224	3.18
15000	6124	3.40

A6. Effect of Contact Time on As(V) Adsorption on nZVI/GAC

Time, min	**As(V) adsorption, q (µg/g)**	**RSD (%)**
15	3320	2.15
30	3460	1.89
60	3502	2.68
120	3578	3.23
180	3610	3.17
360	3686	3.74
480	3714	3.28
720	3780	2.47

A7. Effect of Competitive Ions on As(V) Adsorption at pHs 4.5 and 6.5

Competitive ions	**pH 4.5**			**pH 6.5**		
	As(V) adsorption, q (µg/g) at			**As(V) adsorption, q (µg/g) at**		
	0mM	**1mM**	**10mM**	**0 mM**	**1mM**	**10mM**
PO_4^{3-}	3580	1922	910	3245	1745	805
SiO_3^{2-}	3580	3125	1724	3245	1210	865
SO_4^{2-}	3580	3325	2985	3245	3089	2904
NO_3^-	3580	3410	3214	3245	3127	2995
F^-	3580	3280	3195	3245	2878	2835
Mn^{2+}	3580	3387	3405	3245	2855	2748
Mg^{2+}	3580	3375	3378	3245	2745	2720
Ca^{2+}	3580	3545	3555	3245	2870	2885

A8. Langmuir and Freundlich Isotherm Data for As(V)

Residual conc. of As(V), Ce (µg/L)	**As(V) adsorption, q (µg/g)**	**RSD (%)**
20	480	1.02
110	890	1.10
276	1224	1.24
384	1616	1.78
870	2130	2.41
1180	2820	2.72
1420	3580	3.21
5776	4224	3.18
8876	6124	3.40

A9. FAST Input Parameters for DCBR Experiment

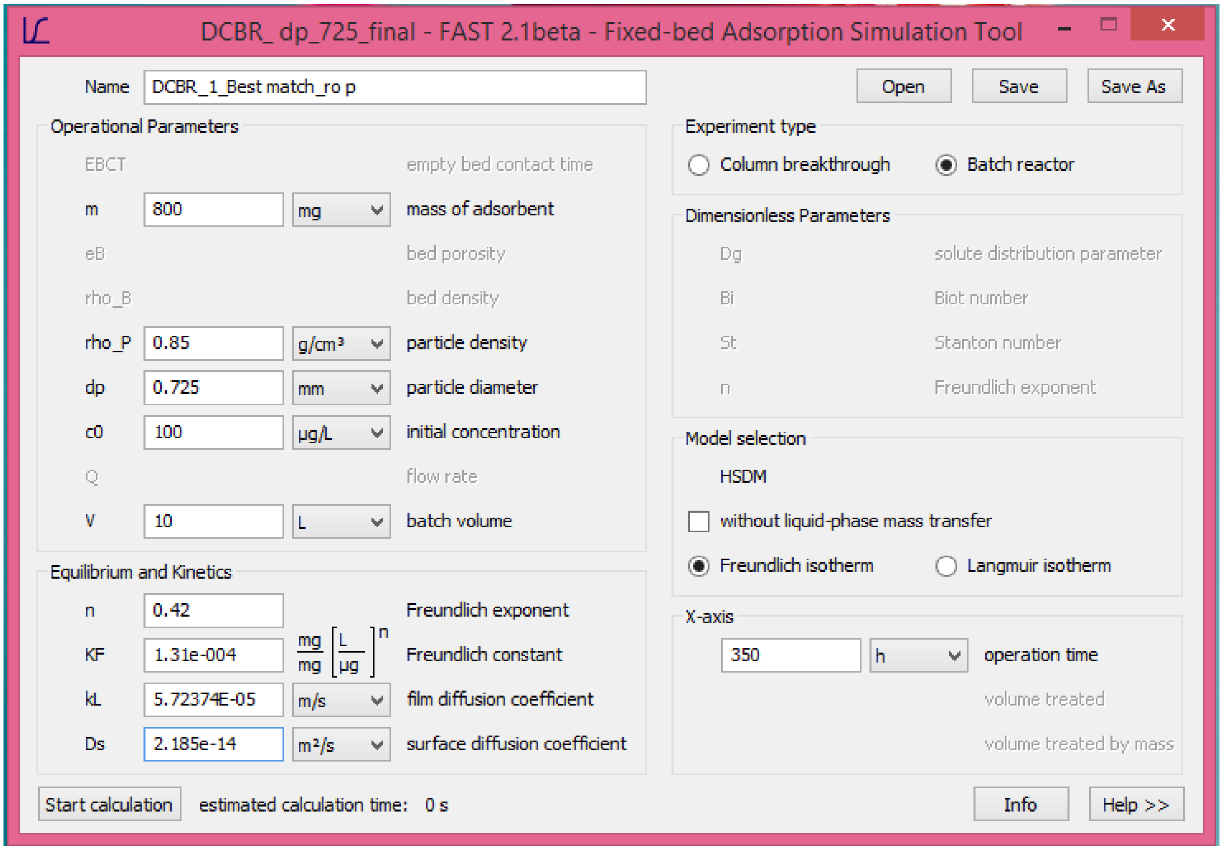

Name: DCBR_1_Best match_ro p

Operational Parameters

EBCT			empty bed contact time
m	800	mg	mass of adsorbent
eB			bed porosity
rho_B			bed density
rho_P	0.85	g/cm³	particle density
dp	0.725	mm	particle diameter
c0	100	µg/L	initial concentration
Q			flow rate
V	10	L	batch volume

Equilibrium and Kinetics

n	0.42		Freundlich exponent
KF	1.31e-004	$\frac{mg}{mg}\left[\frac{L}{\mu g}\right]^n$	Freundlich constant
kL	5.72374E-05	m/s	film diffusion coefficient
Ds	2.185e-14	m²/s	surface diffusion coefficient

Experiment type

○ Column breakthrough ● Batch reactor

Dimensionless Parameters

Dg	solute distribution parameter
Bi	Biot number
St	Stanton number
n	Freundlich exponent

Model selection

HSDM

☐ without liquid-phase mass transfer

● Freundlich isotherm ○ Langmuir isotherm

X-axis

350	h	operation time
		volume treated
		volume treated by mass

estimated calculation time: 0 s

A10. DCBR Modeling Data

Time, h	C/C_0
0	1.000
2	0.936
4	0.909
5	0.889
7	0.873
9	0.859
11	0.846
12	0.835
14	0.825
16	0.815
18	0.807
19	0.799
21	0.791
23	0.784
25	0.777
26	0.771
28	0.764
30	0.758
32	0.753
33	0.747
35	0.742
37	0.737
39	0.733
40	0.728
42	0.723
44	0.719
46	0.715
47	0.711
49	0.707
51	0.703
53	0.699
54	0.696
56	0.692
58	0.689
60	0.686
61	0.682
63	0.679
65	0.676
67	0.673
68	0.670
70	0.667
72	0.665
74	0.662
75	0.659
77	0.657
79	0.654
81	0.652
82	0.649
84	0.647
86	0.644
88	0.642
89	0.640
91	0.638
93	0.636
95	0.633
96	0.631
98	0.629
100	0.627
102	0.625
103	0.623
105	0.622
107	0.620
109	0.618
110	0.616
112	0.614
114	0.613
116	0.611
117	0.609
119	0.608
121	0.606
123	0.604
124	0.603
126	0.601
128	0.600
130	0.598
131	0.597
133	0.595
135	0.594
137	0.593
138	0.591
140	0.590
142	0.589
144	0.587
145	0.586
147	0.585
149	0.583
151	0.582
152	0.581
154	0.580
156	0.579
158	0.577
159	0.576
161	0.575
163	0.574
165	0.573
166	0.572
168	0.571
170	0.570
172	0.569
173	0.568
175	0.567
177	0.566
179	0.565
180	0.564
182	0.563
184	0.562
186	0.561
187	0.560
189	0.559
191	0.558
193	0.557
194	0.556
196	0.556
198	0.555
200	0.554
201	0.553
203	0.552
205	0.552
207	0.551
208	0.550
210	0.549
212	0.548
214	0.548
215	0.547
217	0.546
219	0.546
221	0.545
222	0.544
224	0.543
226	0.543
228	0.542
229	0.541
231	0.541
233	0.540
235	0.540
236	0.539
238	0.538
240	0.538
242	0.537
243	0.536
245	0.536
247	0.535
249	0.535
250	0.534
252	0.534
254	0.533
256	0.533
257	0.532
259	0.531
261	0.531
263	0.530
264	0.530
266	0.529
268	0.529
270	0.528
271	0.528
273	0.527
275	0.527
277	0.527
278	0.526
280	0.526
282	0.525
284	0.525
285	0.524
287	0.524
289	0.523
291	0.523
292	0.523
294	0.522
296	0.522
298	0.521
299	0.521
301	0.521
303	0.520
305	0.520
306	0.519
308	0.519
310	0.519
312	0.518
313	0.518
315	0.518
317	0.517
319	0.517
320	0.517
322	0.516
324	0.516
326	0.516
327	0.515
329	0.515
331	0.515
333	0.514
334	0.514
336	0.514
338	0.513
340	0.513
341	0.513
343	0.513
345	0.512
347	0.512
348	0.512
350	0.511

A11. DCBR Experimental Data

Time, h	**C/C_0**
0	1.00
24	0.82
48	0.75
72	0.71
96	0.58
120	0.57
144	0.56
168	0.53
192	0.51
216	0.51
240	0.52
264	0.49
288	0.49
312	0.49

A12. Experimental and HSDM Predicted Breakthrough Data for EBCT= 0.5 min

HSDM data

BV	C/C_0
0	0.000
150	0.000
300	0.000
450	0.000
600	0.000
750	0.000
900	0.000
1050	0.000
1200	0.000
1350	0.000
1500	0.000
1650	0.000
1800	0.000
1950	0.000
2100	0.000
2250	0.000
2400	0.000
2550	0.000
2700	0.000
2850	0.000
3000	0.000
3150	0.000
3300	0.000
3450	0.000
3600	0.000
3750	0.000
3900	0.000
4050	0.000
4200	0.000
4350	0.000
4500	0.000
4650	0.000
4800	0.000
4950	0.000
5100	0.000
5250	0.000
5400	0.000
5550	0.000
5700	0.000
5850	0.000
6000	0.000
6150	0.000
6300	0.000
6450	0.000
6600	0.000
6750	0.000
6900	0.000
7050	0.000
7200	0.000
7350	0.000
7500	0.000
7650	0.001
7800	0.004
7950	0.020
8100	0.070
8250	0.145
8400	0.221
8550	0.291
8700	0.355
8850	0.412
9000	0.464
9150	0.511
9300	0.554
9450	0.593
9600	0.628
9750	0.661
9900	0.690
10050	0.717
10200	0.742
10350	0.765
10500	0.786
10650	0.805
10800	0.822
10950	0.838
11100	0.852
11250	0.865
11400	0.877
11550	0.888
11700	0.898
11850	0.908
12000	0.916
12150	0.924
12300	0.930
12450	0.937
12600	0.942
12750	0.948
12900	0.952
13050	0.957
13200	0.961
13350	0.964
13500	0.968
13650	0.971
13800	0.973
13950	0.976
14100	0.978

Experimental data

BV	C/C_0
1000	0.010
2000	0.017
3000	0.024
4000	0.072
5000	0.066
6000	0.075
7000	0.080
8000	0.106
9000	0.242
10000	0.352
11000	0.651
12000	0.722
13000	0.942
14000	0.954
15000	1.001

A13. Experimental and HSDM Predicted Breakthrough Data for EBCT= 1.0 min

HSDM data

BV	**C/C$_0$**
0	0.000
150	0.000
300	0.000
450	0.000
600	0.000
750	0.000
900	0.000
1050	0.000
1200	0.000
1350	0.000
1500	0.000
1650	0.000
1800	0.000
1950	0.000
2100	0.000
2250	0.000
2400	0.000
2550	0.000
2700	0.000
2850	0.000
3000	0.000
3150	0.000
3300	0.000
3450	0.000
3600	0.000
3750	0.000
3900	0.000
4050	0.000
4200	0.000
4350	0.000
4500	0.000
4650	0.000
4800	0.000
4950	0.000
5100	0.000
5250	0.000
5400	0.000
5550	0.000
5700	0.000
5850	0.000
6000	0.000
6150	0.000
6300	0.000
6450	0.000
6600	0.000
6750	0.000
6900	0.000
7050	0.000
7200	0.000
7350	0.000
7500	0.000
7650	0.000
7800	0.000
7950	0.000
8100	0.000
8250	0.000
8400	0.001
8550	0.008
8700	0.046
8850	0.145
9000	0.265
9150	0.376
9300	0.471
9450	0.552
9600	0.621
9750	0.679
9900	0.729
10050	0.772
10200	0.808
10350	0.838
10500	0.864
10650	0.885
10800	0.904
10950	0.919
11100	0.932
11250	0.943
11400	0.952
11550	0.960
11700	0.966
11850	0.972
12000	0.976
12150	0.980
12300	0.983
12450	0.986
12600	0.988
12750	0.990
12900	0.992
13050	0.993
13200	0.994
13350	0.995
13500	0.996
13650	0.997
13800	0.997
13950	0.998
14100	0.998

Experimental data

BV	**C/C0**
500	0.009
1000	0.010
1500	0.010
2000	0.024
2500	0.037
3000	0.056
3500	0.063
4000	0.058
4500	0.072
5000	0.069
5500	0.097
6000	0.106
6500	0.082
7000	0.093
7500	0.089
8000	0.090
8500	0.101
9000	0.098
9500	0.111
10000	0.185
10500	0.423
11000	0.387
11500	0.472
12000	0.699
12500	0.989
13000	1.001

A14. Experimental and HSDM Predicted Breakthrough Data for EBCT= 2.0 min

HSDM data

BV	C/C0	BV	C/C0	BV	C/C0
0	0.000	4200	0.000	8400	0.000
150	0.000	4350	0.000	8550	0.000
300	0.000	4500	0.000	8700	0.000
450	0.000	4650	0.000	8850	0.002
600	0.000	4800	0.000	9000	0.019
750	0.000	4950	0.000	9150	0.113
900	0.000	5100	0.000	9300	0.296
1050	0.000	5250	0.000	9450	0.470
1200	0.000	5400	0.000	9600	0.608
1350	0.000	5550	0.000	9750	0.713
1500	0.000	5700	0.000	9900	0.790
1650	0.000	5850	0.000	10050	0.848
1800	0.000	6000	0.000	10200	0.890
1950	0.000	6150	0.000	10350	0.920
2100	0.000	6300	0.000	10500	0.942
2250	0.000	6450	0.000	10650	0.958
2400	0.000	6600	0.000	10800	0.970
2550	0.000	6750	0.000	10950	0.978
2700	0.000	6900	0.000	11100	0.984
2850	0.000	7050	0.000	11250	0.989
3000	0.000	7200	0.000	11400	0.992
3150	0.000	7350	0.000	11550	0.994
3300	0.000	7500	0.000	11700	0.996
3450	0.000	7650	0.000	11850	0.997
3600	0.000	7800	0.000	12000	0.998
3750	0.000	7950	0.000	12150	0.998
3900	0.000	8100	0.000	12300	0.999
4050	0.000	8250	0.000	12450	0.999

Experimental data

BV	C/C0
1000	0.005
2000	0.013
3000	0.017
4000	0.043
5000	0.069
6000	0.057
7000	0.075
8000	0.097
9000	0.125
10000	0.242
11000	0.321
12000	0.677
13000	0.778
14000	0.953
15000	0.923
16000	0.999

A15. Experimental and HSDM Predicted Breakthrough Data for C_0 = 100 μg/L

HSDM data

BV	C/C_0
0	0.000
150	0.000
300	0.000
450	0.000
600	0.000
750	0.000
900	0.000
1050	0.000
1200	0.000
1350	0.000
1500	0.000
1650	0.000
1800	0.000
1950	0.000
2100	0.000
2250	0.000
2400	0.000
2550	0.000
2700	0.000
2850	0.000
3000	0.000
3150	0.000
3300	0.000
3450	0.000
3600	0.000
3750	0.000
3900	0.000
4050	0.000
4200	0.000
4350	0.000
4500	0.000
4650	0.000
4800	0.000
4950	0.000
5100	0.000
5250	0.000
5400	0.000
5550	0.000
5700	0.000
5850	0.000
6000	0.000
6150	0.000
6300	0.000
6450	0.000
6600	0.000
6750	0.000
6900	0.000
7050	0.000
7200	0.000
7350	0.000
7500	0.000
7650	0.000
7800	0.000
7950	0.000
8100	0.000
8250	0.000
8400	0.001
8550	0.008
8700	0.046
8850	0.145
9000	0.265
9150	0.376
9300	0.471
9450	0.552
9600	0.621
9750	0.679
9900	0.729
10050	0.772
10200	0.808
10350	0.838
10500	0.864
10650	0.885
10800	0.904
10950	0.919
11100	0.932
11250	0.943
11400	0.952
11550	0.960
11700	0.966
11850	0.972
12000	0.976
12150	0.980
12300	0.983
12450	0.986
12600	0.988
12750	0.990
12900	0.992
13050	0.993
13200	0.994
13350	0.995
13500	0.996
13650	0.997
13800	0.997
13950	0.998
14100	0.998
14250	0.998
14400	0.999
14550	0.999
14700	0.999
14850	0.999
15000	0.999
15150	0.999
15300	1.000

Experimental data

BV	C/C_0
500	0.009
1000	0.010
1500	0.010
2000	0.024
2500	0.037
3000	0.056
3500	0.063
4000	0.058
4500	0.072
5000	0.069
5500	0.097
6000	0.106
6500	0.082
7000	0.093
7500	0.089
8000	0.090
8500	0.101
9000	0.098
9500	0.111
10000	0.185
10500	0.423
11000	0.387
11500	0.472
12000	0.699
12500	0.989
13000	1.001

A16. Experimental and HSDM Predicted Breakthrough Data for C_0 = 50 µg/L

HSDM data

BV	C/C_0
0	0.000
150	0.000
300	0.000
450	0.000
600	0.000
750	0.000
900	0.000
1050	0.000
1200	0.000
1350	0.000
1500	0.000
1650	0.000
1800	0.000
1950	0.000
2100	0.000
2250	0.000
2400	0.000
2550	0.000
2700	0.000
2850	0.000
3000	0.000
3150	0.000
3300	0.000
3450	0.000
3600	0.000
3750	0.000
3900	0.000
4050	0.000
4200	0.000
4350	0.000
4500	0.000
4650	0.000
4800	0.000
4950	0.000
5100	0.000
5250	0.000
5400	0.000
5550	0.000
5700	0.000
5850	0.000
6000	0.000
6150	0.000
6300	0.000
6450	0.000
6600	0.000
6750	0.000
6900	0.000
7050	0.000
7200	0.000
7350	0.000
7500	0.000
7650	0.000
7800	0.000
7950	0.000
8100	0.000
8250	0.000
8400	0.000
8550	0.000
8700	0.000
8850	0.000
9000	0.000
9150	0.000
9300	0.000
9450	0.000
9600	0.000
9750	0.000
9900	0.000
10050	0.000
10200	0.000
10350	0.000
10500	0.000
10650	0.000
10800	0.000
10950	0.002
11100	0.006
11250	0.020
11400	0.062
11550	0.147
11700	0.252
11850	0.355
12000	0.447
12150	0.528
12300	0.598
12450	0.659
12600	0.710
12750	0.755
12900	0.792
13050	0.824
13200	0.851
13350	0.875
13500	0.894
13650	0.911
13800	0.925
13950	0.937
14100	0.947
14250	0.955
14400	0.962
14550	0.968
14700	0.973
14850	0.977
15000	0.981
15150	0.984
15300	0.987
15450	0.989
15600	0.990
15750	0.992
15900	0.993
16050	0.994
16200	0.995
16350	0.996
16500	0.997
16650	0.997
16800	0.998
16950	0.998
17100	0.998
17250	0.999
17400	0.999
17550	0.999
17700	0.999
17850	0.999
18000	0.999
18150	1.000

Experimental data

BV	C/C_0
1000	0.019
2000	0.047
3000	0.047
4000	0.114
5000	0.087
6000	0.097
7000	0.149
8000	0.183
9000	0.178
10000	0.191
11000	0.251
12000	0.357
13000	0.580
14000	0.562
15000	0.671
16000	0.854
17000	1.002

A17. Experimental and HSDM Predicted Breakthrough Data for C_0 = 20 µg/L

HSDM data

BV	C/C_0
0	0.000
150	0.000
300	0.000
450	0.000
600	0.000
750	0.000
900	0.000
1050	0.000
1200	0.000
1350	0.000
1500	0.000
1650	0.000
1800	0.000
1950	0.000
2100	0.000
2250	0.000
2400	0.000
2550	0.000
2700	0.000
2850	0.000
3000	0.000
3150	0.000
3300	0.000
3450	0.000
3600	0.000
3750	0.000
3900	0.000
4050	0.000
4200	0.000
4350	0.000
4500	0.000
4650	0.000
4800	0.000
4950	0.000
5100	0.000
5250	0.000
5400	0.000
5550	0.000
5700	0.000
5850	0.000
6000	0.000
6150	0.000
6300	0.000
6450	0.000
6600	0.000
6750	0.000
6900	0.000
7050	0.000
7200	0.000
7350	0.000
7500	0.000
7650	0.000
7800	0.000
7950	0.000
8100	0.000
8250	0.000
8400	0.000
8550	0.000
8700	0.000
8850	0.000
9000	0.000
9150	0.000
9300	0.000
9450	0.000
9600	0.000
9750	0.000
9900	0.000
10050	0.000
10200	0.000
10350	0.000
10500	0.000
10650	0.000
10800	0.000
10950	0.000
11100	0.000
11250	0.000
11400	0.000
11550	0.000
11700	0.000
11850	0.000
12000	0.000
12150	0.000
12300	0.000
12450	0.000
12600	0.000
12750	0.000
12900	0.000
13050	0.000
13200	0.000
13350	0.000
13500	0.000
13650	0.000
13800	0.000
13950	0.000
14100	0.000
14250	0.000
14400	0.000
14550	0.000
14700	0.000
14850	0.000
15000	0.000
15150	0.000
15300	0.000
15450	0.000
15600	0.000
15750	0.000
15900	0.000
16050	0.000
16200	0.000
16350	0.001
16500	0.001
16650	0.003
16800	0.006
16950	0.013
17100	0.027
17250	0.054
17400	0.100
17550	0.168
17700	0.247
17850	0.331
18000	0.412
18150	0.487
18300	0.554
18450	0.614
18600	0.667
18750	0.713
18900	0.753
19050	0.788
19200	0.818
19350	0.845
19500	0.867
19650	0.886
19800	0.903
19950	0.917
20100	0.929
20250	0.939
20400	0.948
20550	0.956
20700	0.962
20850	0.968
21000	0.973
21150	0.977
21300	0.980
21450	0.983
21600	0.986
21750	0.988
21900	0.990
22050	0.991
22200	0.992
22350	0.994
22500	0.994
22650	0.995
22800	0.996
22950	0.997
23100	0.997
23250	0.998
23400	0.998
23550	0.998
23700	0.998
23850	0.999
24000	0.999
24150	0.999
24300	0.999
24450	0.999
24600	0.999
24750	1.000

Experimental data

BV	C/C_0
1000	0.049
2000	0.056
3000	0.063
4000	0.157
5000	0.183
6000	0.229
7000	0.194
8000	0.283
9000	0.358
10000	0.413
11000	0.488
12000	0.373
13000	0.458
14000	0.445
15000	0.440
16000	0.494
17000	0.506
18000	0.555
19000	0.861
20000	1.044